Contribution of the Hydrophobic Effect to the Conformational Stability of a Protein

A Doctoral Thesis

by

Kazufumi Takano

Submitted to

the Graduate School of Science,

Osaka University

February, 1998

Contribution of the Hydrophobic Effect to the Conformational Stability of a Protein

A Doctoral Thesis

by

Kazufumi Takano

Submitted to

the Graduate School of Science,

Osaka University

February, 1998

Approval

February, 1998

This thesis is approved as to
style and content by

月原富武

Member-in-Chief

森島淳太郎

Member

則末尚志

Member

油谷克英

Member

Acknowledgments

The present work has been carried out under the direction of Associate Professor Katsuhide Yutani of the Institute for Protein Research, Osaka University. I would like to thank him for his incessant guidance and encouragement throughout this work.

I would like to express my deepest thanks to Dr. Yuriko Yamagata, Osaka University, for her incessant encouragement and helpful advice to X-ray crystallography.

I am deeply indebted to Professor Satoshi Fujii, University of Shizuoka, for his technical advice and helpful suggestion to X-ray crystallography.

I wish sincere thanks to Professor Masakazu Kikuch, Ritsumeikan University, and Dr. Eiko Kanaya, Biomolecular Engineering Research Institute, for their technical advices and helpful suggestions on DNA mutagenesis, expression and purification of human lysozyme. I am also grateful to Dr. Motohisa Oobatake, Riken, for his technical suggestion on computational techniques.

I express my thank to Dr. Kyoko Ogasahara, Osaka University, Dr. Kaori Hiraga, Tokyo University of Pharmacy and Life Science, Mr. Hidetomo Kaneda, Osaka University, and Mr. Jun Funahashi, Osaka University, for their technical supports and useful discussions. I also grateful to Professor Nick Pace, Texas A&M University, Professor George Makhatadze, Texas Tech University, Dr. Allen P. Minton, National Institute of Health, and Dr. Ryota Kuroki, Kirin Brewery Co., Ltd., for their helpful advices and useful discussions.

I thank Takeda Chemical Ind., Ltd. for providing plasmid pGEL125 and Takara Shuzo Co., Ltd. for the mass spectrum measurements of the mutant proteins. The DNA sequence analysis, the numerical calculations on X-ray analysis and the diffraction data collections on X-ray analysis were in part carried out at the Research Center for Protein Engineering, Institute for Protein Research, Osaka University. This work was supported in part by Fellowships from the Japan Society for the Promotion of Science for Japanese Junior Scientists.

I wish to thank all members in the Division of Physical Chemistry, Institute for Protein Research, Osaka University, for their useful discussions and kind friendships.

Finally, I thank my wife, Eriko Takano, and my parents, Teruyoshi Takano and Natsuko Takano, for their incessant understanding and encouragement.

February, 1998

高野 和文

Kazufumi Takano

Contents

Abbreviations Used in This Thesis

3SS	mutant (C77A/C95A) human lysozyme lacking one disulfide bond
3SS mutants	mutants from 3SS human lysozyme
4SS	wild-type human lysozyme (with four disulfide bonds)
4SS mutants	mutants from wild-type human lysozyme
ASA	accessible surface area
B-factor	temperature factor
ΔC_p	heat capacity change between native and denatured states
$\Delta\Delta ASA_{HP}$	change in hydrophobic surface area exposed upon denaturation
ΔG	Gibbs energy change of denaturation
ΔG_{tr}	Gibbs energy change of transfer from organic solvents to water
ΔH	enthalpy change of denaturation
ΔS	entropy change of denaturation
DSC	differential scanning calorimetry
$E^{1\%}_{1cm}$	absorption coefficient (10 mg/ml, 1 cm)
r.m.s.	root mean square
T_d	denaturation temperature
R factor	$\Sigma \mid \mid F_o \mid - \mid F_c \mid \mid / \Sigma \mid F_o \mid$, where F_o and F_c are the observed and calculated structure factor amplitudes, respectively.
R_{merge}	$100 \times \Sigma \mid I_{hi} - \langle I_h \rangle \mid / \Sigma I_{hi}$, where I_{hi} is individual values and $\langle I_h \rangle$ is the mean intensity of the reflection h.

Chapter I

General Introduction

Conformational Stability of a Protein

Proteins are important components for all organisms and are composed of twenty kinds of amino acids. Necessary for their biological functions, proteins each fold to a unique tertiary structure, the "native" conformation, in appropriate solvent environments, depending on the amino acid sequence. These unique conformations support a diverse biological functions. We can now determine tertiary structures at atomic level by X-ray crystallographic analysis (Bernal, 1934; Green et al., 1954; Kendrew et al., 1958), and the unique structures of more than 400 proteins have been determined in order to understand how proteins function.

The native conformation of a protein is denatured by heat, acid or denaturants such as guanidine hydrochloride and urea. The denaturation means the unfolding of the tertiary structure. The denatured protein sometimes irreversibly aggregates, but it can be refolded to the original native conformation again by cooling or diluting the denaturants under appropriate conditions (Anfinsen, 1973). That is, protein denaturation is a reversible reaction according to the following equation.

$$N \Leftrightarrow D \quad (\Rightarrow \text{aggregation}) \tag{I-1}$$

Here, N and D indicate the native and denatured states of a protein, respectively. This equation shows that the protein is in a thermodynamic balance between the native and denatured states. In the energetics of protein denaturation, the conformational stability of a protein means the stability in the native state in Equation I-1 and is defined as the difference in energy between the native and denatured states, that is, the Gibbs energy change of

denaturation (ΔG). This energy change between the N and D states ($\Delta G = G_d - G_n$) is calculated by the following equations.

$$K = [D] / [N] \quad \text{(I-2)}$$

$$\Delta G = - R T \ln K \quad \text{(I-3)}$$

Here, K, [D], [N], R and T represent the equilibrium constant, the protein concentration in the D state, that in the N state, the gas constant and absolute temperature, respectively.

It has been known that the native conformation of a globular protein is stabilized by a Gibbs energy of about only 40 kJ/mol under physiological conditions (Privalov, 1979) resulting from comparatively large changes in both enthalpy and entropy (Brandts, 1964a). So, proteins are said to be marginally stable. This indicates that ΔG value might be remarkably affected if a single hydrogen bond in a protein, which is one of the factors stabilizing the protein conformation, is deleted. In fact, the stability of a mutant protein, in which a single amino acid is substituted, is considerably different from that of a wild-type protein (Yutani et al., 1977, 1987; Matsumura et al., 1988). These facts indicate that the study of the effect of amino acid substitutions on conformational stability can be a fruitful approach to understanding the role of amino acid sequences in protein folding and protein stability. Recent advances in molecular biology allow us to modify the gene of a protein virtually without limitations.

Hydrophobic Effect: A Major Factor Stabilizing the Conformation of a Protein

Hydrophobic effect, hydrogen bonding, and electrostatic interaction are mainly considered as factors stabilizing protein conformations.

Kauzmann (1959) was the first to point out that globular proteins are stabilized mainly by hydrophobic effects (hydrophobic bonding). The hydrophobic effect is described by the thermodynamics of the partitioning of non-polar compounds between water and a non-aqueous phase. The hallmarks of the hydrophobic effect are that the transfer of non-polar compounds into water at ambient temperature is unfavorable due to a decrease in entropy and is associated with a large increase in heat capacity. Tanford (1962) has developed the concept of hydrophobic effect in which the Gibbs energy of the transfer of amino acids from organic solvents to water (ΔG_{tr}) can be used to establish a hydrophobicity scale that is useful for estimating the contributions that buried residues make to the stability of proteins. It has been considered that the environment of an organic solvent can be a model of the interior of a folded protein, because 81 % of the non-polar residues (Ala, Val, Ile, Leu, Met, Phe, Trp and Cys) are buried in the interior of the molecule out of contact with water when the protein folds (Lesser & Rose, 1990). Tanford has then concluded that the stability of the native conformation of a protein in water can be explained entirely on the basis of the hydrophobic effects of the non-polar parts in the molecule. Brandts (1964a, b) has supported the importance of hydrophobic interaction for protein stability by showing that the large excess heat capacity observed for protein denaturation is mainly due to the exposure of non-polar groups.

Mutational analyses have also confirmed that hydrophobic effect is a

stabilizing factor for protein conformations (Yutani et al., 1987; Matsumura et al., 1988). For example, the substitution of Leu with Ala which makes a cavity in the core of T4 lysozyme decreases the stability of the mutant protein (Eriksson et al., 1992), and the substitution of Val with Ile which fills up a cavity in the RNase HI increases the stability (Ishikawa et al., 1993), suggesting that a hydrophobic residue in the interior of a protein contributes toward raising the protein stability.

The hydrophobic scales (ΔG_{tr}) for amino acid side-chains based on the solubility in ethanol and dioxane (Nozaki & Tanford, 1971), *n*-octanol (Fauchere & Pliska, 1974), *N*-methylacetamide (Damodaran & Song, 1986), and cyclohexane (Radzicka & Wolfenden, 1988) have been published. Chothia (1974) has found a linear relationship between Nozaki & Tanford's hydrophobic scale (1971) and the solvent accessible surface area of amino acid side-chains, with a slope of 0.10 kJ/mol Å^2. Pace (1992) has argued on the basis of the data for hydrophobic mutant proteins that the ΔG_{tr} values of *n*-octanol are reasonable for estimating the contribution of the hydrophobic effect to protein stability on an average.

However, even for the same kind of hydrophobic residues, the substitution effect on protein stability is different, depending on the difference in environment surrounding the substitution residue and the structural change due to mutation. For instance, the changes in denaturation Gibbs energy change ($\Delta\Delta G$) for nine different Ile with Val substitutions relative to the wild-type protein ranged from -2.1 to -7.5 kJ/mol (Matthews, 1993). At present, there is no precise estimation of the energetics of the hydrophobic residues stabilizing the protein conformation in various environments because of the lack of sufficient data. It would be expected to

determine exactly how much each hydrophobic residue in the various environments in a tertiary structure contributes to protein stability in order to explain the role of amino acid residues in the conformational stability of a protein. Therefore, it is necessary to accumulate accurate experimental information on the correlation of the stability change due to mutation with the environment of the mutation site and the structural change due to the mutation. The analyses of stability and structure for systematic and comprehensive mutant proteins will provide the answer. Furthermore, the quantitative estimation of the hydrophobic effect on protein stability may allow us to estimate other stabilizing factors.

In recognition of these facts, the contribution of the hydrophobic effect, which is a dominant stabilizing factor, to protein stability was investigated using systematic mutant human lysozymes as a model system by both thermodynamic and structural analyses in this thesis.

Differential Scanning Calorimetry of a Protein

In the process of ordering and disordering under equilibrium conditions, the conformational stability of a protein, the Gibbs energy change of denaturation (ΔG), can be estimated by differential scanning calorimetry (DSC) (Privalov & Khechinashvili, 1974; Becktel & Schellman, 1987), or by analyses of heat or denaturant denaturation curves of a protein using spectroscopic techniques (Hawkers et al., 1984; Pace, 1986). The exact thermodynamic parameters, Gibbs energy change (ΔG), enthalpy change (ΔH), and entropy change (ΔS), of denaturation are directly obtained only from the measurement of adiabatic DSC (Privalov, 1974; Privalov & Potekhin, 1986). The recent developments in sensitive calorimeters have allowed reliable measurement of the energetics for the denaturation process of a protein (Privalov & Khechinashvili, 1974; Privalov et al., 1995; Plotnikov et al., 1997). With this technique, the heat capacity of a protein solution can be measured during heating at a constant rate. The excess heat capacities are accompanied by denaturation of a protein. The denaturation temperature (T_d), calorimetric enthalpy change (ΔH_{cal}), van't Hoff enthalpy change (ΔH_{vH}) and heat capacity change (ΔC_p) of denaturation can be directly obtained from analysis of the DSC curve, as shown in Figure I-1. The temperature functions of the thermodynamic parameters of denaturation can be calculated using the following equations.

$$\Delta H(T) = \Delta H(T_d) - \Delta C_p \, (\, T_d - T \,) \qquad \text{(I-4)}$$

$$\Delta S(T) = \Delta H(T_d) \, / \, T_d - \Delta C_p \ln (\, T_d \, / \, T \,) \qquad \text{(I-5)}$$

$$\Delta G(T) = \Delta H(T) - T \, \Delta S(T) \qquad \text{(I-6)}$$

where ΔC_p is assumed to be independent of temperature (Privalov & Khechinashvili, 1974). DSC measurements should allow us to investigate the thermodynamic parameters for the denaturation of a protein.

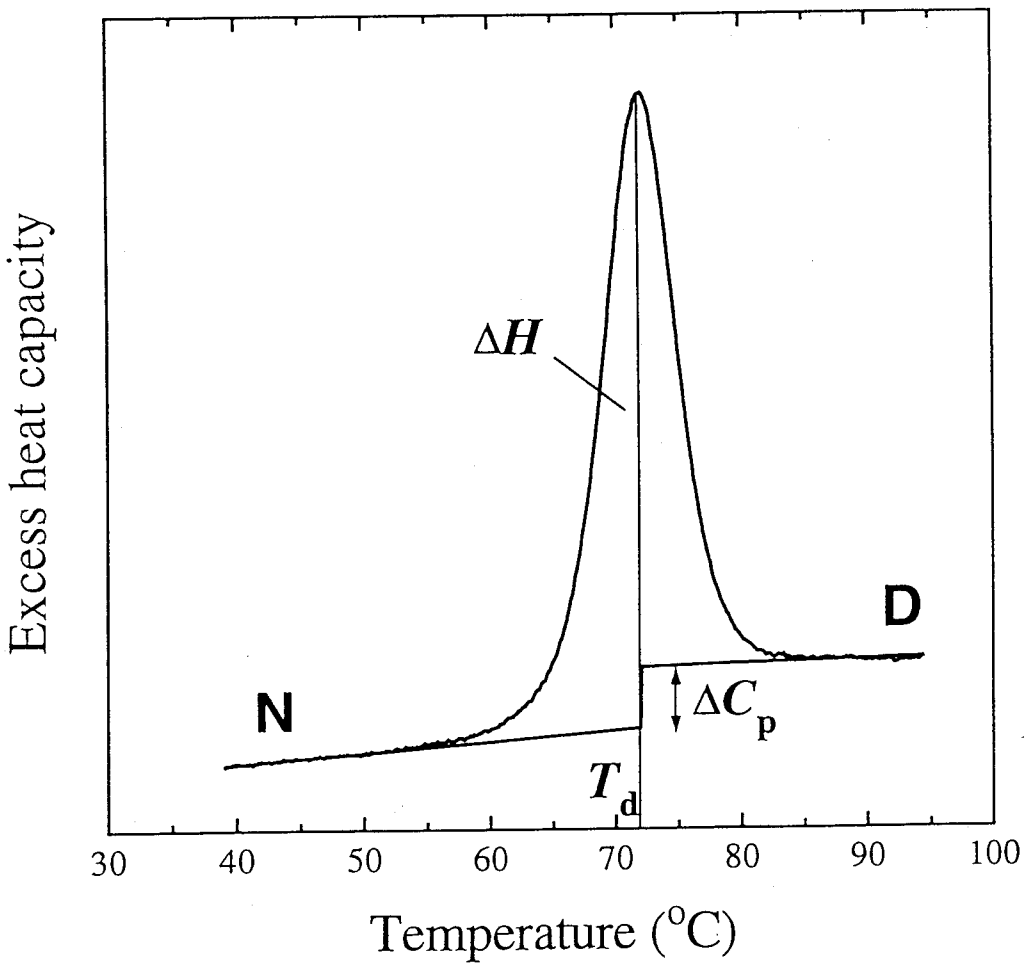

Figure I-1. Typical excess heat capacity curve of a protein.

Structural Analysis of a Mutant Protein

The native structure of a protein can be determined by X-ray crystallography (Bernal, 1934; Green et al., 1954; Kendrew et al., 1958), nuclear magnetic resonance (NMR) (Braun et al., 1983; Driscoll et al., 1990; Ikura et al., 1991), and electron microscopy (Henderson et al., 1990; Stokes & Green, 1990). We need information about native structures at atomic level resolution in order to detect the effects of mutations on the structures.

X-ray crystal structure analysis is the best way to determine the tertiary structure of a protein at atomic resolution. It is becoming a more splendid technique due to remarkable advances in X-ray detectors such as the imaging plate (Miyahara et al., 1986), techniques using synchrotron radiation as the X-ray source (Moffat et al., 1984; Hajdu et al., 1987; Sakabe, 1991), cryogenic techniques (Nakasako et al., 1995), and computational techniques (Jones, 1978; Brunger, 1992; Otwinowski, 1993). For analysis of a mutant structure which is similar to the wild-type one, molecular replacement using the wild-type structure can be utilized as a model without solving the phase problem with some heavy atom derivatives (Green et al., 1954; Blow & Crick, 1959; Rossmann & Blow, 1962; Crowther & Blow, 1967). Thus, we expect to be able to determine many structures of mutant proteins at high resolution if crystals of high quality, sufficient size, small mosaicity, and high stability under X-ray irradiation are obtained. High resolution structural analysis of a mutant protein from X-ray crystallography will provide important information on the energetics which maintain the tertiary structure. X-ray analysis has to reveal the crystal structure of a protein at more than 2.0 Å resolution, because the structure changes due to mutation are small in many cases (Matthews, 1995).

Human Lysozyme: A Model Protein for the Study of Protein Stability

The thermal properties of globular proteins, such as RNase A, hen egg white lysozyme, chymotrypsin, cytochrome *c*, and myoglobin have been well investigated by differential scanning calorimetry (Privalov & Khechinashvili, 1974). These proteins have the following advantages for us. Their structures are known, their thermal unfoldings are reversible, and their refined samples can be easily obtained. The stability of mutant proteins have been studied on a tryptophan synthase α subunit (Yutani et al., 1977, 1987; Hiraga & Yutani, 1996), T4 lysozyme (Matsumura et al., 1988; Eriksson et al., 1992, 1993), barnase (Kellis et al., 1988; Serrano et al., 1992), and staphylococcal nuclease (Shortle et al., 1990). These proteins can be produced by virtually any type of mutant at a specifically targeted residue using site-directed mutagenesis, but they have some defects in structural analysis or reversibility of thermal denaturation. Recent DSC experiments for mutant human lysozymes (Kuroki et al., 1992a, 1992b; Herning et al., 1992a) have thermodynamically analyzed the stabilizing factors of the proteins. These results, combined with X-ray analysis, play an important role in interpreting the stabilizing mechanism of the protein. Human lysozyme has a high reversibility of the unfolding and coordinate at high resolution of the native structure. This protein is the best candidate as a model to study the role of an amino acid sequence in protein stability.

Lysozyme is a ubiquitous enzyme defined as muraminidase catalyzing the hydrolysis of the β (1-4)glycosidic bond in bacterial peptidoglycan, a major component of the bacterial cell wall (Phillips, 1966). Several different types of lysozyme from different species have been characterized, and the complete amino acid sequences have been determined. Human lysozyme is

widely distributed in several human tissues and secretions including milk, tears, and saliva (Peters et al., 1989). It is composed of 130 amino acid residues with four disulfide bonds, and its crystal structure has been determined at 1.5 Å resolution (Artymiuk & Blake, 1981). It is an $\alpha + \beta$ protein with five α-helices and five β-sheets and consists of two domains. The active site is located in the cleft between the domains. The expression system of human lysozyme on yeast, *Saccharomyces cerevisiae*, has been constructed (Yoshimura et al., 1987; Yamamoto et al., 1987; Kikuchi & Ikehara, 1994), and mutant proteins of human lysozyme can be made in principle. The structures of more than ten mutant human lysozymes have been reported (Inaka et al., 1991a, 1991b; Herning et al., 1992a; Kuroki et al., 1992a; Muraki et al., 1992, 1997; Funahashi et al., 1996; Booth et al., 1997). Human lysozyme and its mutants have also been used in studies of the folding process (Herning et al., 1992b; Taniyama et al., 1992), of the secretion and folding mechanism in vivo (Taniyama et al., 1988, 1990; Kanaya & Kikuchi, 1992), and the normal mode refinement of crystal analysis (Kidera et al., 1992, 1994). Recently, amyloidogenic mutant human lysozymes have been attractive as a model of protein misfolding (Pepys et al., 1993; Funahashi et al., 1996; Booth et al., 1997).

Situation of This Thesis in Life Science Research

As described before, a denatured protein can be spontaneously refolded to its native conformation. This fact indicates that the amino acid sequence directs the unique native conformation of the protein. Therefore, if the rules for the relationship between the primary structures (amino acid sequences) and the tertiary structures of proteins, that is "structural principles of protein architecture" are revealed, we are able to predict the tertiary structure from a sequence, and the function from the structure predicted. Moreover, a protein designed with a new function can be constructed. However, this subject has not been achieved, because a protein structure is prescribed not only by a part of the amino acid sequence but also by an extensive interaction (Minor & Kim, 1996). The understanding of these principles is one of the main problems in modern life science research (Gros & Tocchini-Valentin, 1994).

Chothia (1992) has presumed that the basic conformations of proteins are only about 1000 based on a statistical estimation. This brings about the probability of accomplishment of the subject, clarifying the principles of protein architecture. That is, if there is information on all the basic conformations and accurate parameters of energetics for the stabilizing factors of the structures, we can determine which basic conformation is optimal for a sequence (Bowie et al., 1990, 1991). The tertiary structures deposited into protein data bank (PDB) have increased at a surprising rate in the last few years. In contrast, the studies on the energetics of protein conformation have had unsatisfactory progress. Thus, gathering data on the energetics basis of protein conformation is expected.

Purpose and Outline of This Thesis

The final goal of this thesis is elucidation of the principle of how the tertiary and quaternary structures of proteins are coded for in their amino acid sequences. In the present study, we tried to establish a general rule for the relationship between the hydrophobic effect and the conformational stability of a protein using the thermodynamic and structural analyses of a series of mutant proteins, because the hydrophobic effect is the main factor in protein stability.

We focused on hydrophobic mutations in which a larger side-chain is replaced by a smaller one so that steric effects due to mutation are minimal, that is, substitutions from Ile to Val, from Ile to Ala, from Ile to Gly, and from Val to Ala. Human lysozyme contains five Ile and nine Val residues out of 130 residues. In order to elucidate the contribution of hydrophobic residues to the protein stability, the five Ile to Val, nine Val to Ala, five Ile to Ala and two Ile to Gly mutants of the wild-type human lysozyme, and the five Ile to Val and nine Val to Ala mutants of the 3SS (C77A/C95A) human lysozyme, a total of 35 hydrophobic mutants, were constructed. The thermodynamic parameters of denaturation and the crystal structures for the wild-type and these mutant proteins were determined by differential scanning calorimetry and X-ray structural analysis at high resolution, respectively.

In **Chapter II**, the results for wild-type and five mutant proteins from Ile to Val are presented. The thermodynamic results were discussed in light of the high resolution structures.

In **Chapter III**, a correlation between the changes in the stability and the structural features of the mutant proteins was examined using the results of nine mutants from Val to Ala including those of five mutants from Ile to

Val. We found a new correlation between the changes in the stability ($\Delta\Delta G$) and the changes in hydrophobic surface area of all of the hydrophobic residues exposed upon denaturation ($\Delta\Delta ASA_{HP}$) by considering the effect of secondary structural propensity.

In **Chapter IV**, the relationship obtained in Chapter III was applied to the cases of five substitutions of Ile with Ala and two substitutions of Ile with Gly. With this correlation, the contribution of water molecules in the interior of a protein to the conformational stability is represented.

In **Chapter V**, the correlation between $\Delta\Delta G$ and $\Delta\Delta ASA_{HP}$ was tested for its generality using the five substitutions of Ile with Val and nine substitutions of Val with Ala of a greatly perturbed mutant human lysozyme, the 3SS human lysozyme. The 3SS human lysozyme lacks a disulfide bond and is largely destabilized compared with the wild-type protein. The results indicate that changes in ASA (the accessible surface area) value of the hydrophobic residues due to the mutation of globular proteins correspond to changes in conformational stability of about 0.1 kJ/mol $Å^2$.

Chapter VI summarizes the main results and conclusions obtained in this work.

The successive chapters, II to V, correspond to each paper listed at the end of this thesis, [1] to [4], respectively.

Chapter II

Studies on the Five Val Substitutions for Ile of Human Lysozyme*

Introduction

As mentioned in Chapter I, the hydrophobic effect is the major factor stabilizing the conformation of a protein. Studies of the contribution of hydrophobic residues to the protein stability at a single site in a protein have shown a correlation between the stabilities of the mutant proteins and the hydrophobicities of the substituted residues (Yutani et al., 1977, 1987; Matsumura et al., 1988). In addition, other systematic mutational analyses of hydrophobic amino acid residues in proteins have made the same substitutions, such as Ile → Val or Val → Ala at different sites (Kellis et al., 1989; Shortle et al., 1990; Eriksson et al., 1992). For example, nine different Ile to Val substitutions are associated with denaturation Gibbs energy changes that range from 2.1 to 7.5 kJ/mol (Matthews. 1993). The changes in stability might be due to differences in the environment surrounding the residue at various positions, as they cannot result from differences in the hydrophobicity of the side-chain.

Eriksson et al. (1992) have found that the decrease in the denaturation Gibbs energy of phage T4 lysozyme, for a Leu to Ala mutation at different positions, consists of a constant part, from the difference in the hydrophobicity of the side-chain, plus a variable part that depends on the size of the cavity created by the substitution. The constant term agrees with the difference (7.9 kJ/mol) in the hydrophobicity between Leu and Ala estimated

---

* This work is published, titled "Contribution of Hydrophobic Residues to the Stability of Human Lysozyme: Calorimetric Studies and X-ray Structural Analysis of the Five Isoleucine to Valine Mutants" (Takano et al., 1995).

by transfer from water to octanol. This seemed to be a successful way to reconcile a number of conflicting reports concerning the strength of the hydrophobic effect of proteins (Matthews, 1993), in which the hydrophobic values obtained by solvent transfer experiments were different from the differences in the stabilities of the hydrophobic mutant proteins. In the case of mutations in the hydrophobic core of barnase, however, such a correlation between the size of the cavity created by the substitution and the decrease in the denaturation Gibbs energy has not been seen (Buckle et al., 1993). This suggests that more data is needed to precisely describe the differences in the environment surrounding the substituted residues, in order to elucidate the role of hydrophobic residues in the stability of a protein.

Most point mutations are likely to induce relatively small changes in protein stability. Therefore, it is necessary to determine very accurately various thermodynamic parameters for the denaturation of a protein. The most direct and accurate way to determine these parameters is provided by the adiabatic differential scanning calorimetry technique (Privalov & Khechinashvili, 1974). By this technique, we can directly obtain thermodynamic parameters, such as the denaturation temperature (T_d), the denaturation enthalpy change (ΔH), and the denaturation heat capacity change (ΔC_p) of a protein. From these values, all of the thermodynamic parameters in the denaturation of a protein at a given temperature (T, Kelvin) can be calculated using Equations I-4 to I-6.

In our laboratory, we have reported calorimetric studies of mutant human lysozymes that substitute Pro (Herning et al., 1992), lack a disulfide bridge (Kuroki et al., 1992a), and create a calcium binding site (Kuroki et al., 1992b). Since they are combined with an X-ray structure analysis of each

mutant protein, we could explain the thermodynamic parameters of the denaturation of the proteins, taking into account their environment in the protein structure (Oobatake & Ooi, 1993). In this chapter, we focus on substitutions of Ile by Val, which result in the deletion of a methylene group.

Human lysozyme is an $\alpha + \beta$ protein with five α-helices and five β-strands, and consists of two domains (Artymiuk & Blake, 1981). The active site is located in the cleft positioned between the two domains. The belt consisting of the hydrophobic core lies in the interior of the protein, with a V shape through the two domains, as shown in Figure II-1. Five Ile residues in the protein are included in the belt of the hydrophobic core. Ile23 and Ile106 are located at the edge of the hydrophobic belt. Ile56 and Ile89 face each other at the bend of the V shape, connected to Ile59 through Phe57. All of the mutated residues are buried in the interior of the molecule and have small solvent accessible surface areas (ASA) (Table II-6). A large cavity, which includes internal water molecules, exists in the hydrophobic belt.

The thermodynamic parameters for the denaturation of the five Ile mutants were determined by scanning calorimetry and their three-dimensional structures were solved at high resolution by X-ray crystallography. The thermodynamic results are discussed in light of the high resolution X-ray structures of the five Ile mutants of human lysozyme.

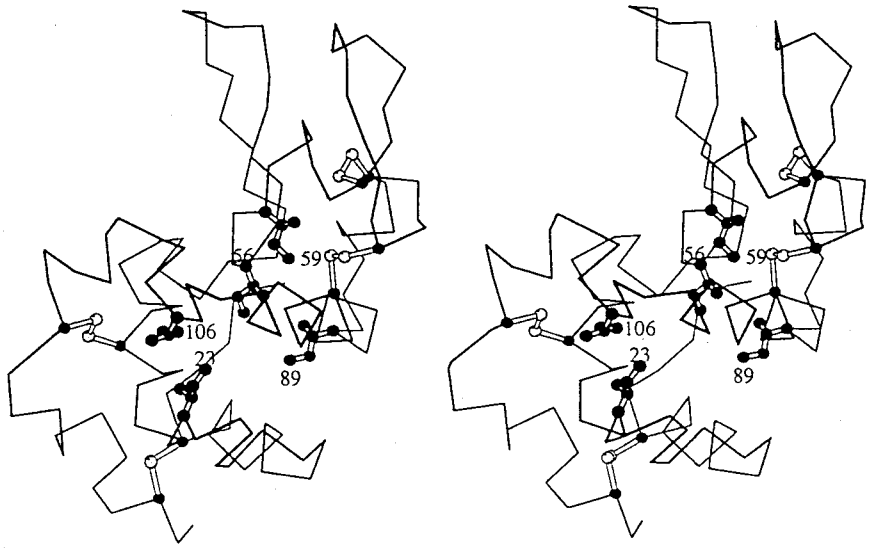

Figure II-1. Stereo drawing of the wild-type human lysozyme structure. The positions of the substituted Ile residues are indicated. This was generated by the program MOLSCRIPT (Kraulis, 1991). The open circles represent sulfur atoms of disulfide bonds.

Materials and Methods

Materials

Human lysozyme from the sputum duct was purchased from Elastin Products Company. For purification, the lysozyme was applied to an Asahipak ES-502C column, and was eluted with a linear gradient of 0 M to 0.36 M Na_2SO_4 in 50 mM sodium-phosphate buffer (pH 6.5). The main active fraction was collected.

Mutagenesis was performed by the polymerase chain reaction (PCR) to obtain the five mutant human lysozymes in which the Ile residues at positions 23, 56, 59, 89, and 106 were replaced by Val. The genes encoding the signal sequence and the mutated human lysozyme were combined with the large *Xho*I-*Sma*I fragment from pERI8602 (Taniyama et al., 1988) to construct the expression plasmids. *Saccharomyces cerevisiae* AH22R$^-$ (Miyanohara et al., 1983) was used for the host strain, and was cultivated in modified Burkholder minimal medium (Toh-e et al., 1973) supplemented with 8 % (w/v) sucrose. Secreted mutant human lysozymes were purified as described by Kikuchi et al. (1988).

The purified wild-type and mutant human lysozymes were dialyzed extensively against distilled water, and were lyophilized for storage. All other chemicals were reagent grade.

Differential scanning calorimetry (DSC)

Calorimetric measurements were carried out with a DASM4 adiabatic microcalorimeter equipped with an NEC personal computer. The scan rate was 1.0 K/min. This system is the same as that reported by Yutani et al.

(1991). Sample solutions for DSC measurements were prepared by dissolving the lysozyme in 0.05 M glycine buffer between pH 2.4 and 3.2. The lysozyme concentrations were 0.7 to 1.5 mg/ml. The concentrations of the protein solutions were determined spectrophotometrically using $E^{1\%}_{1cm}$ = 25.65 at 280 nm for human lysozyme (Parry et al., 1969) and its mutants. Data analysis was done using the Origin software (MicroCal Inc., Northampton, MA).

X-ray crystallography

Crystals of the wild-type and all mutant proteins were obtained using the hanging drop vapor diffusion method. Typically, a 10 mg/ml protein solution (2 μl) was mixed in a 1:1 ratio with the crystallization reservoir solution (2.5 M NaCl, 20 mM acetate, pH 4.5). Suitably sized (> 0.2 mm x 0.2 mm x 0.5 mm) rod-shaped crystals grew at 10 °C in one to four weeks. As the exceptional case, X-ray quality crystals of I23V could be grown by macroseeding. All of the crystals of the mutant proteins are isomorphous with our wild-type crystals (Table II-3).

Diffraction data were collected at 10 °C by the oscillation method on a Rigaku R-AXIS IIC imaging plate mounted on a Rigaku RU300 rotating anode X-ray generator (CuK_α, radiation, 40 kV 200 mA). The crystal-to-detector distance and the exposure times were 60 mm and 30 to 40 minutes, respectively, for 1.5° oscillation. The data to 1.58 Å resolution were processed with the software provided by Rigaku (Table II-3). The data below 1.8 Å resolution were excluded from the refinements, due to their low accuracy and high R_{merge} values of ca 15 %.

The crystal structure of the wild-type human lysozyme has been refined at 1.5 Å resolution (Artymiuk & Blake, 1981), but the parameters for the solvent molecules have not been deposited in the Protein Data Bank (data set name: 1LZ1). Furthermore, the unit cell dimensions of our mutant and wild-type proteins significantly differed from the published dimensions (a = 57.13, b = 60.99, c = 32.87 Å). Therefore, we independently refined the crystal structure of the wild-type protein to use in the comparison between the wild-type and mutant structures. Of the wild-type and mutant proteins, all the crystals belong to the space group $P2_12_12_1$. All refinements were performed using the program X-PLOR (Brunger, 1992). The procedures are as follows: (1) positional refinement as a rigid body using the coordinates of the wild-type structures (1LZ1 for the wild-type structure and our wild-type model for the mutant proteins), (2) restrained least-squares refinement of all atomic positions, (3) restrained least-squares refinement of the thermal parameters, (4) detection of solvent molecules using the program FLAPPER (Fujii, S., unpublished), (5) repeating (2) to (4). The criteria for selecting the solvent molecules were to have hydrogen-bonding geometry contacts of 2.4 to 3.5 Å (except for one peak assigned as a Na^+, which binds to carbonyl oxygen and water molecules with contacts of 2.1 to 2.3 Å) with protein atoms or with existing solvent, excluding contacts to carbon atoms within 3.2 Å, to have temperature factors less than 50 $Å^2$, and to have electron densities more than the 2.5 σ level in F_o - F_c maps. All numerical calculations were carried out on NEC engineering workstations at the Research Center for Protein Engineering, Institute for Protein Research, Osaka University.

The coordinates of the five mutant human lysozymes, I106V, I23V, I56V, I59V and I89V, have been deposited in the Brookhaven Protein Data Bank, accession nos, 1YAM to 1YAQ.

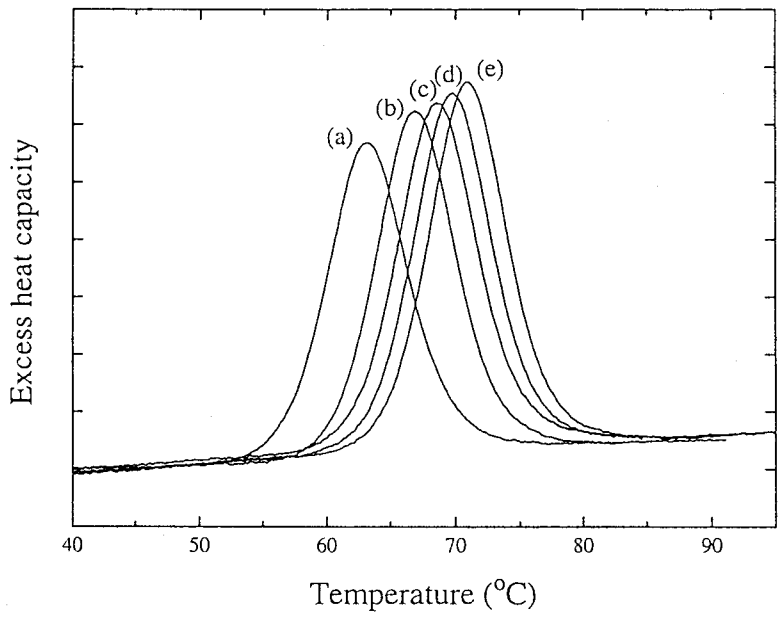

Figure II-2. Typical excess heat capacity curves of the mutant human lysozyme (I106V) at pH 2.70 (a), 2.92 (b), 3.04 (c), 3.10 (d), and 3.14 (e). The increments of excess heat capacity were 10 kJ/mol K.

Results

Differential scanning calorimetries of the wild-type and mutant human lysozymes

In order to evaluate the contribution of the amino acid substitutions to the conformational stability, we determined the thermodynamic parameters for the denaturation of the wild-type and Ile mutant human lysozymes using a differential scanning calorimeter. Figure II-2 shows typical excess heat capacity curves resulting from calorimetric recordings of the mutant human lysozyme (I106V) at acidic pHs (pH 2.70 to 3.14). Each protein considered in this study gave an excess heat capacity curve with similar characteristics. The acidic pH region was chosen because of the high reversibility of the thermal denaturation of the mutant proteins, as well as the wild-type protein. The denaturation temperature (T_d), the denaturation enthalpy changes (calorimetric (ΔH_{cal}) and van't Hoff (ΔH_{vH}) enthalpy changes), and the denaturation heat capacity change (ΔC_p) were obtained directly from analyses of the heat capacity curves (Table II-1). The data for the wild-type protein, which were obtained in this study to compare with those of the mutant proteins, agree with those reported previously (Kuroki et al., 1992b). The denaturation temperatures decreased linearly with decreasing pH, in the pH range from 2.4 to 3.2, for all the mutant and the wild-type human lysozymes (Figure II-3(a) to (f)). The T_d values of the mutant proteins were lower than those of the wild-type protein at the measured pHs. The decreases in T_d among the mutant proteins were different from each other, in spite of the same kind of substitution. Figure II-4(a) to (f) shows the temperature

dependence of the calorimetric enthalpies of the wild-type and the mutant proteins examined at different pHs. The slopes of the mutant proteins, I23V, I56V, and I106V, were similar to that of the wild-type one, but those of the other two mutant proteins, I89V and I59V, are different. These results indicate that ΔC_p was affected by different magnitudes by the same kind of substitution. Each slope coincided with the average of ΔC_p obtained from the excess heat capacity curves, within experimental errors.

The thermodynamic parameters of denaturation as a function of temperature can be calculated using Equations I-4 to I-6. We could obtain the most reliable thermodynamic parameters at 64.9 °C, because many experimental data with high accuracy for all the mutant proteins are available near 65 °C. Table II-2 shows the denaturation thermodynamic parameters of the five mutant and the wild-type proteins at the same temperature, 64.9 °C, which is the denaturation temperature of the wild-type protein at pH 2.7. These results show the following. (1) The stabilities (T_d and $\Delta\Delta G$) of all the mutant proteins decreased as compared with that of the wild-type protein. (2) The calorimetric enthalpy changes ranged from 457 to 484 kJ/mol. (3) The changes in ΔH were bigger than those in ΔG and were compensated by ΔS.

Table II-1. Thermodynamic parameters for denaturation of wild-type and Ile to Val mutant human lysozymes at different pHs.

	pH	T_d (°C)	ΔH_{cal} (kJ/mol)	ΔH_{vH} (kJ/mol)	ratio $\Delta H_{cal}/\Delta H_{vH}$	ΔC_p[a] (kJ/mol K)
Wild-type	3.02	70.1	515	536	0.96	7.4
	2.88	67.6	490	510	0.96	7.7
	2.72	65.6	481	502	0.96	4.9
	2.71	65.4	485	506	0.96	6.7
	2.71	65.3	481	506	0.95	6.7
	2.53	61.3	452	473	0.96	5.4
	2.46	61.4	456	481	0.95	6.7
					0.96	6.5 ± 1.1
I23V	2.90	67.5	477	519	0.92	6.9
	2.70	63.7	473	502	0.94	3.2
	2.53	60.3	444	481	0.92	6.3
	2.46	59.8	431	464	0.93	4.7
					0.93	5.3 ± 2.0
I56V	3.03	67.5	498	506	0.98	4.8
	2.88	64.4	460	485	0.95	4.0
	2.70	61.7	469	485	0.97	4.4
	2.69	61.5	444	481	0.92	6.6
	2.66	60.6	444	464	0.95	6.6
	2.53	57.9	444	464	0.95	7.4
					0.95	5.6 ± 1.6
I59V	3.03	67.4	469	502	0.93	4.6
	2.88	64.4	460	481	0.96	4.0
	2.71	61.3	435	464	0.94	5.6
	2.70	61.9	456	477	0.96	4.6
	2.66	60.6	435	473	0.92	4.8
	2.46	57.7	423	444	0.95	3.7
					0.94	4.6 ± 0.8
I89V	3.14	72.0	540	565	0.96	6.0
	3.14	71.7	536	561	0.96	6.7
	2.92	67.9	510	544	0.94	6.8
	2.71	62.9	464	485	0.96	8.4
	2.46	59.4	439	469	0.94	5.1
					0.95	6.7 ± 1.4
I106V	3.14	71.3	510	510	1.00	5.6
	3.14	71.1	494	515	0.96	5.9
	3.14	71.0	494	506	0.98	4.8
	3.10	69.8	477	506	0.94	6.0
	3.04	68.7	469	494	0.95	6.5
	2.92	67.0	464	494	0.94	5.5
	2.85	65.5	469	481	0.97	6.0
	2.70	63.2	452	460	0.98	4.8
	2.61	60.6	444	452	0.98	4.4
	2.46	58.3	410	427	0.96	3.4
					0.97	5.3 ± 1.0

[a] ΔC_p was obtained from each calorimetric curve.

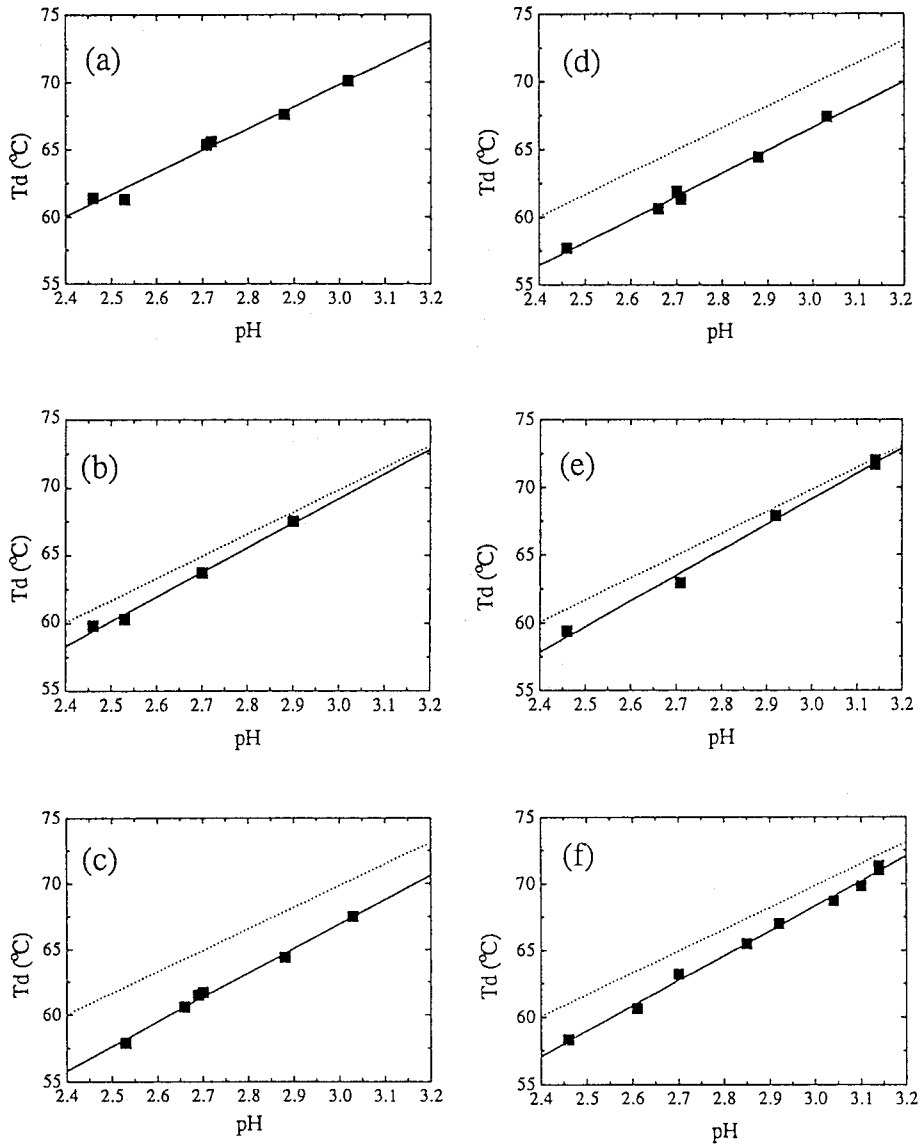

Figure II-3. The denaturation temperature versus pH. The continuous line in each Figure shows a linear regression of calorimetric results obtained at different pHs for the wild-type and the five mutant human lysozymes in Table II-1. The dotted lines of the wild-type protein in (b) to (f) are depicted for comparison. Figures (a) to (f) represent the wild-type protein, I23V, I56V, I59V, I89V, and I106V, respectively.

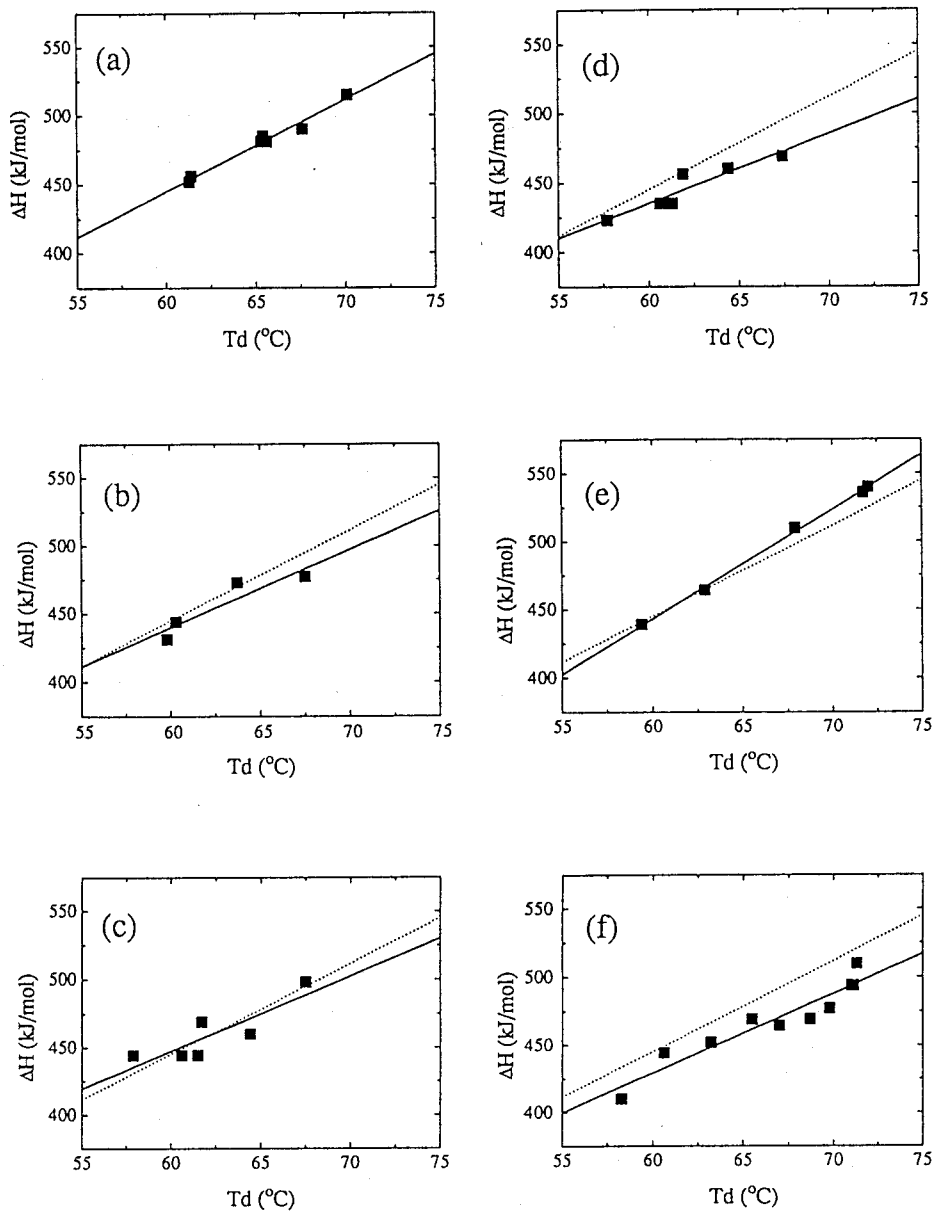

Figure II-4. The calorimetric enthalpy change as a function of the denaturation temperature. The continuous line in each figure shows a linear regression of results for the wild-type and the five mutant human lysozymes as shown in Table II-1. The dotted lines of the wild-type protein in (b) to (f) are depicted for comparison. Figures (a) to (f) represent the wild-type protein, I23V, I56V, I59V, I89V, and I106V, respectively.

Table II-2. Thermodynamic parameters for denaturation of Ile to Val mutant human lysozymes at the denaturation temperature (64.9 °C) of the wild-type protein at pH2.7.

	T_d (°C)	ΔT_d (°C)	ΔC_p[a] (kJ/mol K)	ΔH_{cal} (kJ/mol)	$\Delta\Delta G$ (kJ/mol)	$\Delta H_{cal}/\Delta H_{vH}$
Wild-type	64.9 ± 0.5		6.6 ± 0.5	477 ± 4	(0)	0.95
I23V	63.8 ± 0.4	-1.1	5.8 ± 1.8	468 ± 11	-1.5 ± 0.4	0.93
I56V	61.3 ± 0.3	-3.6	5.6 ± 1.7	475 ± 13	-5.0 ± 0.4	0.97
I59V	61.5 ± 0.4	-3.4	5.0 ± 1.0	461 ± 7	-4.6 ± 0.4	0.94
I89V	63.5 ± 0.6	-1.4	8.0 ± 0.3	484 ± 3	-2.0 ± 0.8	0.95
I106V	62.7 ± 0.3	-2.2	5.9 ± 0.7	457 ± 10	-3.0 ± 0.4	0.96

[a] ΔC_p was obtained from the slope of ΔH against T_d (Figure II-4).

X-ray structures of the mutant human lysozymes

Data collection and refinement statistics for the wild-type and the five mutant human lysozymes are summarized in Table II-3. The overall X-ray structures of the examined mutant proteins were essentially identical to that of the wild-type structure. The r.m.s. deviations for the main-chain atoms between the wild-type and each mutant are 0.09 to 0.14 Å, as shown in Table II-4. These values are somewhat smaller than the experimental error and the difference between the wild-type structures (PDB data, 1LZ1 and our model) independently crystallized and refined. The coordinate error of each structure was estimated to be about 0.2 Å from the Luzzati plot (1952). To better understand the errors in our structures, two kinds of I59V mutant structures were refined using two different crystals. The r.m.s. deviations for all atoms, backbone atoms, and atoms within 6 Å from the Val at position 59, between these structures are 0.18 Å, 0.07 Å, and 0.07 Å, respectively. The differences in the average *B*-factors of the main-chain atoms and the side-chain atoms between the wild-type and mutant structures are in good agreement, within 1.4 $Å^2$ and 1.6 $Å^2$, respectively (Table II-3). In sum, all of the structures were equally refined, and they are highly accurate.

The crystal structures in the vicinity of the respective mutation sites are shown in Figure II-5. The r.m.s. deviations between the wild-type and mutant structures for the atoms within a sphere of 6.0 Å from the $C^{\delta 1}$ atom in the methyl group of Ile in the wild-type protein are listed in Table II-4. To examine the conformational change around each mutation site, the r.m.s. deviations are compared with those around other hydrophobic cores in Table II-4, and indicate that all the values around the mutation sites were bigger than those around the other sites, especially in I59V.

Two interesting examples were provided by I56V and I59V, which have the smaller side-chain solvent-accessible surface areas at the mutation sites and larger denaturation Gibbs energy changes. The I59V mutant adopts the largest structural change of all mutant structures, and some prominent characteristic features are observed. First, a newly bound water molecule appeared in the cavity created by the Ile Val mutation. The new water is fixed by two hydrogen bonds with the carbonyl oxygen of Ala92 and one of the internal waters found in the wild-type and mutant crystal structures. The *B*-factor of the newly bound water is 24.0 $Å^2$ which is smaller than the averaged value (36.5 $Å^2$) of the solvent molecules. To our knowledge, this is the first example in which a cavity created by the replacement of a bulky hydrophobic residue with a smaller residue contains a solvent molecule. Matsumura et al. (1988) have found a water molecule in the cavity created by the rotational change of the Tyr side-chain substituted at Ile3 of T4 phage lysozyme. In this case, the side-chain of Tyr is not located in the original hydrophobic core, but is largely exposed to the solvent. Second, the side-chain conformation around the C^{α}-C^{β} bond of Val59 was quite different from the corresponding one of the parent Ile residue. Ile59 in the wild-type human lysozyme has the gauche$^-$ conformation (χ_1 angle, -67°). However, the conformation of Val59 is gauche$^+$ (χ_1 angle, 53°; see Table II-5). Third, the main-chain atoms of Val59 moved by 0.3 to 0.5 Å as compared to the shift of 0.16 Å found in the other Val substitution. A shift of the main-chain atoms is also observed in residues Gly55 and Ala42, which are connected by hydrogen bonding in the β-sheet. As a result, it is somewhat surprising that the hydrogen bond distance in the β-sheet is not changed. The *B*-factors do not vary significantly from those of the wild-type protein.

In contrast, when Ile56 was replaced by Val, the movements of the surrounding atoms were smaller than those of the other mutants. The maximal shift in the vicinity of Val56 is only 0.23 Å for the $C^{\varepsilon 2}$ atom of Phe57. The movement tends to shift toward the cavity formed by the mutation. The bound water molecules that are neighboring position 56 in the wild-type structure do not move in response to this mutation.

Mutation of Ile89, which faces Ile56, to Val caused movement resembling the case of I56V. The $C^{\delta 2}$ atom of Leu12 moves by 0.31 Å. The maximal movement of the main-chain atoms occurs in the C-terminal residue Val130, as also observed in I106V. In the case of I23V, movements were observed in the loop region (residues 99 to 105) facing positron 23, rather than in the vicinity of residue 23. The largest backbone shift, 1.0 Å, is in the oxygen atom of Pro103. The B-factors of the atoms in the vicinity of Pro103 are also significantly larger than the corresponding ones of the wild-type structure. It is likely that an increase in the flexibility in the loop region involving Pro103 is induced. In contrast, the mutation of Ile106, which is located near Ile23, to Val caused no significant change. The maximal shift in the surrounding atoms of Val106 is 0.3 Å for the $C^{\eta 2}$ atom of Trp109. The backbone shift is less than 0.2 Å, except for Val130 of the C-terminal residue.

Table II-3. X-ray data collection and refinement statistics for the wild-type and Ile to Val mutant human lysozymes.

	Wild-type	I23V	I56V	I59V	I89V	I106V
Data collection						
Cell dimension (Å)						
a	56.74	56.51	56.71	56.92	56.78	56.76
b	61.10	61.26	60.85	61.07	61.02	61.05
c	33.77	33.75	33.72	33.74	33.77	33.80
Resolution (Å)	1.58	1.58	1.58	1.58	1.58	1.58
No. of crystal	1	1	1	1	1	1
No. of measured reflections	47,280	45,777	49,674	44,290	46,765	45,192
No. of independent reflections	13,655	14,564	15,567	13,955	14,968	14,486
Completeness of data (%)	82.4	88.6	94.1	84.3	90.4	87.4
R_{merge} (%)[a]	3.96	4.62	5.71	4.20	4.48	5.48
Refinement						
No. of atoms	1226	1206	1216	1182	1215	1191
No. of solvent atoms	197	178	188	154	187	163
Resolution range (Å)	8-1.8	8-1.8	8-1.8	8-1.8	8-1.8	8-1.8
No. of reflections used	9,688	10,279	10,658	9,998	10,459	10,225
Completeness of data (%)	86.3	91.8	95.4	88.9	93.2	91.3
R factor[b]	0.153	0.158	0.160	0.162	0.164	0.162
r.m.s. of dev. (bond: Å)	0.009	0.009	0.008	0.008	0.009	0.008
r.m.s. of dev. (angle: °)	1.47	1.52	1.47	1.48	1.48	1.48
Mean *B* (main-chain) (Å^2)	13.0	14.4	13.7	13.8	13.7	13.8
Mean *B* (side-chain) (Å^2)	17.5	19.1	18.3	18.6	18.5	18.5

[a] $R_{merge} = 100 \times \Sigma \mid I - \langle I \rangle \mid / \Sigma \langle I \rangle$.

[b] R factor $= \Sigma \mid\mid F_o \mid - \mid F_c \mid\mid / \Sigma \mid F_o \mid$.

Table II-4. The r.m.s. deviation (Å) of atoms between the wild-type and mutant structures.

	I23V	I56V	I59V	I89V	I106V
All residues					
Main-chain atoms	0.14	0.09	0.13	0.10	0.10
Atoms within 6.0 Åfrom mutation site					
No. of atoms	60	53	61	48	55
All atoms	0.15	0.12	0.46	0.15	0.14
Main-chain atoms	0.12	0.07	0.21	0.10	0.11
Side-chain atoms	0.18	0.14	0.61	0.18	0.15
Atoms in some hydrophobic core for comparison					
Position of center	Ile56	Ile59	Ile23	Ile23	Ile56
No. of atoms	55	60	60	60	56
All atoms	0.10	0.09	0.08	0.08	0.09
Main-chain atoms	0.08	0.08	0.07	0.09	0.07
Side-chain atoms	0.11	0.09	0.10	0.07	0.12

(a)

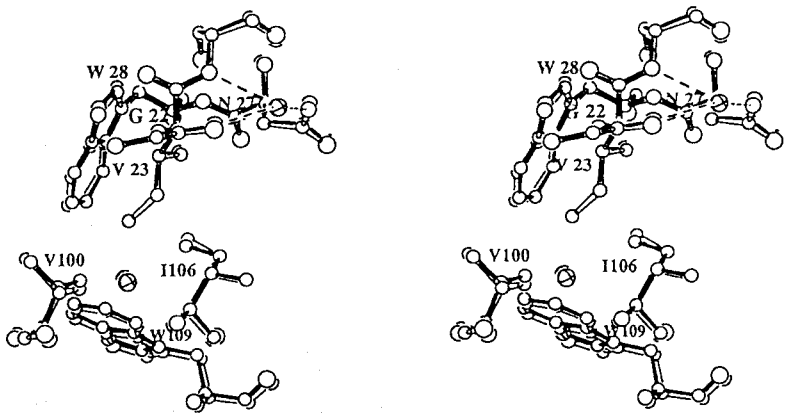

(b)

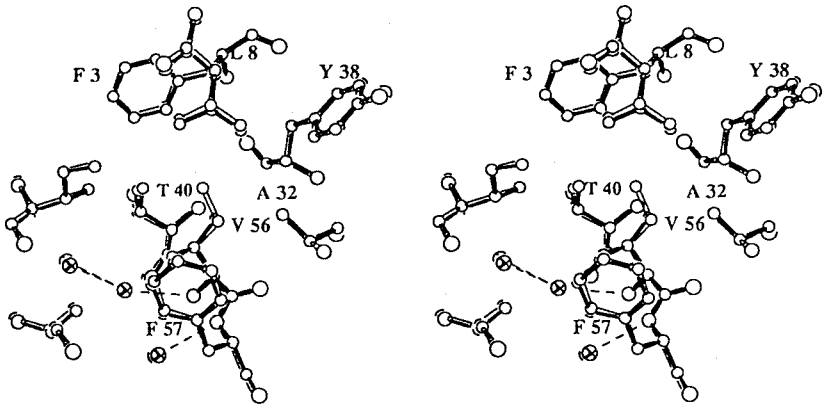

(c)

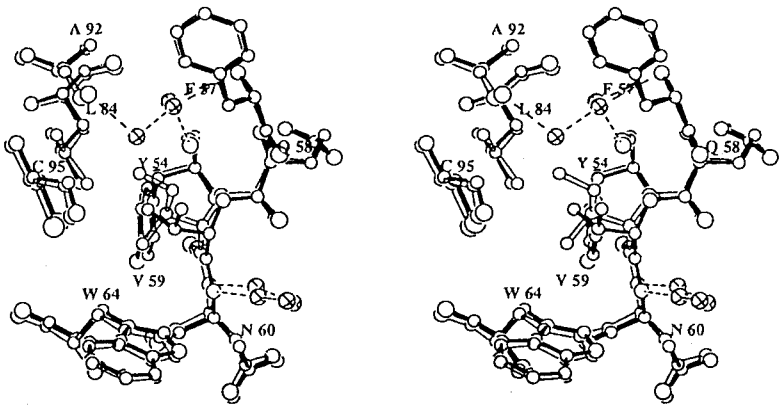

Figure II-5 (a)-(c) (legend overleaf)

(d)

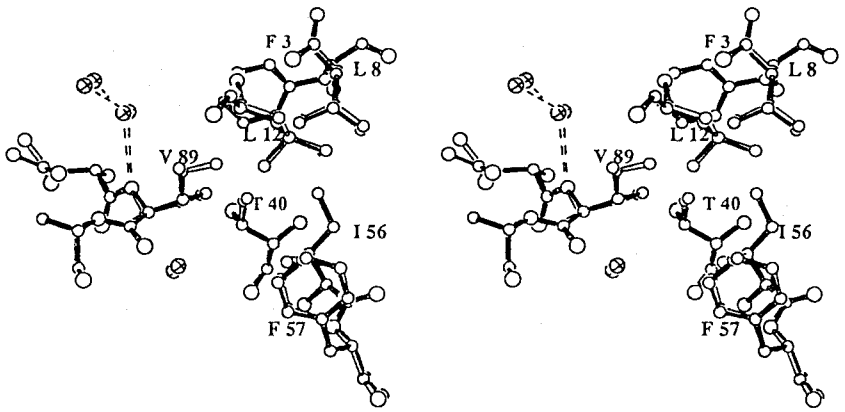

(e)

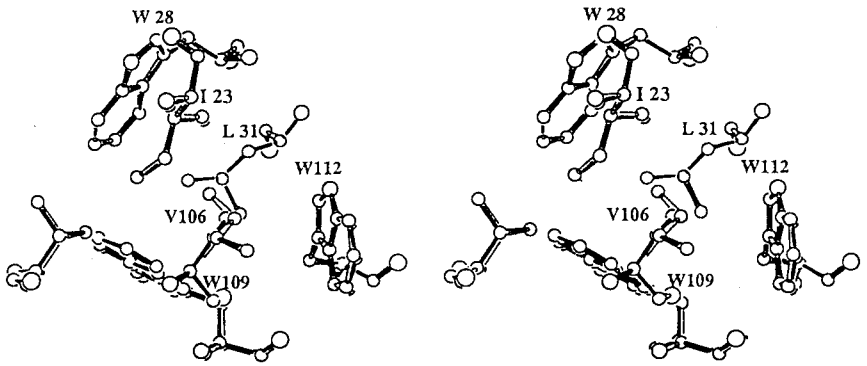

Figure II-5. Stereo drawings (Johnson, 1976) showing the mutant structure in the vicinity of the mutation sites. The wild-type (open bonds) and mutant structures (filled bonds) are superimposed. (a) I23V; (b) I56V; (c) I59V; (d) I89V; and (e) I106V. Solvent water molecules are drawn as cross-circles. Broken lines indicate hydrogen bonds.

Table II-5. Side-chain conformations of Ile and substituted Val residues for human lysozyme.

Residue	χ_1(°)[a]	χ_2(°)
Ile23	-52	160
Val23	-58	
Ile56	-162	161
Val56	-161	
Ile59	-67	175
Val59	53	
Ile89	65	168
Val89	57	
Ile106	-172	77
Val106	-169	

[a] Because of the difference in the IUPAC-IUB definition of the side-chain angles between Ile and Val, 120° is added to the χ_1 value for Val.

Table II-6. Structural characteristics at the substitution sites (Ile) of the wild-type human lysozyme.

	ASA (%)[a]	No. of methyl(ene) groups[b]	*B*-factor (Å^2)[c]
Position 23	6	18	4.8
Position 56	1	22	10.2
Position 59	2	18	11.2
Position 89	4	21	12.7
Position 106	6	29	13.3

[a] Accessible surface area of Ile in comparison with the exposed value of 175 Å^2. The ASA was calculated by the method of Kabsch and Sander (1983).

[b] Number of -CH_2- and -CH_3 groups within a sphere of 6Å radius surrounding $C^{\delta 1}$ atom of Ile.

[c] *B*-factor of $C^{\delta 1}$ atom of Ile.

Discussion

It can be considered that the removal of a methylene group by the substitution of Ile to Val in the interior of a protein affects the conformational stability due to the difference in hydration of the substituted residue, the changes in the van der Waals interactions, the cavities created, or the structural rearrangements caused by the mutation.

Thermodynamic properties of denaturation of the mutant human lysozymes

There are only a few reports on the differences in the denaturation enthalpies ($\Delta\Delta H$) between a wild-type and mutant protein, as compared with those describing changes in the denaturation Gibbs energy ($\Delta\Delta G$), although the accumulation of these data would be useful for analyzing the mechanism of protein stability. This may be due to the difficulty in measuring small differences in the thermodynamic parameters (Sturtevant, 1994). To minimize the error of estimation from the experimental results in this chapter (Table II-2), the thermodynamic parameters of the denaturation of the mutant proteins are compared at the denaturation temperature (64.9 °C) of the wild-type protein at pH 2.7. Near 65 °C, the ΔH values of all the mutant proteins were obtained directly at different pHs. Table II-2 indicates that the changes in ΔH are larger than those of ΔG, and the ΔH of each mutant protein is substantially different, despite the sameness of the substitution. The results suggest that the destabilization mechanism of the mutant proteins differs, depending on the location of the mutation sites.

Denaturation Gibbs energy changes ($\Delta\Delta G$) by the substitution of Ile to Val have been examined in several proteins, such as five nuclease mutants (Shortle et al., 1990), four barnase mutants (Serrano et al., 1992a), and three

chymotrypsin inhibitor 2 mutants (Jackson et al., 1993). The values of $\Delta\Delta G$ have ranged from -2.1 to -7.5 kJ/mol, except for 0.4 kJ/mol in the mutant (I76V) of chymotrypsin inhibitor 2, which is confirmed to have a structural rearrangement due to the mutation (Jackson et al., 1993). In the case of human lysozyme the decreases in the Gibbs energy change (-1.5 to -5.0 kJ/mol) were generally small as compared with the other proteins reported. The difference in the transfer Gibbs energy from organic solvent (*n*-octanol) to water between Ile and Val is 3.4 kJ/mol (Fauchere & Plisk, 1983). The values of $\Delta\Delta G$ for three of the mutant proteins (I23V, I89V, and I106V) were smaller than the value in the transfer Gibbs energy of the substituting residues, which suggests that the decrease in the stability of the mutant proteins, due to the removal of a methylene group, is compensated by some structural changes.

Correlation between the locations of the mutation sites and the changes in the thermodynamic parameters of the mutant human lysozymes

The mutation sites of Ile $\rightarrow$ Val in this study are located in a loop, a turn, and a β-sheet, which are mostly buried in the interior of the molecule. The accessible surface area (ASA) values are from 2 to 11 $Å^2$ (Table II-6) (99 to 94 % buried, in comparison with the completely exposed value of 175 $Å^2$). Pace (1992) has suggested that different experimental values of the denaturation Gibbs energy change, due to the removal of a methylene group should be corrected to the same solvent accessibility (100 % buried). In our case, the mutations of the more buried residues (1 and 2 % of ASA) were less stable than those of the less buried ones (6 %) (the dotted line in Figure

II-6(a)), but the $\Delta\Delta G$ values were not reconciled by correction for the solvent accessibility (the continuous line in Figure II-6(a)).

For barnase, a statistical correlation has been found between the $\Delta\Delta G$ values and the number of -CH_2- and -CH_3- groups within a 6 Å radius sphere surrounding the deleted methylene group (Serrano et al., 1992a). Figure II-6(b) shows the correlation between the number of side-chain methylene groups (Table II-6), within a radius of 6 Å of the group deleted from the wild-type protein, and the $\Delta\Delta G$ values of the mutant proteins. All of our $\Delta\Delta G$ values were lower in magnitude than those expected from the barnase data (the continuous line in Figure II-6(b)), indicating that the mutant human lysozymes were not destabilized to the same extent, in spite of the greater number of methylene groups at the mutation site. The enthalpy changes of the mutant proteins also do not correlate with the number of methylene groups at the mutation site (Figure II-6(c)), which may be related to the strength of the van der Waals interactions.

The variation in the stability might be related to the mobility of the protein molecule at the mutation site (Alber et al., 1987; Yutani et al., 1991; Herning et al., 1992; Lee, 1993). The crystallographic *B*-factor (thermal factor) of the side-chain atoms of a protein is related to the mobility of the atoms. Figure II-6(d) shows the correlation between the $\Delta\Delta G$ and the *B*-factors of the methylene group of Ile for the wild-type human lysozyme at the mutation site (Table II-6). A linear correlation seems to exist, except for I23V.

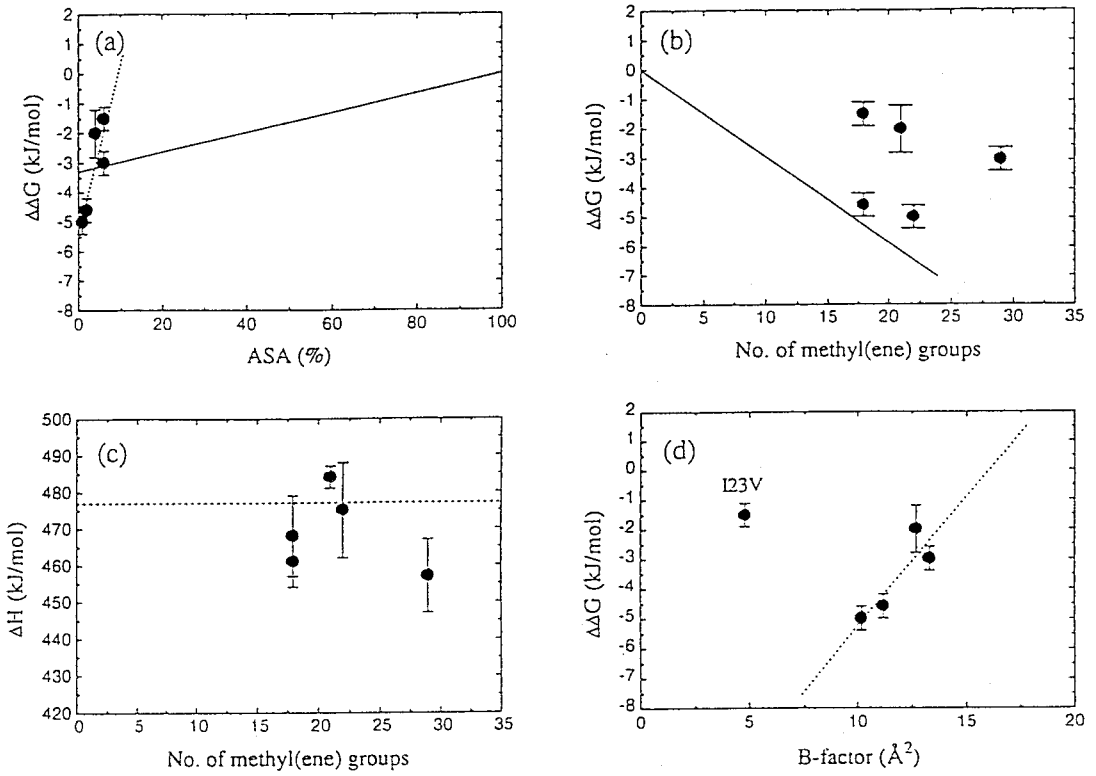

Figure II-6. Correlation between the thermodynamic parameters of denaturation for the mutant proteins at 64.9 °C and the structural characteristics of the mutated site in the wild-type structure. (a) $\Delta\Delta G$ of each mutant protein and the accessible surface area (ASA) of the substituted residue in the wild-type structure. The continuous line shows the values estimated from the transfer Gibbs energy of a methylene group at each ASA value. The dotted line shows the linear regression of all the proteins. (b) $\Delta\Delta G$ and the number of side-chain methylene groups within 6 Å of each Ile. The continuous line shows the best fit of the barnase data to a linear equation obtained by Serrano et al. (1992a). (c) ΔH and the number of side-chain methylene groups within 6 Å of each Ile. The dotted line shows ΔH of the wild-type protein. (d) $\Delta\Delta G$ and *B*-factors of the methylene group of Ile for the wild-type protein at each mutation site. The dotted line shows the linear regression of four proteins (excluding I23V).

Correlation between changes in thermodynamic parameters and structural changes of the mutant human lysozymes

The overall structure of all the mutant human lysozymes examined was identical to that of the wild-type, and only slight structural rearrangements were observed locally around the mutation sites. No significant correlation between the difference in the thermodynamic parameters and the local structural changes were found, although the X-ray structures for both mutant proteins were examined thoroughly. The accumulation of subtle structural changes that we cannot detect in the structural examination may be the cause of the extensive differences in the thermodynamic parameters.

We calculated the total changes in the ASA values between the wild-type and the mutant X-ray structures to examine the effects of subtle structural changes (Table II-7). To reduce the errors due to structural fluctuations of the surface residues for calculation of the changes in ASA values, we searched for hydrophobic residues that might be affected by the substitution, using the energy-minimized wild-type structures with the deletion of the methylene group of each Ile, calculated by a the program, X-PLOR (Brunger, 1992). Then, we calculated the ΔASA values of these residues (affected by the substitution) using the refined wild-type and mutant X-ray structures. Figure II-7(a) shows the correlation between $\Delta\Delta G$ and the changes in the ASA values of the hydrophobic residues affected by the substitution. The linear regression of the data the (dotted line in Figure II-7(a)) for all the mutant lysozymes was close to the expected line (the continuous line in Figure II-7(a)) obtained from the transfer Gibbs energy of a hydrophobic group from *n*-octanol to water between Ile and Val (3.4 kJ/mol) (Fauchere & Pliska, 1983) and the decrease in the ASA values (23

Å^2) (Makhatadze & Privalov, 1993) by the substitution. This correlation is better than that between $\Delta\Delta G$ and the ASA values of Ile for the wild-type structure (Figure II-6(a)). This suggests that the total changes in the ASA values may play an important role in the conformational stability of the protein. In the case of some mutant proteins (I23V, I89V, and I106V), the accumulation of subtle structural changes (rearrangements) might compensate for the destabilization due to the removal of a methylene group by the mutation. We also calculated the difference in the ASA values of all the hydrophobic residues between the wild-type and each mutant lysozyme (Table II-7). Figure II-7(b) shows the correlation between $\Delta\Delta G$ of the mutant proteins and the changes in the ASA values of all the hydrophobic residues. The data (the dotted line in Figure II-7(b)) are far from the expected line (the continuous line in Figure II-7(b)) from the transfer Gibbs energy of a hydrophobic group. The calculation with all the hydrophobic residues may result in larger errors, due to ambiguity in the structures of the surface residues. We should note that the changes in the ASA values were negative, indicating that small collapses are caused by the substitution.

Eriksson et al. (1992) have reported interesting results on the relationship between created cavity size and $\Delta\Delta G$: the decrease in protein stability by a hydrophobic mutation consists of a constant energy term, due to the difference in the hydrophobicity between the wild-type and substituting residues, and an energy component that depends on the size of the cavity created by the substitution. We also determined the sizes of the cavities the crystal structures of the wild-type and mutant human lysozymes using the procedure of Connolly (1985, 1993) with a probe radius r = 1.2 Å The van der Waals radii of the atoms used were 1, 1.8, 1.7, 1.6, and 1.9 Å

for hydrogen, carbon, nitrogen, oxygen, and sulfur, respectively. Water molecules were not included in the volume calculations. In the wild-type structure, five cavities were found, and their sizes ranged from 8.0 to 123.3 $Å^3$. The sizes of the cavities created at the substitution sites of the mutant proteins were from 8.4 to 24.4 $Å^3$ (Table II-7). Assuming that the structure is not affected by the deletion of a methylene group, each cavity volume can be theoretically calculated by the deletion of a methylene group from the coordinates of the wild-type structure (B in Table II-7). The observed value of I59V was bigger than the theoretical value, in which one new water molecule was inserted at the mutation site, but the other ones were smaller, indicating a decrease in the cavity volume at the mutation site. I59V and I89V have bigger differences (positive and negative, respectively), which would cause the structural rearrangements (changes) around the mutation sites. The cavity of I23V was not detected with a probe radius of either 1.1, 1.2 or 1.25 Å, suggesting that the cavity size becomes smaller than the probe radius or that the probe connects to the protein surface.

Although Hubbard et al. (1994) have reported that a probe size of 1.25 Å is optimal for detecting cavities and their associated solvent, we used a probe size of 1.2 Å to allow comparison with results reported previously (Eriksson et al., 1992). Figure II-7(c) shows the correlation between the $\Delta\Delta G$ values of the mutant proteins and the sizes of the cavities at the mutation sites. The deviations from the theoretical line proposed by Eriksson et al. (1992) can come from differences in the side-chain rotamer angles, differences in the side-chain conformational entropy differences in the bond angles and bond lengths, and any other differences between the structures of the wild-type and mutant proteins (Eriksson et al., 1993). The data of three

of the mutant proteins, I59V, I89V, and I106V, were higher than the theoretical line, suggesting that structural rearrangements improve their stability elsewhere. In the case of I23V, in which a cavity was not detected at the mutation site, the filling of the cavity may have improved the stability. On the other hand, we examined the correlation between the changes in the total cavity volume of the mutant lysozymes and $\Delta\Delta G$ (Figure II-7(d)). This gives a better correlation with the line expected by Eriksson et al. (1992). We should note that the changes in the total cavity volume of all the mutant proteins, except for I59V, were negative, showing a decrease in the total volume by the substitution. This means that the removal of a methylene group by the mutation affects the overall structure of the mutant proteins, although to a small extent.

The thermodynamic parameters of denaturation should depend on the denatured state of proteins, because they are defined as the difference in the energies of the native and denatured states, and amino acid substitutions affect the conformation in the denatured state (Shortle et al., 1990; Dill & Shortle, 1991). In this case, we would be able to describe more precisely the relationship between the thermodynamic parameters and the changes in the conformational structure, if we had some more information about the denatured states of the mutant proteins. The denatured state of a protein can be studied by NMR experiments (Evans et al., 1991).

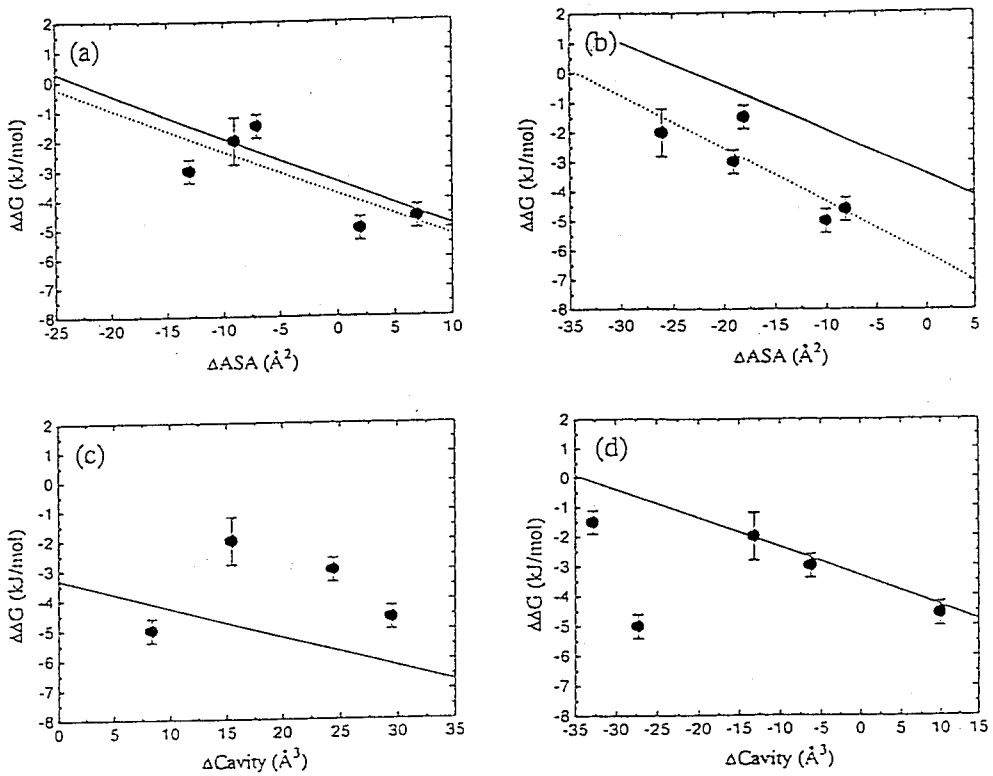

Figure II-7. Correlation between the thermodynamic parameters of denaturation for the mutant proteins at 64.9 °C and the structural characteristics obtained from its mutant structure. (a) $\Delta\Delta G$ and the decrease in the ASA values of the hydrophobic residues affected by the mutations. The continuous line shows the value (0.148 kJ/mol Å^2) obtained from the transfer Gibbs energy of a methylene group (-3.4 kJ/mol, Fauchere & Pliska, 1983) and the surface area created by the deletion of a methylene group (23 Å^2, Makhatadze & Privalov, 1993), where we assume that $\Delta\Delta G$ values of -3.4 kJ /mol correspond to ΔASA of zero when the cavity created by the deletion of a methylene group is completely buried and other residues are not affected. Dotted line shows the linear regression of all the proteins. (b) $\Delta\Delta G$ and the decrease in the ASA values of all the hydrophobic residues. The continuous line represents the same line shown in (a) and the dotted line the linear regression of all proteins. (c) $\Delta\Delta G$ and the difference in the cavity volume of each mutant protein at the mutation site from that of the wild-type structure. The continuous line is that proposed by Eriksson et al. (1992). (d) $\Delta\Delta G$ and difference in the total cavity volume of each mutant protein from that of the wild-type structure. The continuous line is that the line proposed by Eriksson et al. (1992).

Table II-7. Changes in solvent-accessible surface area (ASA) values and cavity volume between the wild-type structure and each mutant structure of human lysozyme.

	ASA[a]		Cavity[d]			
			Cavity volume at substitution site			
	ΔASA[b] (affected) ($Å^2$)	ΔASA[c] (all) ($Å^2$)	Observed (A) ($Å^3$)	Model (B)[e] ($Å^3$)	(A-B) ($Å^3$)	ΔTotal cavity volume[f] ($Å^3$)
I23V	-7	-18	g	g		-32.8
I56V	2	-10	8.4	13.1	-4.7	-27.2
I59V	7	-8	29.5	16.6	12.9	10.0
I89V	-9	-26	15.5	30.2	-14.7	-13.1
I106V	-13	-19	24.4	28.7	-4.3	-6.2

[a] The ASA was calculated by the method of Kabsch and Sander (1983).

[b] Difference in ASA values of the hydrophobic residues affected by the substitution between the wild-type and each mutant protein, defined as the ΔASA = ASA(mutant) - ASA(wild-type).

[c] Difference in ASA values of all the hydrophobic residues between the wild-type and each mutant protein, defined as the ΔASA = ASA(mutant) - ASA(wild-type).

[d] The cavity volume was calculated using the procedure of Connolly (1985, 1993) with a probe radius 1.2 Å.

[e] Volume of the cavity remaining after deleting a methylene group from the coordinates of the wild-type structure.

[f] Difference in total cavity volume between the wild-type (209.1 $Å^3$) and each mutant protein, defined as the ΔVol. = Vol.(mutant) - Vol.(wild-type).

[g] Cavity is not detected.

Conclusion

(1) The thermodynamic parameters for denaturation of the five Ile to Val mutant human lysozymes obtained by calorimetry differed from each other, depending on the location of the mutation.

(2) The changes in the thermodynamic parameters of denaturation had a better correlation with the accumulation of subtle structural changes, such as total changes in ASA values, than with changes in the local structural characteristics at each substitution site.

(3) Rearrangements of the overall structure partially compensated for the destabilization due to the removal of the methylene group by the mutation.

Chapter III

Studies on the Nine Ala Substitutions for Val of Human Lysozyme**

Introduction

Calorimetry and X-ray structural analyses have been used to study human lysozymes of Pro mutants (Herning et al., 1992), disulfide mutants (Kuroki et al., 1992a) and a calcium-binding mutant (Kuroki et al., 1992b). We have also reported studies of hydrophobic mutant human lysozymes in which Ile was substituted by Val in the interior of the molecule resulting in the deletion of a methylene group. To elucidate the role of hydrophobic residues of human lysozyme in conformational stability, we focused on the Val residues located in various regions in the protein. Each residue was substituted by Ala which removes two methylene groups equivalents. Human lysozyme (130 residues, 4 S-S bridges) contains nine Val residues, as shown in Figure III-1. The side-chains of Val93, Val99 and Val100 are in an α-helix and are nearly completely buried in the protein. The side-chains of Val121, Val125 and Val130 in the C-terminal region are also mostly buried in the inside of the molecule. In contrast, the side-chains of Val2, Val74 and Val110 are mostly exposed to solvent in the native protein (Table III-1).

In this chapter, the thermodynamic parameters characterizing the denaturation of the nine Val mutants were determined using scanning calorimetry, and their three-dimensional structures were determined at high resolution by X-ray crystallography. We will use these results to gain a better understanding of the hydrophobic effect.

** This work is published, titled "Contribution of the Hydrophobic Effect to the Stability of Human Lysozyme: Calorimetric Studies and X-ray Structural Analyses of the Nine Valine to Alanine Mutants" (Takano et al., 1997a).

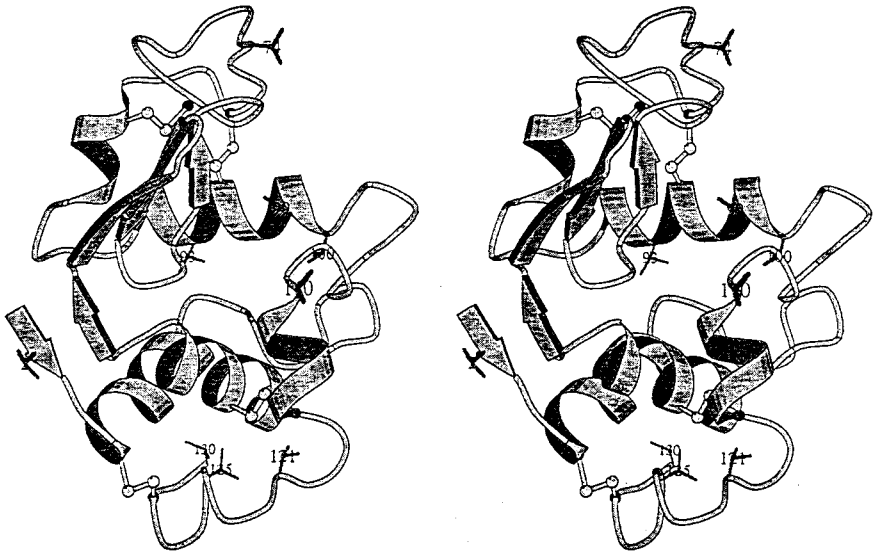

Figure III-1. Stereo drawing of the wild-type human lysozyme structure. The positions of the substituted Val residues are indicated. The structure was generated by the program MOLSCRIPT (Kraulis, 1991). The open circles represent sulfur atoms of disulfide bonds.

Table III-1. Structural characteristics of Val residues in the wild-type human lysozyme[a]

	ASA (%)[a]	χ_1 (°)
Val 2	72	-178
Val 74	75	-84
Val 93	3.0	174
Val 99	1.9	175
Val 100	0	-57
Val 110	71	174
Val 121	15	-69
Val 125	16	-66
Val 130	2.4	-65

[a] ASA (%) = [$ASA(Val)^{fold}$ / $ASA(Val)^{extended}$] × 100. The $ASA(Val)^{extended}$ is the value for a polypeptide as a reference for the unfolded state (Oobatake & Ooi, 1993). The ASA was calculated using the procedure of Connolly (1985, 1993) with a probe radius of 1.4 Å.

Materials and Methods

Mutant Proteins

Mutagenesis, expression and purification of the Val mutant human lysozymes were performed as described in Chapter II. Furthermore, the preparations for V74A, V100A and V110A were applied to an Asahipak ES-502C column and were eluted with a linear gradient of 0 to 0.36 M Na_2SO_4 in 0.05 M sodium-phosphate buffer at different pH (pH 5.5) because the heat denaturation curves of these mutant proteins gave two peaks in calorimetric measurements. The proteins collected from the main peak showed a single transition curve in DSC. The mass spectrum (Sciex API.III mass spectrometer) of the purified proteins was used to confirm the identity of the mutant proteins.

Differential scanning calorimetry (DSC)

Calorimetric measurements and data analyses were carried out as described in Chapter II.

X-ray crystallography

Mutant human lysozymes were crystallized, diffraction data collected, and the structures refined as described in Chapter II. All the crystals belong to the space group $P2_12_12_1$.

The coordinates of the nine mutant human lysozymes, V100A, V110A, V121A, V125A, V130A, V2A, V74A, V93A and V99A, have been deposited in the Brookhaven Protein Data Bank, accession nos, 1OUB to 1OUJ.

Results

Differential scanning calorimetry (DSC) of mutant human lysozymes

In order to determine the thermodynamic parameters of denaturation, DSC measurements of Val to Ala mutant human lysozymes were made at acidic pHs between 2.5 and 3.2. In this pH region, the denaturation of the mutants was reversible. Typical excess heat capacity curves are shown in Figure III-2. The proteins gave similar results. The denaturation temperature (T_d), the calorimetric enthalpies (ΔH_{cal}), the van't Hoff enthalpies (ΔH_{vH}) and the heat capacity changes (ΔC_p) were obtained directly from analyses of these curves (Table III-2). The T_d values were sensitive to pH and increased linearly with pH. The temperature dependences of ΔH_{cal} for the nine Val mutant lysozymes were linear. The ΔC_p values obtained from the slopes by least-squares fitting (Table III-3) were coincident within experimental error with the average of the values obtained from the excess heat capacity curves (Table III-2).

The thermodynamic parameters for denaturation of the mutant proteins at the denaturation temperature of the wild-type protein, 64.9 °C, and at pH 2.7 were calculated (Table III-3) using Equations I-4 to I-6.

As shown in Table III-3, the effects of the deletion of two methylene groups (Val → Ala) on the stability of human lysozyme were different in each mutant protein. The changes in ΔG ranged from +2.2 to -6.3 kJ/mol and the changes in ΔH ranged from +7 to -17 kJ/mol, compared with the wild-type protein.

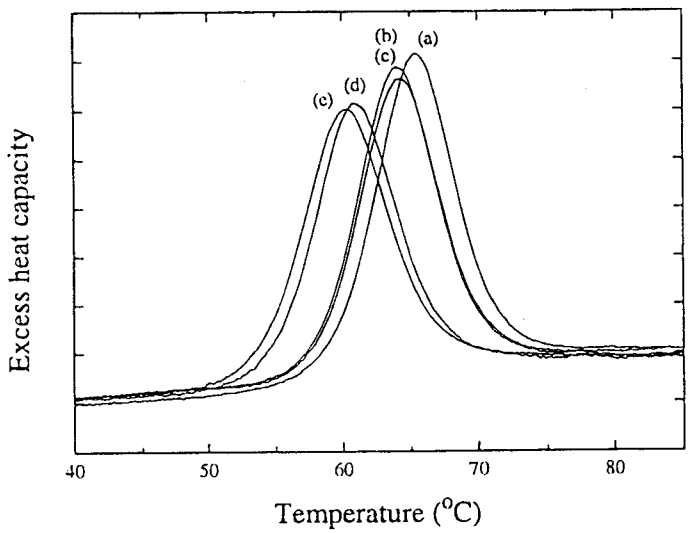

Figure III-2. Typical excess heat capacity curves of the wild-type and mutant human lysozymes at pH 2.71. (a) wild-type; (b) V74A; (c) V100A; (d) V125A and (e) V2A. The increments of excess heat capacity were 10 kJ/mol K.

Table III-2. Thermodynamic parameters for denaturation of Val to Ala mutant human lysozymes at different pHs.

	pH	T_d (°C)	ΔH_{cal} (kJ/mol)	ΔH_{vH} (kJ/mol)	ratio $\Delta H_{cal}/\Delta H_{vH}$	ΔC_p[a] (kJ/mol K)
V2A	3.17	68.7	490	502	0.98	7.0
	2.88	63.7	464	473	0.98	6.7
	2.71	60.3	439	456	0.96	6.4
	2.55	57.6	418	431	0.97	4.5
					0.97	6.2 ± 1.4
V74A	2.88	67.1	490	510	0.96	6.6
	2.71	64.1	469	502	0.94	5.6
	2.55	61.0	452	481	0.94	6.4
					0.94	6.2 ± 0.7
V93A	3.17	71.1	502	531	0.95	7.4
	3.02	68.3	490	523	0.94	4.4
	3.02	68.6	494	527	0.94	3.8
	2.88	66.1	473	510	0.93	4.4
	2.71	62.6	448	494	0.91	4.6
	2.55	59.8	435	464	0.94	4.9
					0.94	4.9 ± 1.4
V99A	3.02	67.8	481	506	0.95	6.4
	2.88	65.2	464	490	0.95	4.6
	2.71	62.1	448	469	0.96	6.3
	2.55	59.2	423	448	0.94	6.1
					0.95	5.9 ± 1.0
V100A	3.17	72.1	490	536	0.91	4.7
	3.02	69.9	485	540	0.90	3.3
	2.71	64.3	456	498	0.92	4.5
	2.55	61.5	448	477	0.94	4.3
					0.92	4.2 ± 0.8
V110A	3.02	71.2	515	540	0.95	5.8
	2.88	69.7	510	540	0.94	4.6
	2.71	66.5	494	527	0.94	4.1
	2.55	63.8	477	498	0.96	4.6
					0.95	4.8 ± 0.9
V121A	3.17	69.9	490	494	0.99	5.8
	2.88	64.2	456	469	0.97	6.7
	2.71	60.5	435	448	0.97	4.9
	2.55	57.4	410	427	0.96	6.6
					0.97	6.0 ± 1.0
V125A	3.17	69.6	498	515	0.97	4.6
	2.88	64.3	469	494	0.95	4.8
	2.71	61.0	452	460	0.98	6.3
	2.55	58.1	435	448	0.97	4.3
	2.55	58.0	435	444	0.98	4.8
					0.97	5.0 ± 0.9
V130A	3.17	70.6	502	531	0.95	3.6
	3.02	68.0	485	523	0.93	3.2
	2.88	65.7	469	510	0.92	4.6
	2.71	62.4	452	481	0.94	6.7
	2.55	59.6	435	464	0.94	7.0
					0.94	5.0 ± 2.0

[a] ΔC_p was obtained from each calorimetric curve.

Table III-3. Thermodynamic parameters for denaturation of Val to Ala mutant human lysozymes at the denaturation temperature (64.9 °C) of the wild-type protein at pH2.7.

	T_d (°C)	ΔT_d (°C)	ΔC_p[a] (kJ/mol K)	ΔH_{cal} (kJ/mol)	$\Delta\Delta G$ (kJ/mol)	$\Delta H_{cal}/\Delta H_{vH}$
Wild-type[b]	64.9 ± 0.5		6.6 ± 0.5	477 ± 4	(0)	0.95
V2A	60.3 ± 0.2	-4.6	6.5 ± 0.5	468 ± 4	-6.3 ± 0.2	0.98
V74A	63.8 ± 0.1	-1.1	6.2 ± 0.4	476 ± 2	-1.5 ± 0.2	0.95
V93A	62.6 ± 0.2	-2.3	6.4 ± 0.4	466 ± 4	-3.1 ± 0.3	0.93
V99A	61.9 ± 0.02	-3.0	6.6 ± 0.5	463 ± 3	-4.1 ± 0.1	0.95
V100A	64.1 ± 0.2	-0.8	4.2 ± 0.4	461 ± 3	-1.1 ± 0.3	0.92
V110A	66.4 ± 0.4	+1.5	5.2 ± 0.4	484 ± 2	+2.2 ± 0.6	0.95
V121A	60.4 ± 0.2	-4.5	6.4 ± 0.3	460 ± 3	-6.0 ± 0.3	0.98
V125A	60.9 ± 0.1	-4.0	5.4 ± 0.1	472 ± 0.5	-5.5 ± 0.1	0.97
V130A	62.3 ± 0.1	-2.6	6.3 ± 0.6	464 ± 5	-3.5 ± 0.1	0.93

[a] ΔC_p was obtained from the slope of ΔH against T_d.
[b] Chapter II.

X-ray structures of mutant human lysozymes

Data collection and refinement statistics for the nine Val to Ala mutant human lysozymes are summarized in Table III-4. The mutant structures seemed to be essentially the same fold as the wild-type structure except at the substituted residue. The r.m.s. deviations and the changes in the *B*-factor of each residue for the main-chain atoms between the wild-type and each mutant are shown in Figures III-3(a) to (i) and III-4(a) to (i), respectively. Figures III-3(j) and III-4(j) show those between V74A and V74A2, respectively. V74A2 is the structure of the same protein obtained from smaller crystal to estimate the errors in our structures. In Figure III-3, there were no differences more than 0.4 Å between the mutant and wild-type structures except for the C-terminal regions of V125A and V130A. The differences between V74A and V74A2 are small: the averages of the r.m.s. deviations for all of the atoms and the main-chain atoms were 0.11 Å and 0.06 Å, respectively. Judging from this reference (Figure III-3(j)), differences over 0.2 Å might reflect meaningful structural change, and indicate that substitutions affect the area around the mutation site and also other parts of the molecule far from the site. For most of the mutant proteins, the largest shift was near residues 71 to 74, a loop on the surface with the largest *B*-factors in the protein. In Figure III-4, the *B*-factors of some mutants are larger than those of the wild-type, especially V2A. This might be due to the smaller crystal size of the V2A mutant. Note that V74A2 had larger *B*-factors than those of V74A (Figure III-4(j)).

The crystal structures in the vicinity of the mutation sites are illustrated in Figure III-5. V93A, V100A, V125A and V130A were substituted in the interior of the protein, and the residues around the mutation

site shifted toward the created cavity (Figures III-5(c), (e), (h) and (i)). Such shifts have not been observed for the Ile to Val mutant lysozymes in Chapter II. The shifts observed here may be caused by creation of a larger cavity due to the deletion of two methylene groups or by an increase in the flexibility of the main-chain due to the substitution with Ala. The Val to Ala mutants examined did not contain any solvent molecules in the cavities, although this has been observed in one Ile mutant (see Chapter II).

(i) V93A, V99A and V100A substitutions in the α-helix in the interior of a protein

Val93, 99 and 100 are all located in an α-helix (residues 90 to 100) in the center of the protein and have small solvent accessible surface areas of side-chain. For V93A, the Leu15 and Met17 residues facing the side-chain of Val93 shifted toward the created cavity without movement of the mutated residue which is in the center of the α-helix (Figure III-5(c)). The largest shift in the vicinity of Ala93 was 0.7 Å for the sulfur atom of Met17. In contrast, V100A substituted at the edge of the α-helix underwent a shift of Ala100 itself toward the cavity (Figure III-5(e)) and the loop regions (residues 101 to 109) (Figure III-3(e)) followed. The C^{β} atom of Ala100 moved 0.8 Å, and some main-chain atoms in residues 101 to 109 moved 0.4 Å. The mutation of Val99, whose side-chain was sandwiched between Trps (64 and 109), resulted in shifts and an increase in *B*-factors in the following loop region (Figures III-3(d) and III-4(d)). The substitutions in this α-helix (residues 90 to 100) mainly affected the surrounding residues.

(ii) V121A, V125A and V130A substitutions in the C-terminal region of a protein

The changes in structure for V121A, V125A and V130A were quite different, although Val121 and Val125 have similar ASA values in the β-turn. When Val121 was replaced by Ala, the movements were smaller than those of the other mutant proteins (Figures III-3(g) and III-5(g)). The average of the r.m.s. differences for the main-chain atoms between V121A and the wild-type was 0.08 Å. V125A had structural changes in the residues in the C-terminal region (residues 119 to 130) due to the movement of Ala125 toward the created cavity (Figures III-3(h) and III-5(h)). The maximal shift (0.7 Å) of the main-chain atoms was for the C^{α} atom of Gln126. The movements of V130A were largely observed only in residues 129 and 130 (Figures III-3(i) and III-5(i)). The r.m.s. differences for the main-chains of the residues 129 and 130 were 0.5 and 1.4 Å, respectively.

(iii) V2A, V74A and V110A substitutions on the surface of a protein

The deletions of the methylene groups on the surface of the protein allowed water molecules to move closer to the protein molecule (Figures III-5(b) and (f)). Between the two V74A structures (V74A & V74A2), the water molecules ordered on the first hydration phase surrounding the mutation site were identical, but when ordered in a second phase, they varied.

Table III-4. X-ray data collection and refinement statistics for Val to Ala mutant human lysozymes.

	V2A	V74A	V93A	V99A	V100A	V110A	V121A	V125A	V130A	V74A2[a]
Data collection										
Cell (Å)										
a	57.09	56.64	56.65	56.73	56.56	56.80	56.77	56.70	56.70	56.61
b	61.23	61.01	60.85	61.09	61.00	60.91	60.92	61.12	61.12	61.01
c	33.60	33.77	33.86	33.92	33.70	33.83	33.82	33.76	33.76	33.79
Resolution (Å)	1.8	1.8	1.8	1.8	1.8	1.8	1.8	1.8	1.8	1.8
No. of measured reflections	34394	35925	36666	35708	33859	34707	35004	36385	35420	34497
No. of indeendent reflections	10331	10564	11122	10408	10366	10973	10733	10428	10915	10843
Completeness of data (%)	90.0	93.1	98.0	91.1	91.3	95.9	94.0	91.3	96.1	95.6
$I/\sigma I$ (1.9-1.8 Å)	5.5	11.4	9.1	6.4	4.9	6.9	5.2	7.0	6.4	4.9
R_{merge} (%)[b]	5.4	3.7	4.0	5.1	5.1	3.4	4.6	4.6	5.3	6.8
Refinement										
No. of atoms	1181	1228	1237	1220	1203	1234	1216	1192	1243	1208
No. of solvent atoms	154	201	210	193	176	207	189	165	216	181
Resolution range (Å)	8-1.8	8-1.8	8-1.8	8-1.8	8-1.8	8-1.8	8-1.8	8-1.8	8-1.8	8-1.8
No. of reflections used	9945	10311	10827	10036	9912	10504	10313	10148	10504	10407
Completeness of data (%)	88.2	92.1	96.8	89.1	88.8	93.6	92.0	90.4	93.8	93.0
R factor[c]	0.173	0.160	0.159	0.168	0.160	0.153	0.154	0.158	0.158	0.170
r.m.s. of dev. (bond:Å)	0.009	0.008	0.008	0.009	0.009	0.008	0.009	0.008	0.008	0.008
r.m.s. of dev. (angle:°)	1.52	1.49	1.51	1.50	1.50	1.49	1.53	1.50	1.51	1.50
Mean *B* (main-chain) (Å^2)	17.0	13.3	13.0	13.8	14.6	13.6	14.5	14.7	13.2	14.9
Mean *B* (side-chain) (Å^2)	22.1	17.7	17.4	18.7	19.3	18.3	19.2	19.2	17.5	19.4

[a] This is the same protein as V74A and is obtained from a smaller crystal as a reference to estimate the errors in the structure.

[b] $R_{merge} = 100 \times \Sigma \mid I_{h,i} - \langle I_h \rangle \mid / \Sigma \langle I_{hi} \rangle$. $I_{h,i}$ are individual values, and $\langle I_h \rangle$ is the mean value of the intensity of reflection *h*.

[c] *R* factor = $\Sigma \mid\mid F_o \mid - \mid F_c \mid\mid / \Sigma \mid F_o \mid$.

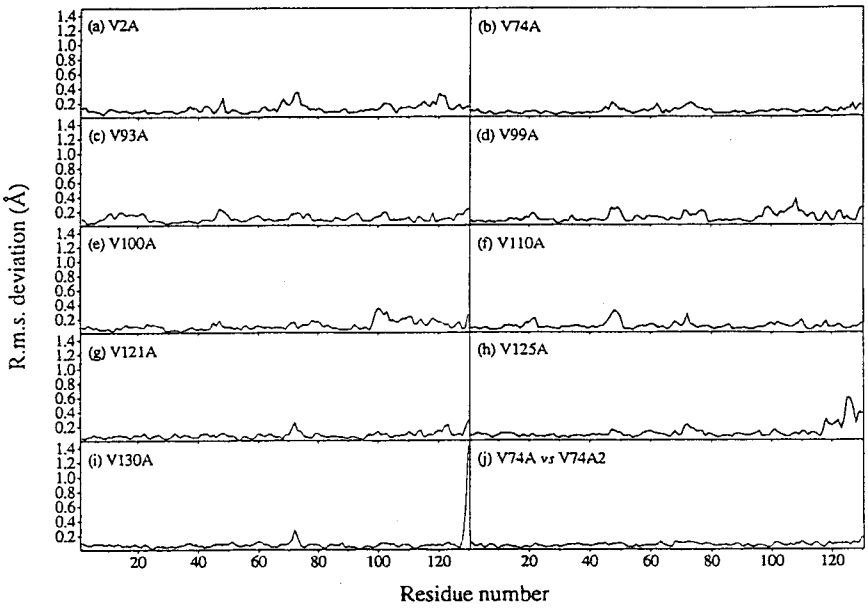

Figure III-3. The r.m.s. deviations for the main-chain atoms between each mutant and the wild-type structure after a least-squares fit of both structures, using the main-chain atoms (Figure (a) to (i)) and those between V74A and V74A2 as a reference (Figure (j)). Figures (a) to (i) represent V2A, V74A, V93A, V99A, V100A, V110A, V121A, V125A and V130A, respectively.

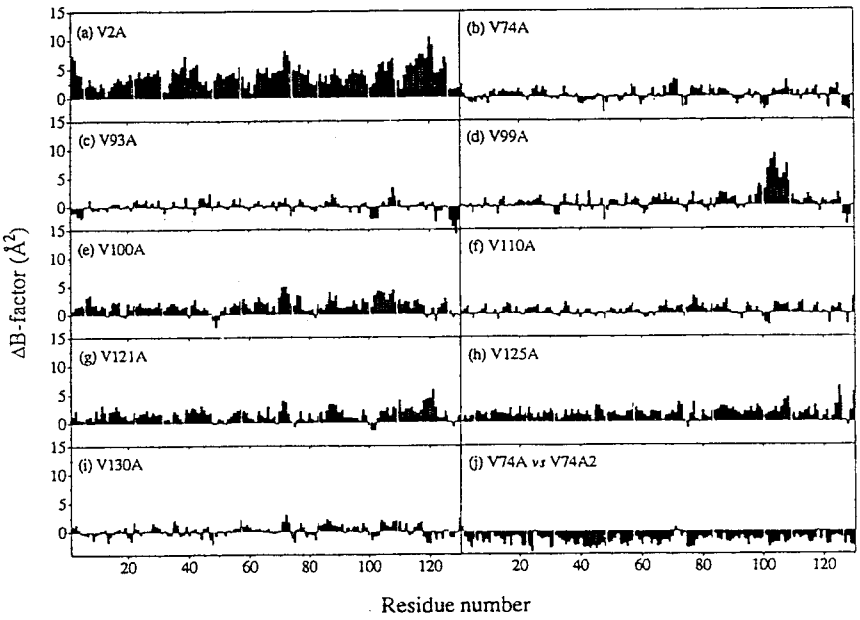

Figure III-4. The differences in the *B*-factors of each residue for the main-chain atoms between each mutant and the wild-type structure (Figure (a) to (i)) and those between V74A and V74A2 as a reference (Figure (j)). Figures (a) to (i) represent V2A, V74A, V93A, V99A, V100A, V110A, V121A, V125A and V130A, respectively.

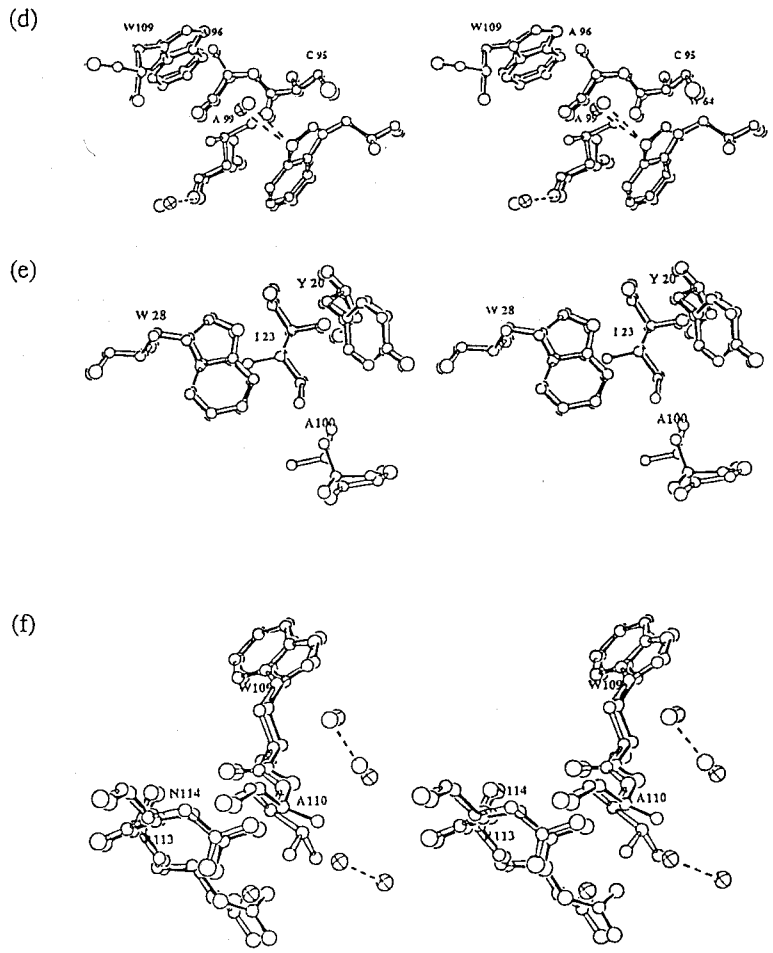

Figure III-5 (d)-(f) (legend overleaf)

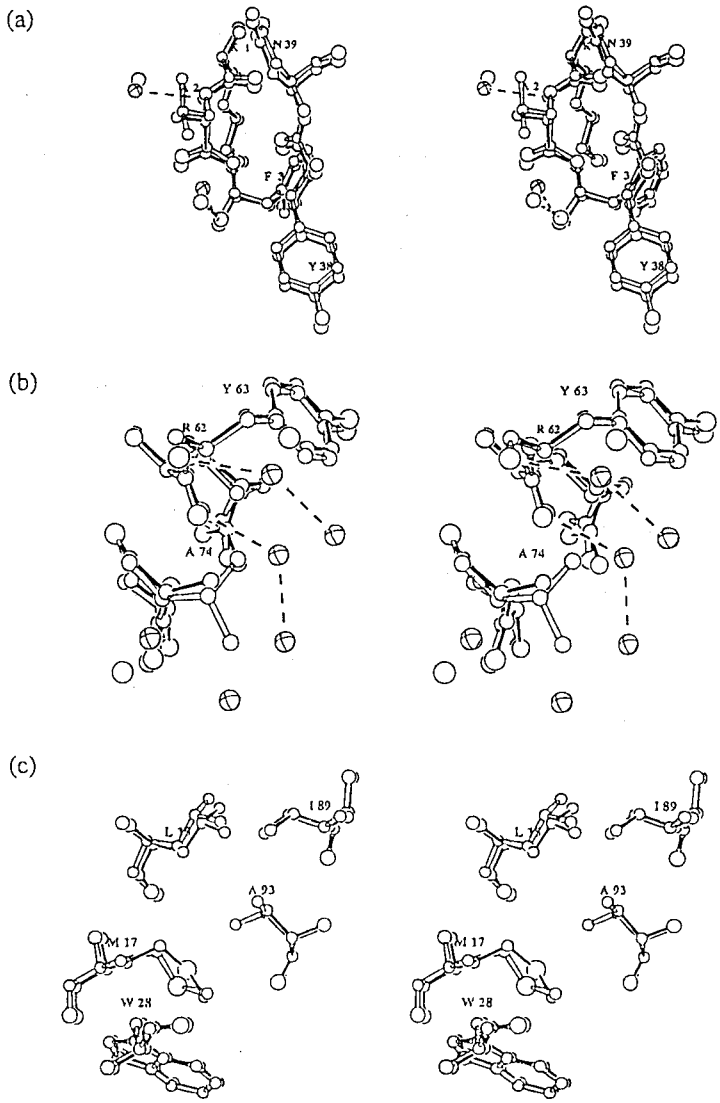

Figure III-5 (a)-(c) (legend overleaf)

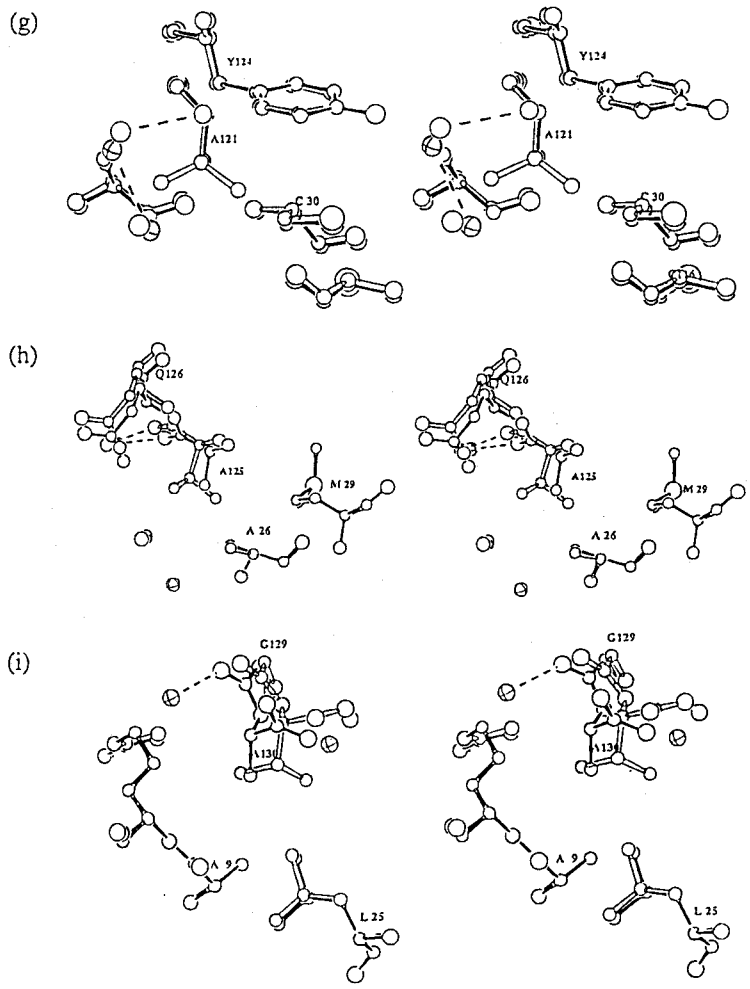

Figure III-5. Stereo drawings (Johnson, 1976) showing the structure in the vicinity of the mutation sites. The wild-type (open bonds) and mutant structures (filled bonds) are superimposed. Figures (a) to (i) represent V2A, V74A, V93A, V99A, V100A, V110A, V121A, V125A and V130A, respectively. Solvent water molecules are drawn as open circles (wild-type) and cross circles (mutants). The broken lines indicate hydrogen bonds.

Discussion

The changes in the thermodynamic properties for the denaturation of the Val to Ala mutants of human lysozyme differed considerably (Table III-3). Our primary goal is to understand the observed differences. The changes in the structures of Val to Ala mutant lysozymes were also different (Figure III-5). We examined the correlations between the changes in the thermodynamic parameters of the denaturation and the following structural features of the proteins: (i) the structural characteristics at each mutation site in the wild-type structure, (ii) the structural differences at each mutation site between the wild-type and the mutant structures and (iii) the structural differences throughout the whole structures between the wild-type and the mutant structures, including five Ile to Val mutants of human lysozyme. For mutant proteins in which methylene groups have been removed, the thermodynamic parameters for denaturation should depend on structural characteristics of the protein, such as accessible surface area (ASA) (Pace, 1992), packing density (Serrano et al., 1992a), and cavity volume (Eriksson et al., 1992).

In addition, the strain due to a Val side-chain in the native protein may be relieved in the Ala mutant. The conformation of Val residues in the wild-type structure are listed at Table III-1. Although the χ_1 value of Val74 deviates from the low energy minima (Zimmerman et al., 1977), its side-chain is highly exposed and flexible: the B-factors for the side-chain were larger than those of other Val side-chains. Therefore, Val74 has little strain. No unfavorable side-chain conformations of the Val residues were found in the present study.

Correlation of $\Delta\Delta G$ with Accessible Surface Area (ASA) of Each Substituted Residue

Pace (1992) has suggested that values of $\Delta\Delta G$ of hydrophobic mutant proteins could be corrected to the same accessibility, namely 100 % buried. For six proteins, the average $\Delta\Delta G$ values, which are divided by the fraction buried for the side-chain in the wild-type proteins, of 15 Val to Ala and 20 Ile to Val mutants are 10.7 and 4.6 kJ/mol, respectively (Pace et al., 1996). These values are similar to ΔG_{tr} from cyclohexane, 9.3 for Val → Ala and 3.7 for Ile → Val (Pace, 1995; Radzika & Wolfenden, 1988). In case of the human lysozyme,the average corrected $\Delta\Delta G$ values were decidedly lower than other results, 4.3 for Val → Ala and 3.3 for Ile → Val, except for V2A, V74A and V110A the residues of which are quite accessible to the solvent. These values are more similar to the ΔG_{tr} values from octanol, 5.2 for Val → Ala and 3.3 for Ile → Val, than those from cyclohexane (Fauchere & Pliska, 1983). The reason for this is probably that the unfolded state for human lysozyme is less accessible to the solvent, mainly due to the 4 disulfide bonds in human lysozyme, than for most of the other proteins that have been used in similar studies (Pace et al., 1990, 1992).

Figure III-6(a) shows the relation between the accessible surface area (%) of the side-chain for each mutation residue in the wild-type structure and the denaturation Gibbs energy changes. However, we did not find good correlation between them. We then tried to calculate the changes in ASA value using the mutant protein structures.

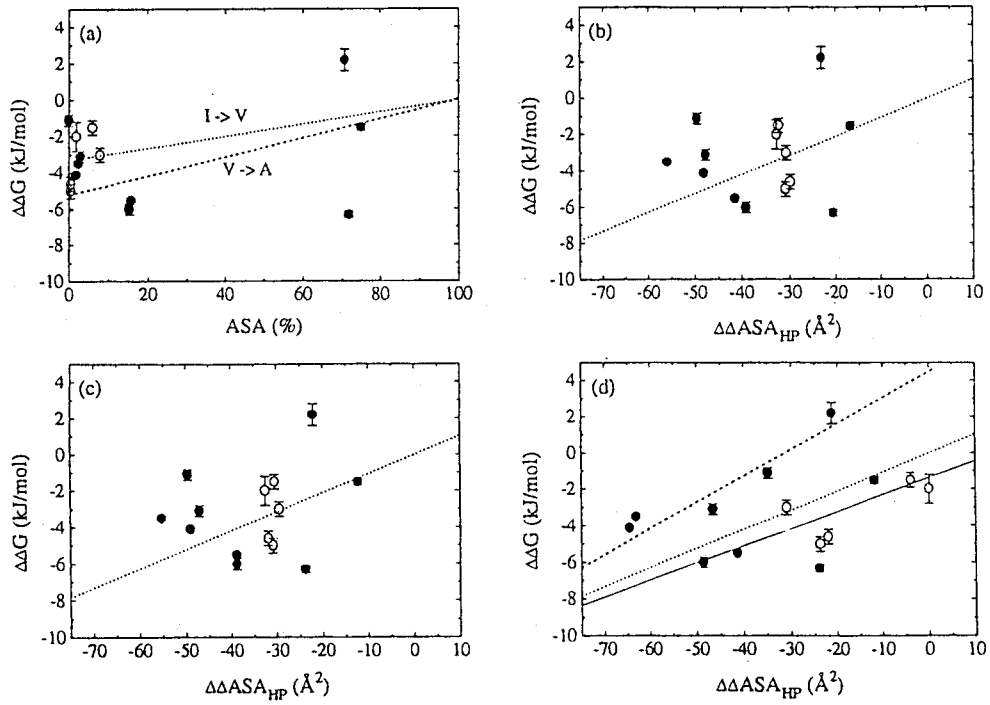

Figure III-6. Correlation of accessible surface area (ASA) or changes in hydrophobic surface area exposed upon denaturation ($\Delta\Delta ASA_{HP}$) with the thermodynamic parameters of denaturation for the mutant proteins at 64.9 °C ($\Delta\Delta G$). Val → Ala mutants are shown as solid circles and Ile → Val as open circles. (a) $\Delta\Delta G$ and the accessible surface area (ASA) (%) of the substituted residue in the wild-type structure. The broken (Val → Ala) and dotted (Ile → Val) lines show the values estimated from the transfer Gibbs energy of a hydrophobic group from n-octanol to water (Fauchere & Pliska, 1983). (b) $\Delta\Delta G$ and the difference in ΔASA for each substituted residue calculated using just the wild-type structure with the mutant structure modeled by deleting the methylene groups from the coordinates of the wild-type structure. (c) $\Delta\Delta G$ and the difference in ΔASA for each substituted residue calculated using both the wild-type and the mutant structure. (d) $\Delta\Delta G$ and the difference in ΔASA for all of the hydrophobic residues calculated using the wild-type and the mutant structure. The continuous and broken lines show the linear regression of the mutant protein on the non-secondary structures (V74A, V121A, V125A, I23V, I56V, I89V and I106V) and the mutants on the α-helices (V93A, V99A, V100A and V110A), respectively. The dotted lines in Figures (b) to (d) indicate the values expected from the transfer Gibbs energy of a methylene group (0.11 kJ/mol Å^2) (Fauchere & Pliska, 1983; Connolly, 1983, 1993).

Correlation of ΔΔG with Changes in Hydrophobic Surface Area Exposed upon Denaturation ($\Delta\Delta ASA_{HP}$)

The ASA values of the Val residues in human lysozyme varied from 0 to 75 % (Table III-1). We estimated the changes in hydrophobic surface area exposed upon denaturation ($\Delta\Delta ASA_{HP}$) using the following equation, where $\Delta\Delta ASA_{HP}$ is a measure of the changes in hydrophobic surface area exposed upon denaturation.

$$\begin{aligned}\Delta\Delta ASA_{HP} &= (\Delta ASA_{mutant})_{HP} - (\Delta ASA_{wild})_{HP} \\ &= (ASA^{extended}_{mutant} - ASA^{fold}_{mutant})_{HP} - (ASA^{extended}_{wild} - ASA^{fold}_{wild})_{HP} \\ &= (ASA^{extended}_{mutant} - ASA^{extended}_{wild})_{HP} - (ASA^{fold}_{mutant} - ASA^{fold}_{wild})_{HP} \qquad \text{(III-1)}\end{aligned}$$

$ASA^{extended}$ was calculated using the actual polypeptide with extended conformation (Oobatake & Ooi, 1993). Yu et al. (1995) have observed a strong relationship between $\Delta\Delta ASA$ based on the wild-type structure and the changes in the Gibbs energy of the unfolding for mutations in BPTI (bovine pancreatic trypsin inhibitor). We estimated $\Delta\Delta ASA_{HP}$ values in three ways: two of them give values just for the substituted residue, but the other is concerned with all hydrophobic residues. The $\Delta\Delta ASA_{HP}$ values in Figures III-6(b) to (d) represent the difference between the ΔASA for each substituted residue in the wild-type structure and that in the model mutant structure deleting the methylene groups based on the coordinates of the wild-type structure (Model), the difference between ΔASA values for each substituted residue in the wild-type and the mutant structure, and the difference between the ΔASA for all of the hydrophobic residues in the wild-type and the mutant

structure, respectively. In most reports (e.g., Jackson et al., 1993; Yu et al., 1995; Tamura & Sturtevant, 1995), wild-type structures are used for evaluation of ΔASA for mutant proteins like that in Figure III-6(b). The $\Delta\Delta ASA_{HP}$ values in Figures III-6(b) and III-6(c) were essentially the same, indicating that the conformational changes at the substitution sites are not large enough to affect the ASA values. However, the correlations between $\Delta\Delta ASA_{HP}$ and $\Delta\Delta G$ were poor. The relationship of $\Delta\Delta G$ with $\Delta\Delta ASA_{HP}$ of all of the hydrophobic residues showed less scatter from the line (dotted) expected from the transfer Gibbs energy of a methylene group (Figure III-6(d)) than those with the $\Delta\Delta ASA_{HP}$ of each substituted residue (Figure III-6(c)). These results suggest that the substitutions involve structural rearrangements of the overall structure, which affect the stabilities, and confirm structural changes of residues far from substitution site (Figure III-3).

We should note that the data points were scattered on the expected line as shown in Figure III-6(a) to (d), suggesting that other factors also affected the conformational stability. Residues exposed on the surface of a protein will have little interaction with other residues. At positions Val2, Val74 and Val110, the side-chains were highly exposed, however, the $\Delta\Delta G$ values were -6.3, -1.5 and +2.2 kJ/mol, respectively. Because Val2, Val74 and Val110 are located on the β-sheet, long loop and α-helix, respectively, the difference in stability among them may depend on the secondary structure at the substitution site. Table III-5 lists the $\Delta\Delta G$ values measured by DSC and the $\Delta\Delta G$ expected from the hydrophobicity corrected for ASA values of each substitution (Fauchere & Pliska, 1983; Pace, 1992). As shown in Table III-5, for the substitutions of Val by Ala on the α-helix, the Gibbs

energy changes are smaller than the expected values. The secondary structure propensities of Val and Ala are different: the ranking in an α-helix is Ala > Val, and the ranking in a β-sheet is Val > Ala (Chou & Fasman, 1978). The stabilities of proteins substituted in an α-helix (Dao-Pin et al., 1990; Serrano et al., 1992b; Blaber et al., 1993; Pinker et al., 1993) and in a β-sheet (Kim & Berg, 1993; Smith et al., 1994; Minor & Kim, 1994; Otzen & Fersht, 1995) have been examined. For most of them, the ranking of the stabilities is coincident with the ranking of the secondary structure propensities of Chou & Fasman (1978). In the present case, data over the expected line (the dotted line) in Figures III-6(a) to (d) might contain the influence of the secondary structure propensities. When the mutants on non-secondary structures were considered, the correlation between $\Delta\Delta G$ and $\Delta\Delta ASA_{HP}$ had a correlation coefficient of 0.88 for 7 points (V74A, V121A, V125A, I23V, I56V, I89V and I106V, as shown by the continuous line in Figure III-6(d)). A similar analysis of the mutants on the α-helices showed a very good correlation with the correlation coefficient of 0.95 for 4 points (V93A, V99A, V100A and V110A), as shown by the broken line in Figure III-6(d). In this connection, the correlation coefficients of all data for Figures III-6(c) and III-6(d) were only 0.22 and 0.37, respectively. These results indicate that the secondary structure propensities of the amino acid residues in α-helices compensated for the destabilization due to the removal of the methylene groups and also that the α-helix propensity corrections may apply at completely buried sites if there is no steric strain as in this study. Thus, V110A was more stable than the wild-type protein because the increment in stabilization due to helix propensity was greater than the small decrease in stability due to the removal of methylene groups located largely on the

protein surface. In contrast, V2A was less stable than expected due to the unfavorable β-sheet propensity. It has been reported that α-helix propensity and β-sheet propensity contribute 2.3 and -3.8 kJ/mol to the stability of Val to Ala substitutions (Pace, 1995).

The mutant proteins with similar measured $\Delta\Delta G$ and expected $\Delta\Delta G$ values were V74A and I106V (Table III-5). The discrepancy was also small for V99A, V125A, I59V and I89V. V74A (Figure III-3(b)), I89V and I106V (Chapter II) are the mutant proteins with the smallest structural changes. These results suggest that $\Delta\Delta G$ correlates with the ASA value corrected for the accessibility, if the structure is not affected by the substitution and the substitution site is not located in the secondary structure.

Table III-5. Comparison of measured $\Delta\Delta G$ with $\Delta\Delta G$ expected from hydrophobicity corrected using the ASA value of each substitution residue for Val and Ile mutant human lysozymes (in kJ/mol).

	Position of substitution	Measured $\Delta\Delta G$ (A)	Expected $\Delta\Delta G$[a] (B)	Discrepancy (A-B)
V93A	α-Helix	-3.1	-5.0	+1.9
V99A	α-Helix	-4.1	-5.1	+1.0
V100A	α-Helix	-1.1	-5.2	+4.1
V110A	α-Helix	+2.2	-1.5	+3.7
V2A	β-Sheet	-6.3	-1.5	-4.8
V121A	β-Turn[b]	-6.0	-4.4	-1.6
V125A	β-Turn[b]	-5.5	-4.4	-1.1
V74A		-1.5	-1.3	-0.2
V130A	C-Terminal	-3.5	-5.1	+1.6
I59V	β-Sheet	-4.6	-3.3	-1.3
I23V	β-Turn[b]	-1.5	-3.1	+1.6
I56V	β-Turn[b]	-5.0	-3.3	-1.7
I106V	β-Turn[b]	-3.0	-3.0	0
I89V		-2.0	-3.2	+1.2

[a] These were calculated using the transfer Gibbs energy from *n*-octanol to water (Fauchere & Pliska, 1983). When fully buried, $\Delta\Delta G$ of Val → Ala and Ile → Val are -5.2 and -3.3 kJ/mol, respectively. ASA (%) of Ile residues (23, 56, 59, 89 and 106) calculated in the same way as Val residues (in Table III-1) are 6.0, 0.5, 0.5, 1.9 and 3.9, respectively.
[b] Defined by Rose et al. (1985).

Correlation of $\Delta\Delta G$ with Cavity Volume and with Packing Density

Eriksson et al. (1992, 1993) have found the relationship between the created cavity volume and $\Delta\Delta G$ in Leu → Ala and Phe → Ala mutant T4 lysozymes:

$$\Delta\Delta G = \Delta\Delta G_{tr} + \Delta\Delta G_{cav} + \Delta\Delta G_{other} \qquad \text{(III-2)}$$

where $\Delta\Delta G_{tr}$ is the difference in the hydrophobicity of the amino acids, $\Delta\Delta G_{cav}$ is an energy component that depends on the size of the cavity created by substitution and $\Delta\Delta G_{other}$ represents other energy terms that may result from differences in the side-chain rotamer angles, differences in the side-chain conformational entropy, differences in the bond angles and bond lengths, and any other differences between the structures of the wild-type and the mutant proteins. For barnase, the correlation between $\Delta\Delta G$ and cavity volume has not been seen in Ile → Val mutants (Buckle et al., 1993), but in Ile → Ala mutants there is an approximately linear relationship between them (Buckle et al., 1996). Five Ile mutant human lysozymes have shown some correlation with the line derived by Eriksson et al. (1992) for the changes in the total cavity volume and $\Delta\Delta G$ (Chapter II).

We have determined the size of the cavities in the Val mutant crystal structures using the procedure of Connolly (1985, 1993) with a probe radius of r = 1.20 Å. The reason for using this program and this probe size was to allow comparison with previous reports (Eriksson et al., 1992, 1993; Chapter II). The van der Waals radii of the atoms in the new version of the Connolly procedure are improved compared to those used in the previous study

(Chapter II). The cavity volumes of Ile mutants were also recalculated for comparison.

A cavity at each mutation site of Val to Ala mutants of human lysozyme was not detected, except for V93A, indicating that the cavity size became smaller than the probe radius or that the probe connected with the protein surface. Therefore, we also calculated the cavity volume of each model structure obtained by the deletion of the methylene groups from the coordinates of the wild-type structure (Model). However, the cavity volume could again only be calculated for Model-V93A. The detected cavity volume of V93A and Model-V93A corresponded to one deleted methylene group. Next, we tried calculations using smaller probe radii of 1.15, 1.10, 1.05 and 1.00 Å. For these smaller probe radii, V99A, V100A, Model-V99A and Model-V100A had cavities which were equivalent to one methylene group. These results indicate that it is difficult to determine the cavity volume of these mutant proteins with Val → Ala mutations.

Figures III-7(a) and (b) show the correlation between $\Delta\Delta G_{cav}$ (= $\Delta\Delta G$ - $\Delta\Delta G_{tr}$) and the total cavity volume changes between the wild-type and the mutant proteins for the probe sizes 1.20 and 1.40 Å which is typically assumed to be the radius of a water molecule. Here, the $\Delta\Delta G_{tr}$ values were corrected for the accessibility of each residue. The correlations between them were poor, but these results show that cavity detection was highly dependent on the probe radius (Hubbard & Argos, 1995).

The $\Delta\Delta G$ values for mutations in the hydrophobic core of chymotrypsin inhibitor 2 correlate with the packing density (the number of methylene groups within 6 Å of the removed atoms) (Jackson et al., 1993),

and the partly exposed minicore correlates with a mixture of the ASA and the packing density (Otzen et al., 1995). In the case of the human lysozyme mutants, the correlation between the packing density and $\Delta\Delta G$ is shown in Figure III-7(c). The correlation with only the mutants in the interior of the protein was poor, and the data were far from the line (the dotted line in Figure III-7(c)) obtained from barnase and chymotrypsin inhibitor 2 (Otzen et al., 1995).

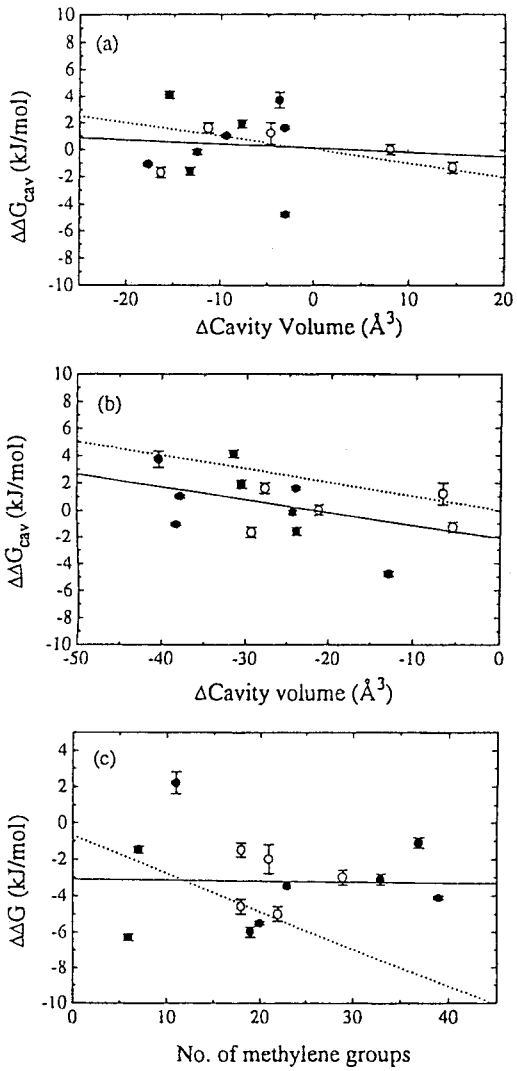

Figure III-7. Correlation of cavity volume and packing density with the thermodynamic parameters of denaturation for the mutant proteins. Val → Ala mutants are shown as solid circles and Ile → Val as open circles. The continuous lines show the linear regression of all the proteins. (a) $\Delta\Delta G_{cav}$ (= $\Delta\Delta G$ - $\Delta\Delta G_{tr}$) and the difference in the total cavity volume between each mutant protein and the wild-type structure using the probe size 1.20 Å (Connolly, 1983, 1993). (b) $\Delta\Delta G_{cav}$ (= $\Delta\Delta G$ - $\Delta\Delta G_{tr}$) and the difference in the total cavity volume between each mutant protein and the wild-type structure using the probe size 1.40 Å (Connolly, 1983, 1993). The $\Delta\Delta G_{tr}$ values in Figures (a) and (b) are corrected by the accessibility of each residues. The dotted lines in Figures (a) and (b) indicate that proposed by Eriksson et al. (1992). (c) $\Delta\Delta G$ and the packing density (number of methylene groups within 6 Å of the removed atoms). The dotted line shows the best fit of the barnase and chymotrypsin inhibitor 2 data to a linear equation obtained by Otzen et al. (1995).

Correlation of ΔH with $\Delta\Delta ASA_{HP}$

There are only a few data on the differences in the enthalpy changes ($\Delta\Delta H$) between wild-type and mutant proteins. One reason may be the large error in measurements for ΔH. As described in Chapter II, to minimize the error we measured at several pHs for each protein and determined the thermodynamic parameters at the temperature (near 65 °C) where the ΔH values were obtained directly by the measurements. The plots of T_d vs. ΔH (not shown) indicate the obvious differences between proteins.

No attempt has been made previously to correlate $\Delta\Delta H$ values with changes in the accessibility of mutant proteins. Makhatadze & Privalov (1995) have estimated that the enthalpy change ($\Delta H^{vdW} + \Delta H^{hyd}$) of non-polar atoms at 65 °C using a model compound is 80 J/mol Å^2. The correlation between the denaturation enthalpies of the mutant human lysozymes and $\Delta\Delta ASA_{HP}$ of each mutation site is shown in Figure III-8(a). The comparison with the total structural changes including the Ile mutant lysozymes (Figure III-8(b)) showed better correlation than with the local ones. However, the correlation coefficient is still low (0.56). This suggests that other factors which are particular for each position of a protein also affect the enthalpy change of denaturation.

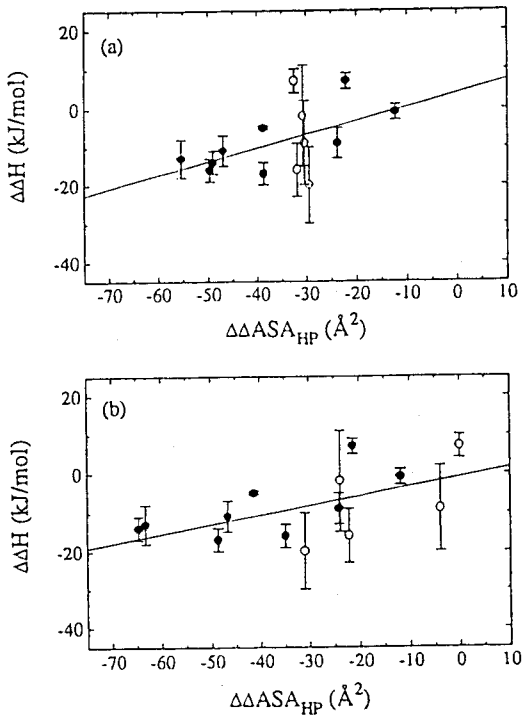

Figure III-8. Correlation of changes in hydrophobic surface area exposed upon denaturation ($\Delta\Delta ASA_{HP}$) with enthalpy changes of denaturation for the mutant proteins at 64.9 °C ($\Delta\Delta H$). Val → Ala mutants are shown as solid circles and Ile → Val as open circles. The continuous lines show the linear regression of all the proteins. (a) $\Delta\Delta H$ and the difference in ΔASA for each substituted residue using the wild-type and the mutant structure (correlation coefficient = 0.49). (b) $\Delta\Delta H$ and the difference in ΔASA for all of the hydrophobic residues using the wild-type and the mutant structure (correlation coefficient = 0.56).

Chapter IV

Studies on the Five Ala and Two Gly Substitutions for Ile of Human Lysozyme[+]

Introduction

The interior of globular proteins is well packed (Richards, 1977). However, the packing is not always perfect. Some cavities exist in protein structures (Rashin et al., 1986). Studies of cavity-forming mutant proteins have shown that the empty cavity destabilized the protein (Eriksson et al., 1992; Buckle et al., 1996). Moreover, cavities frequently contain water molecules (Rashin et al., 1986; Kossiakoff et al., 1992; Ernst et al., 1995), and cavities engineered by mutation occasionally contain water molecules (Fitzgerald et al., 1994; Pederson et al., 1994; Buckle et al., 1996; Matthews, 1996; Chapter II). There is a question as to whether water molecules in the interior of a protein stabilize or destabilize the protein structure.

The effect of buried water molecules on protein stability has been studied using (1) cavity-filling mutants to remove buried water molecules and (2) cavity-creating mutants to introduce buried water molecules. Although several studies have been reported, there are conflicting views regarding the effect of the buried water molecules on the protein stability. In the first case, yeast iso-1-cytochrome *c* (Das et al., 1989; Hickey et al., 1991; Lett et al., 1996) and neutral protease (Vriend et al., 1991) have increased stability, but

---

[+] This work is published, titled "Contribution of Water Molecules in the Interior of a Protein to the Conformational Stability" (Takano et al., 1997b).

BPTI (Berndt et al., 1993) and subtilisin (Pedersen et al., 1994) have decreased stability resulting from the removal of water molecules. In the second case, the water molecule introduced in V149A of T4 lysozyme has been regarded as the reason for the unexpectedly large loss of stability (Matthews, 1996), but the presence of the water molecule in I76A mutant of barnase has been considered as having a stabilizing effect (Buckle et al., 1996). In order to understand the role of buried water molecules in the stability of proteins, it will be useful to more precisely examine the environment surrounding buried water molecules.

We have reported studies on the structure and stability of 14 hydrophobic mutant human lysozymes in which Ile or Val were substituted by Val or Ala, respectively (Chapters II and III), including I59V with a buried water molecule in the cavity created by the mutation. It was found that the correlation between $\Delta\Delta G$ (changes in stability) and $\Delta\Delta ASA_{HP}$ (changes in hydrophobic surface area exposed upon denaturation) is good for the hydrophobic cavity-creating mutants, if the effect of the secondary structural propensity is taken into account (Chapter III). This systematic analysis should be useful to estimate the contribution of introduced water molecules to protein stability, because changes in the total hydrophobic surface area of the protein due to mutations have been considered.

In this chapter, we focused on Ile to Ala or Gly (I23A, I56A, I59A, I89A, I106A, I56G and I59G) mutants of human lysozyme, in which a larger hydrophobic side-chain was replaced by a smaller one and a cavity was created at each mutation site. All five Ile residues in human lysozyme are almost completely buried in the native structure. Ile23, 56, 89 and 106 are in turn/loops and Ile59 is in a β-sheet. We solved the mutant structures, except

for I56G, by X-ray crystallography and determined the thermodynamic parameters of denaturation using DSC (differential scanning calorimetry). These data have important implications for the understanding of the hydrophobic effect with regard to protein stability.

Material and Methods

Mutant proteins

Mutagenesis, expression and purification of the Ile to Ala/Gly mutant human lysozymes were performed as described in Chapter II. DNA sequence analysis was carried out using an automated DNA sequencer (Applied Biosystems Inc.) at the Research Center for Protein Engineering, Institute for Protein Research, Osaka University.

X-ray crystallography

Mutant human lysozymes were crystallized, diffraction data collected, and the structures refined (Brunger, 1992) as described in Chapter II. For I23A, the crystal was small (0.1 mm x 0.1 mm x 0.3 mm). The data set was collected using synchrotron data at the Photon Factory (Tsukuba); this made use of the Weissenberg camera (Sakabe, 1991) on beam line 6B. The data was processed with DENZO (Otwinowski, 1990). All the crystals belong to the space group $P2_12_12_1$.

The coordinates of the six mutant human lysozymes, I106A, I23A, I56A, I59A, I59G and I89A, have been deposited in the Brookhaven Protein Data Bank, accession nos, 2HEA to 2HEF.

DSC measurements

Calorimetric measurements and data analyses were carried out as described in Chapter II. The thermodynamic parameters for denaturation as a function of temperature were calculated using Equations I-4 to I-6.

Results

Structures of mutant human lysozymes

Table IV-1 shows X-ray data collection and refinement statistics for Ile to Ala/Gly mutant human lysozymes, except for I56G. All mutant structures determined were essentially identical to the wild-type structure. However, we have shown that the substitutions in Ile to Val and Val to Ala mutant human lysozymes affected not only the mutation sites but also other parts far from the sites, although the structural changes were not great (Chapters II and III). Therefore, when investigating the relationship between changes in thermodynamic parameters and structures due to mutations, we should also consider subtle structural changes by rearrangements of the overall structure.

The mutations at positions 56 and 89 in the same core and at position 23 in another core caused small structural changes around each mutation site. The mean rms deviations for main-chain atoms within 6 Å from C^{α} at each substitution residue (position 23, 56 or 89) between the wild-type and mutant structures were 0.22, 0.08 and 0.14 Å, respectively. The cavities created in the I23A, I56A and I89A structures remained empty. In contrast, new water molecules were found in the created cavities in I106A, I59A and I59G. The mean rms deviations within 6 Å from C^{α} at each substitution residue between the wild-type and mutant proteins of I106A, I59A, and I59G were 0.39, 0.26, and 0.27 Å, respectively. The water molecule in I106A made two hydrogen bonds[++] with the surrounding residues (Asp27 and Trp28) (Figure IV-1(a)). We have already observed an additional water molecule in the cavity of I59V (Chapter II). In the cases of I59A and I59G, each cavity contained two

additional water molecules (Wat1 and Wat2), resulting in the formation of a hydrogen bonding network with water molecules around the residue at position 59 (Figure IV-1(b) and (c)). The water molecules in I59A were equivalent to those in I59G. One (Wat1) of two waters was at the same position as that in I59V, the other (Wat2) was new. The Wat1 water molecules in I59A and I59G had three hydrogen bonds with the carbonyl oxygen of Ala92, one of the internal waters and the Wat2 water newly introduced. An internal water molecule having a hydrogen-bond with the side-chain of Trp64 in the wild-type structure made new hydrogen bonds with the Wat2 water molecules in I59A and I59G instead of that with Trp64. Consequently, the side-chain of Trp64 was not hydrogen bonded in the I59A and I59G structures.

Table IV-2 lists the volumes of the cavities occupied by water molecules, the number of internal water molecules in the cavities, and the number of hydrogen bonds made by each internal water molecule, in order to compare with the data from statistical surveys of naturally occurring cavities (Rashin et al., 1986; Hubbard et al., 1994; Williams et al., 1994). The mean cavity volume per water in a protein structure is reported to be 25.6 $Å^3$ and 94 % of cavity solvents are forming three or four hydrogen bonds (Hubbard et al., 1994). For the new cavities in I59A, I59G and I106A in the present study, the cavity volumes per water were 25.6, 32.6, and 42.2 $Å^3$, respectively. The water molecules detected in these cavities also participated in hydrogen-bonding with two or three atoms (Table IV-2).

[++] Hydrogen bonds between solvent molecule and protein molecule, or between solvent molecules are considered to be formed when the distances between the solvent oxygen and the protein atoms oxygen or nitrogen, or between the solvent oxygens are 2.4 to 3.5 Å.

Table IV-1. X-ray data collection and refinement statistics for Ile to Ala/Gly mutant human lysozymes.

	I23A	I56A	I59A	I89A	I106A	I59G
Data Collection						
Cell dimension (Å)						
a	56.80	56.73	56.97	56.75	56.99	57.12
b	61.22	61.04	60.36	60.97	60.90	60.87
c	33.76	33.80	33.51	33.74	33.77	33.70
Resolution (Å)	2.0	1.8	1.8	1.8	1.8	1.8
No. of measured reflections	21,591	35,090	33,207	36,537	29,620	35,373
No. of independent reflections	5,702	10,237	9,981	10,724	9,899	10,885
Completeness of data (%)	67.7	90.0	88.6	94.0	87.4	95.1
(outer shell)	(56.2)	(86.6)	(79.3)	(84.6)	(67.4)	(88.0)
$I/\sigma I$ of outer shell	5.7	5.7	4.8	7.3	2.8	5.7
R_{merge} (%)[a]	7.1	5.9	5.7	3.3	6.7	5.7
(outer shell)	(18.5)	(11.3)	(15.5)	(8.5)	(16.2)	(13.1)
Refinement						
No. of atoms	1,258	1,214	1,227	1,198	1,205	1,219
No. of solvent atoms	232	188	201	172	179	194
Resolution range (Å)	8-2.2	8-1.8	8-1.8	8-1.8	8-1.8	8-1.8
No. of reflection used	4,109	9,879	9,604	10,128	9,111	10,518
Completeness of data (%)	66.3	88.0	86.8	90.4	81.1	93.5
R factor[b]	0.124	0.153	0.157	0.160	0.156	0.160
r.m.s.d. bond (Å)	0.008	0.008	0.009	0.009	0.009	0.009
r.m.s.d. angle (°)	1.52	1.49	1.46	1.52	1.56	1.50
rmsd *B*-factor (main-chain) (Å^2)	1.7	1.3	1.3	1.2	1.5	1.2
rmsd *B*-factor (side-chain) (Å^2)	2.9	2.8	2.8	2.9	3.2	2.9

[a] $R_{merge} = 100\ \Sigma\ |\ I_{h,i} - \langle I_h \rangle\ |\ /\ \Sigma\ I_{hi}$. $I_{h,i}$ are individual values, and $\langle I_h \rangle$ is the mean value of the intensity of reflection *h*.

[b] *R* factor = $\Sigma||F_o| - |F_c|| / \Sigma|F_o|$.

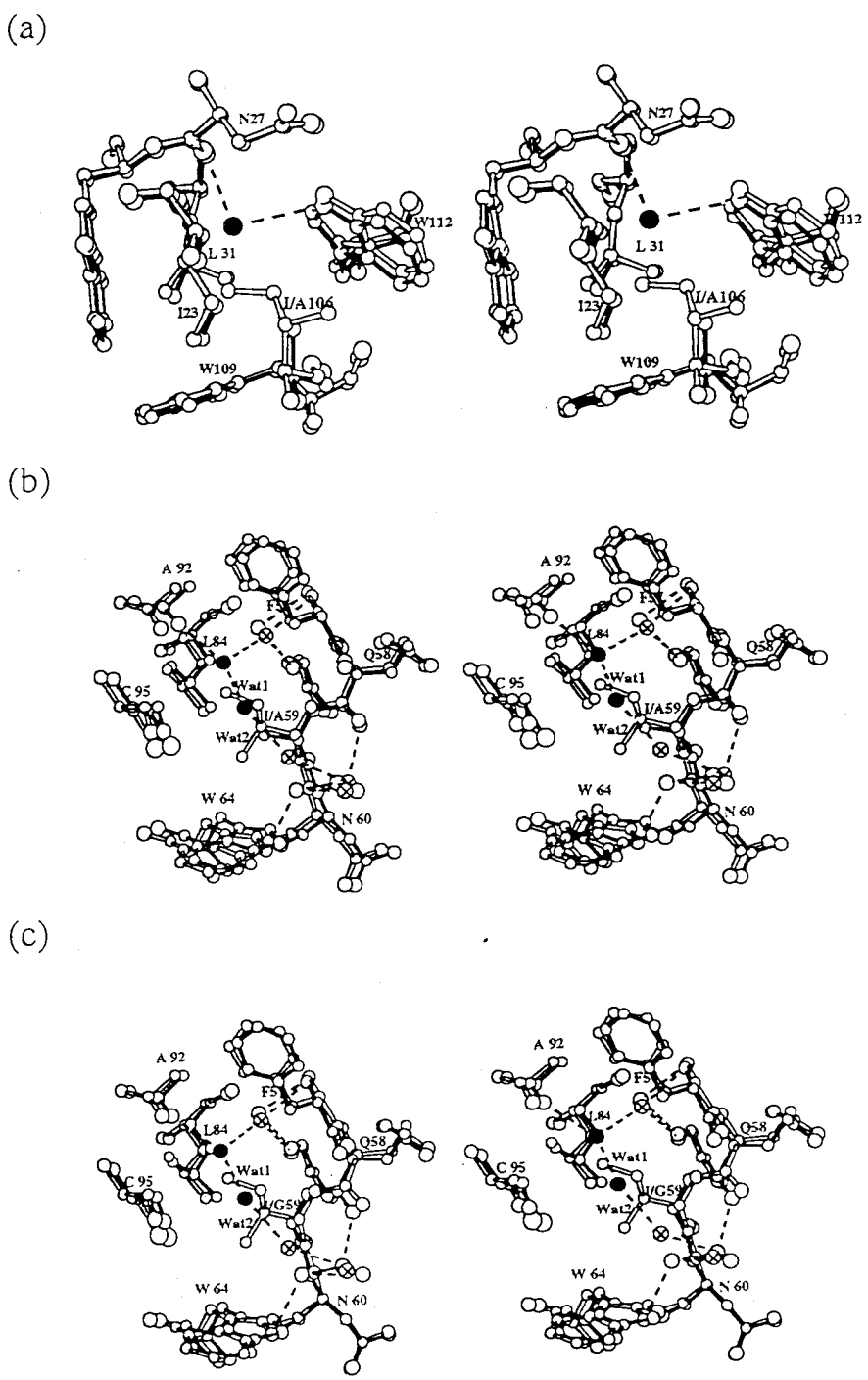

Figure IV-1. Stereodrawings (Johnson, 1976) showing the structure in the vicinity of the mutation site. The wild-type (open bonds) and typical mutant structures (filled bonds) are superimposed. Panels (a) to (c) represent I106A, I59A and I59G, respectively. Solvent water molecules are drawn as open circles (wild-type), crossed circles (mutants), and solid circles (introduced in mutants). The broken lines indicate hydrogen bonds.

Table IV-2. Structural characteristics of solvated cavity at the substitution sites of the mutant human lysozymes.

	Cavity volume[a] ($Å^3$)	No. of internal water molecules	No. of hydrogen bonds made by each internal water molecules		
				with protein atoms	with internal waters
I59A	51.1	2	Water 1	1	2
			Water 2		2
I59G	65.1	2	Water 1	1	2
			Water 2		2
I106A	42.2	1		2	

[a] Cavity volume was calculated using the procedure of Connolly (1993) with a probe radius 1.4 Å. Water molecules were removed from the structure for the purpose of calculating cavity volume.

Stability of mutant human lysozymes

DSC measurements of Ile to Ala/Gly mutant human lysozymes were carried out at acidic pHs (pH 2.5 to 3.1) where the denaturation of human lysozyme is reversible. Table IV-3 shows the denaturation temperature (T_d), the calorimetric enthalpies (ΔH_{cal}), the van't Hoff enthalpies (ΔH_{vH}), and the heat capacity changes (ΔC_p) of each measurement for the mutant proteins. Since the secretions in yeast of I23A and I56G were about twenty and fifty times lower, respectively, than that of the wild-type protein, only two and one measurements for I23A and I56G, respectively, could be done. In the measurement of I56G, only the peak temperature of denaturation was determined because the protein concentration was low (about 0.3 mg/ml). The thermodynamic parameters of denaturation at a constant temperature, 64.9 °C, and pH 2.7 were calculated using these data as shown in Table IV-4. All mutants were destabilized relative to the wild-type protein, but the decrease in the stability was quite different among the mutant proteins. The mutants with the additional water molecules in the created cavities, I59A and I106A were destabilized less than the other Ile to Ala mutants.

To examine the role of a methylene group in conformational stability, the $\Delta\Delta G$ values associated with the removal of a methylene group at each Ile residue were recalculated. The substitutions from Val to Ala, Val to Gly, and Ala to Gly could be estimated from the differences between the observed data of Ile to Val and Ile to Ala mutant proteins, of Ile to Val and Ile to Gly, and of Ile to Ala and Ile to Gly, respectively. The substitutions of Val to Ala at positions 59 and 106 showed only small decreases in the stability (Table IV-5). This means that the water molecules introduced in the cavities of the I59A and I106A structures compensate for the destabilizations of Val59 →

Ala and Val106 → Ala substitutions.

The calorimetric enthalpy changes ranged from 441 to 480 kJ/mol, for the mutant proteins with the additional water molecules (Table IV-4). This range was equivalent to that for the mutants with empty cavities, including Ile to Val and Val to Ala mutants, from 440 to 484 kJ/mol (Chapters II and III). We detected no effect of introduced water molecules on the enthalpy term.

Table IV-3. Thermodynamic parameters for denaturation of Ile to Ala/Gly mutant human lysozymes at different pHs.

	pH	T_d (°C)	ΔH_{cal} (kJ/mol)	ΔH_{vH} (kJ/mol)	ΔC_p[a] (kJ/mol K)
I23A	2.96	62.0	439	464	4.5
	2.67	56.2	410	431	6.3
					5.4 ± 0.9
I56A	3.08	60.2	413	427	6.0
	2.96	58.5	405	427	6.7
	2.81	54.2	379	385	6.1
	2.67	52.3	372	382	6.4
	2.50	48.2	346	351	5.1
					6.1 ± 0.6
I59A	3.12	66.5	485	510	7.8
	2.98	64.5	481	502	6.8
	2.80	61.5	460	481	5.0
	2.66	59.1	444	477	5.0
	2.49	55.9	423	452	3.5
					5.6 ± 1.7
I89A	3.09	62.9	444	460	6.3
	2.95	61.1	431	452	7.0
	2.80	57.7	409	431	4.5
	2.66	55.4	389	410	5.8
	2.50	52.6	374	399	7.2
					6.2 ± 1.1
I106A	3.10	69.7	469	498	6.6
	2.96	67.4	456	477	4.9
	2.80	64.1	435	464	4.1
	2.66	61.3	418	452	5.7
	2.51	57.7	403	427	4.8
					5.2 ± 1.0
I56G	2.73	62.7	-	-	-
I59G	3.16	60.4	419	427	3.4
	3.02	59.2	412	418	3.6
	2.82	54.6	396	408	2.7
	2.70	52.0	380	388	2.6
	2.49	48.1	353	375	3.3
					3.1 ± 0.4

[a] ΔC_p was obtained from each calorimetric curve.

Table IV-4. Thermodynamic parameters for denaturation of Ile to Ala/Gly mutant human lysozymes at the denaturation temperature (64.9°C) of the wild-type protein at pH 2.7.

	T_d (°C)	ΔT_d (°C)	ΔC_p[a] (kJ/mol K)	ΔH_{cal} (kJ/mol)	$\Delta\Delta G$ (kJ/mol)	$\Delta H_{cal}/\Delta H_{vH}$
Wild-type[b]	64.9 ± 0.5		6.6 ± 0.5	477 ± 4	(0)	0.95
I23A	56.8	-8.1	5.0	454	-10.6	0.94
I56A	52.4 ± 0.4	-12.5	5.6 ± 0.2	440 ± 2	-15.5 ± 0.5	0.95
I59A	59.7 ± 0.2	-5.2	6.1 ± 0.4	480 ± 4	-7.2 ± 0.3	0.95
I89A	56.2 ± 0.3	-8.7	6.9 ± 0.2	458 ± 2	-11.3 ± 0.4	0.97
I106A	61.9 ± 0.3	-3.0	5.6 ± 0.3	441 ± 2	-3.9 ± 0.4	0.94
I59G	52.2 ± 0.6	-12.7	5.2 ± 0.5	444 ± 5	-16.0 ± 0.8	0.97

[a] ΔC_p was obtained from the slope of ΔH_{cal} against T_d.

[b] Chapter II

Table IV-5. $\Delta\Delta G$ values for mutant human lysozymes at 64.9 °C. (kJ/mol)

Position	Ile → Val[a]	Val → Ala[b]	Ile → Ala
23	-1.5	-9.1	-10.6
56	-5.0	-10.5	-15.5
59	-4.6	-2.6	-7.2
89	-2.0	-9.3	-11.3
106	-3.0	-0.9	-3.9

	Ile → Gly	Val → Gly[c]	Ala → Gly[d]
59	-16.0	-11.4	-8.8

[a] Chapter II.
[b] Difference between the data of mutants of Ile → Val and Ile → Ala.
[c] Difference between the data of mutants of Ile → Val and Ile → Gly.
[d] Difference between the data of mutants of Ile → Ala and Ile → Gly.

Discussion

Cavity created in mutant proteins

In a well-defined crystal structure, atoms (including solvent) with *B*-factors in the range 0-40 $Å^2$ are usually well defined. When the *B*-factor exceeds about 60 $Å^2$, the atom is sufficiently mobile or disordered that it can no longer be seen reliably in electron density maps (Matthews, 1993). The *B*-factors of the Wat1 and Wat2 waters of I59A, the Wat1 and Wat2 waters of I59G, and the additional water in I106A were 12.6, 20.7, 14.7, 26.1 and 46.5 $Å^2$, respectively. These water molecules were clearly detected in both $2F_o - F_c$ and $F_o - F_c$ electron density maps, but there was no electron densities in the created cavities of the other mutant proteins including Ile to Val and Val to Ala mutants (Chapters II and III).

Statistical studies of cavities in protein structure (Rashin et al., 1986; Hubbard et al., 1994; Williams et al., 1994; Buckel et al., 1996) have shown that cavities usually have some polar surface and most buried waters form hydrogen bonds with protein atoms. In the I23A, I56A and I89A mutant human lysozymes, which had no water molecules in the cavities created, there were some polar atoms surrounding each cavity. For example, the hydroxyl group of Ser36 was 3.57 Å distant from the $C^{\gamma 1}$ atoms of Ile56, and the oxygen atom of an interior water was 3.42 Å from $C^{\gamma 2}$ of Ile56 in the wild-type structure. In the structure of an amyloidogenic mutant human lysozyme (I56T), the $O^{\gamma 1}$ atom of Thr56 has formed a hydrogen bond with the internal water molecule (Funahashi et al., 1996).

Using the program, X-PLOR (Brunger, 1992), we searched to see if water molecules could form hydrogen bonds in the cavities created in the

mutant structures and the model mutant structures generated by deleting the methylene groups based on the coordinate of the wild-type structure. The calculation was carried out as following. (1) A ghost water molecule was introduced in the mutant and model structures at the position of $C^{\gamma 1}$, $C^{\gamma 2}$, or $C^{\delta 1}$ atoms of each Ile residue in the wild-type structure. (2) Only the water was energy-minimized. (3) Water molecule with low energy was searched. For all of the cavities created at the substitution sites of I23A, I56A and I89A, suitable sites for water molecules were detected. Figure IV-2 represents the structures in the vicinity of residue 56 in the wild-type (a) and I56A (b) to (d), for example, and those of the residue 59 in the wild-type (e) and I59A (f), for reference. The detected water molecules (dummy waters), which made hydrogen bonds with O^{γ} of Ser36 and an internal water molecule, respectively, are drawn in Figures IV-2(c) and (d). Although polar atoms capable of hydrogen bonding with water molecules exist in the cavities, we could not find water molecules in the created cavities in the case of I56A. A molecular dynamic study has suggested that the free energy of introduction of water into an empty cavity may be unfavorable, (Wade et al., 1991), supporting the empty cavity in the case of I56A. It should be pointed out that cavities in which a water molecule can not be detected via X-ray crystallography may still be solvated, at least transiently (Ernst et al., 1995).

We also calculated the size of the cavities in the real mutant structures and model mutant structures created by deleting side-chain methylene groups based on the coordinate of the wild-type structure. This was done by attempting to insert a probe sphere of a given radius (Connolly, 1993) to examine whether there is enough space for water occupancy. For I106A, I59A and I59G which contain water molecules in the created cavities, the

structures with the water molecules removed were used. As shown in Table IV-6, only the mutant proteins containing additional water molecules were found to have large cavities detected with a probe radius 1.6 Å, which is larger than that typically assumed to be the radius of a water molecule (1.4 Å). This indicates that a cavity volume exceeding the theoretical minimum is necessary for introducing water molecules.

Table IV-6. Cavity volume of the model and mutant structures

	Cavity volume at substitution site (Å^3)					
	Model			Mutant		
Probe size	1.4 Å	1.5 Å	1.6 Å	1.4 Å	1.5 Å	1.6 Å
I23A	a	a	a	a	a	a
I56A	78.4	49.1	a	51.3	18.7	a
I59A	57.2	51.1	32.7	51.1[b]	45.0[b]	38.1[b]
I89A	43.3	23.5	a	15.6	a	a
I106A	62.7	45.9	39.7	42.2[b]	36.3[b]	32.0[b]
I56G	129.9	120.1	112.3	-	-	-
I59G	94.4	84.2	77.5	65.1[b]	59.8[b]	55.6[b]

[a] Cavity was not detected.

[b] Water molecules were removed from the structure for the purpose of calculating cavity volume.

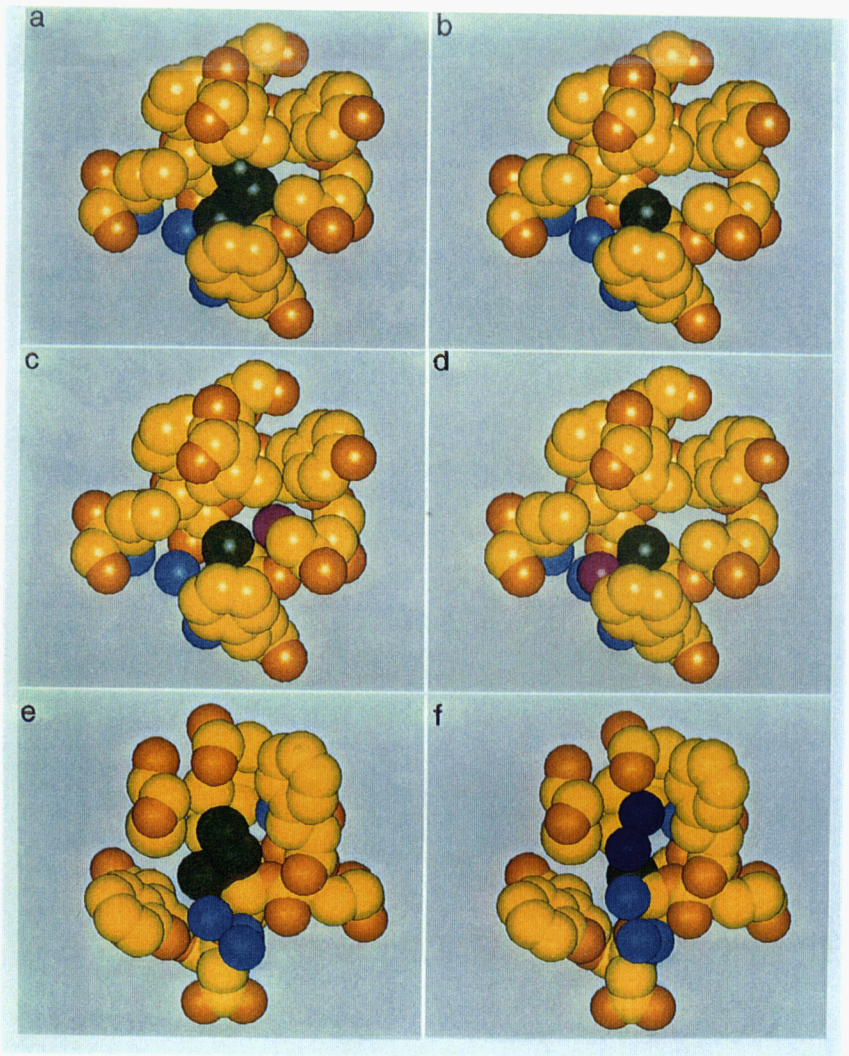

Figure IV-2. Structures in the vicinity of the residue 56 in the wild-type (a) and I56A (b) to (d), and those of the residue 59 in the wild-type (e) and I59A (f). In panels (c) and (d), dummy waters, which were estimated to be energetically favorable using the program, X-PLOR (Brunger, 1992), are drawn. The dummy waters in panels (c) and (d) made hydrogen bonds with O^{γ} of Ser36 and an internal water molecule, respectively. The side-chain atoms of the residues 56 and 59, carbon atoms, oxygen and nitrogen atoms, interior waters, introduced waters and the dummy water molecules are represented by green, yellow, orange, blue, dark blue and purple, respectively.

Contribution of hydrophobic effect to protein stability

The substitutions of Ile → Val → Ala → Gly might remove hydrophobic effect without introducing new interactions. We have investigated the contribution of the hydrophobic effect to the protein stability using the five Ile to Val and the nine Val to Ala mutants of human lysozyme (Chapters II and III), and found a correlation between $\Delta\Delta G$ (differences between species of denaturation Gibbs energy change) and $\Delta\Delta ASA_{HP}$ (differences between species of the hydrophobic surface area exposed upon denaturation) for the hydrophobic cavity-creating mutants, if the effect of the secondary structural propensity was taken into account (Chapter III). $\Delta\Delta ASA_{HP}$ can be calculated by Equation III-1.

In this correlation, the mutations used are divided into three types, according to the differences in the secondary structural propensities of amino acids by the mutations (Chou & Fasman, 1978). Type I is for the mutations of Val to Ala in α-helices (represented by black in Figure IV-3), that is, mutations for which the secondary structural propensity would be expected to increase the stability of the protein, Type II is for the mutations of Ile/Val to Ala/Gly at β-sheet (blue), that is, mutations for which the secondary structural propensity would be expected to decrease the stability of the protein, and Type III includes the mutations at turn/loop and the mutations of Ile to Val and Ala to Gly at β-sheet (red), which are insensitive to the secondary structural propensity.

We examined the correlation between $\Delta\Delta G$ and $\Delta\Delta ASA_{HP}$ for the hydrophobic mutations (Figure IV-3(a)). The substitutions of I23A, V23A, I56A, V56A, I89A, V89A and A59G with no water molecules in the cavities created belonging to the type III were represented by the red solid squares in

Figure IV-3(a). There was a good correlation, yielding Equation IV-1 (red continuous line in Figure IV-3).

$$\Delta\Delta G \text{ (kJ/mol)} = 0.12\ (\pm 0.01)\ \Delta\Delta ASA_{HP}\ (\text{Å}^2) - 0.87\ (\pm 0.80)$$
(correlation coefficient of 0.94 for 14 points) (IV-1)

The value of the slope in this correlation, 0.12 kJ/mol Å^2, was comparable with that of accessible surface areas of amino acid side-chains plotted against hydrophobicity, 0.10 kJ/mol Å^2, estimated by Chothia (1974). This correlation should be useful for estimating contribution of the water molecules introduced in the mutants to the protein stability.

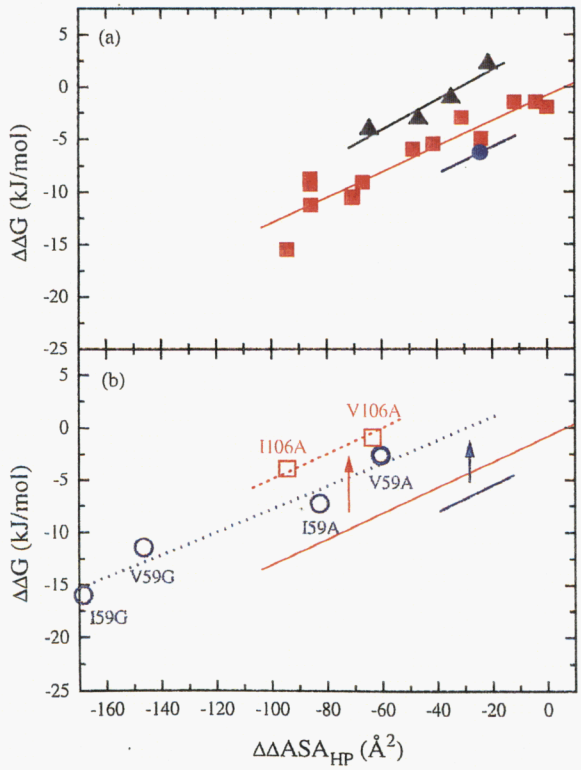

Figure IV-3. Correlation of $\Delta\Delta ASA_{HP}$ (changes in hydrophobic surface area exposed upon denaturation) with $\Delta\Delta G$ for the mutant proteins with empty cavities (a) and with solvated cavities (b). The mutants with solvated cavities are shown as open symbols and labeled. The mutants of the type I are represented by black solid up-triangles (with empty cavity). The black continuous line shows the linear regression of the type I mutants with empty cavity (black solid up-triangles). The mutants of the type II are represented by blue solid (with empty cavity) and open (with solvated cavity) circles. The blue broken line shows the linear regression of the type II mutants with solvated cavity (blue open circles). The mutants of the type III are represented by red solid (with empty cavity) and open (with solvated cavity) squares. The red continuous line shows the linear regression of the type III mutants with empty cavity (red solid squares). The red broken line is drawn with reference to the red continuous line. The ASA values were calculated using the procedure of Connolly (1993).

Contribution of introduced water molecules to protein stability

The factors stabilizing protein structures, such as hydrophobic effects, electrostatic interactions and hydrogen bonds, have been extensively analyzed by studies with site-directed mutagenesis (e.g., Yutani et al, 1987, Serrano et al., 1990, Dao-pin et al., 1991). Studies of the contribution of buried water molecules to protein stability, however, are lacking. The contribution to conformational stability of buried water molecules introduced by cavity-creating mutations removing mainly hydrophobic interactions could be more reasonably estimated, than when bulkier side-chains are introduced, which usually cause strain and unfavorable van der Waals contacts (Karpusas et al., 1989). A few observations on water molecules in created cavities have been reported (Chapter II; Buckle et al., 1996; Matthews, 1996). In this study, we studied three new mutants, I59A, I59G and I106A, with additional water molecules in the created cavities. We tried to estimate the contribution of the water molecules to the protein stability, using the correlation between $\Delta\Delta G$ and $\Delta\Delta ASA_{HP}$ of all of hydrophobic residues, so that subtle structural changes by rearrangements of the overall structure would be taken into account.

The mutant proteins with the additional water molecules did not obey the correlation obtained with the mutants with the empty cavities (Figure IV-3(b)). For I106A and V106A with one additional water molecule belonging to the type III, the decreases in the stabilities were smaller than those expected from their $\Delta\Delta ASA_{HP}$ values (red open squares in Figure IV-3(b)). However, the difference in the correlation between I106A and V106A corresponded to the difference in the hydrophobic effect between them (the slope of the red dashed line in Figure IV-3(b)). The expected $\Delta\Delta$G values of

I106A and V106A using $\Delta\Delta ASA_{HP}$ could be estimated from Equation IV-1 to be -12.2 and -8.5 kJ/mol, respectively. These values were about 8 kJ/mol smaller than measured values ($\Delta\Delta G$) of the mutant proteins.

Results similar to those at position 106 were also observed in I59A, V59A, I59G and V59G belonging to the type II (blue open circles in Figure IV-3(b)). The stabilities of these mutants were about 7 kJ/mol higher than those expected from their $\Delta\Delta ASA_{HP}$ values (as shown by the blue arrow). The substitutions of Ile59 $\rightarrow$ Ala/Gly stabilized the mutant proteins by two additional water molecules to the same degree as I106A and V106A stabilized by one additional water molecule. These results indicate that all water molecules do not contribute equally to stability, owing to differences in the environment of water molecules in proteins, such as the number of hydrogen bonds.

I56G was not so destabilized, as revealed by about 10 °C increase in the T_d value, as compared to I56A mutant protein at same pH (Table IV-3). Furthermore, the model structure of I56G had a large cavity volume detected with a probe radius 1.6 Å (Table IV-6). Although this crystal structure was unsolved, we would expect I56G to contain some additional water molecules within the cavity created, and/or other structural changes in the I56G structure minimizing the destabilization.

The change in stability ($\Delta\Delta G$) of I76A mutant barnase with an additional water molecule in the cavity is -7.9 kJ/mol, while the average $\Delta\Delta G$ value of other Ile/Leu to Ala mutant barnases is -16.0 kJ/mol (Buckle et al., 1996), indicating the favorable contribution of the water molecule to conformational stability of a protein. In the case of I59V in human lysozyme belonging to the type III, however, the water molecule introduced made little

contribution to the stability (Table IV-5). In the I59V structure, the side-chain conformation of Val59 has been quite different from the corresponding one of the parent Ile residue, due to the additional water molecule (Chapter II). The side-chain of Val59 in I59V would be a less stable conformation than that of Ile59 in the wild-type (Zimmerman et al., 1977). For the V149A mutant of T4 lysozyme, which contains a water molecule in the created cavity and is greatly destabilized (Matthews, 1996), unfavorable structural changes contributing to the conformational stability might be caused by the mutation, and the water molecule did not compensate for the destabilization due to the structural changes.

In the native state, hydrogen bonds are formed between the additional water molecules and polar atoms surrounding the cavity of the mutant proteins. Upon denaturation, their hydrogen bonds should still be satisfied by solvent waters. Thus the hydrogen bonds in the folded protein reduce the unfavorable cost of dehydrating polar groups in protein folding (Makhatadze & Privalov, 1993). On the other hand, when a water molecule is introduced in the interior of a protein, the decrease in entropy of transferring the water molecule from solvent to the interior of a protein corresponds to an unfavorable free energy cost, maximally 10 kJ/mol at 65 °C (Dunitz, 1994). Because the stabilization due to the introduced water molecules in the mutant human lysozymes was about 8 kJ/mol, hydrogen bonds (interaction) between the additional water molecules and polar atoms contributed maximally about 18 kJ/mol to the conformational stability. Funahashi et al. (1996) have previously estimated the contribution of a hydrogen bond in the interior between an internal water molecule and a polar atom at 23 kJ/mol.

For molecular dynamics simulations, Helms & Wade (1995) have

shown that hydration of cavity in the active site of cytochrome P450cam (1PHE) is favorable by 11.6 kJ/mol, and Zhang & Hermans (1996) have shown that free energies for transfer of water into cavities in the crystal structure of subtilisin (1CSE) are -13.0 to -50.2 kJ/mol.

Chapter V

Studies on the Five Val Substitutions for Ile and Nine Ala Substitutions for Val of Human Lysozyme Lacking a Disulfide Bond between Cys77 and Cys95[#]

Introduction

Human lysozyme is a globular protein with 130 residues and four disulfide bonds (Figure V-1). We have constructed systematic hydrophobic mutants of human lysozyme (Chapters II to IV), and found the correlation between $\Delta\Delta G$ and the changes in hydrophobic surface area exposed upon denaturation ($\Delta\Delta ASA_{HP}$) by considering the effects of secondary structure propensity (Chapter III) and water molecules in the cavity (Chapter IV). In this correlation, the coefficient of the correlation (slope; 0.12 kJ/mol Å^2) is comparable with that of accessible surface areas of amino acid side-chains plotted against the hydrophobicity of side-chains (0.10 kJ/mol Å^2) estimated by Chothia (1974). It is important to test empirically whether this correlation, hydrophobic effect to protein stability, is common to globular proteins. We focused on a series of hydrophobic mutants from a mutant human lysozyme with a great perturbation, C77A/C95A mutant human lysozyme (3SS).

The 3SS human lysozyme lacking one disulfide bond between Cys77 and Cys95 has been largely destabilized compared to the wild-type human lysozyme (4SS) (Kuroki et al., 1992a). The destabilization is caused by a great decrease in enthalpy (Kuroki et al., 1992a), although entropy in the denatured state could be expected to be increased due to the deletion of a disulfide bond. That is, (i) this protein is perturbed at both the native and denatured states, (ii) the differences in properties between the perturbed protein and the intact (wild-type) protein have been analyzed in detail as described above (Kuroki et al., 1992a), and (iii) the experiment results of both proteins could be compared at the same conditions using the same kind of mutations. Then, we constructed five Ile to Val and nine Val to Ala mutants (3SS mutants) from the 3SS protein, analyzed their conformational

stabilities using differential scanning calorimetry and their crystal structures at high resolution. The results were compared with those of the mutants (4SS mutants) from the 4SS protein (Chapters II to IV). The five Ile residues are almost completely buried in the folded protein. The side-chains of Val93, 99, 100, 121 and 125 are also mostly buried in the inside of the molecule. In contrast, the side-chains of Val2, 74 and 110 are mostly exposed to solvent in the native protein. Val130 is the C-terminal residue (Figure V-1).

Using the results obtained from DSC and X-ray analysis of the 3SS mutants, the correlation between $\Delta\Delta G$ and $\Delta\Delta ASA_{HP}$ for the 3SS and 4SS mutants was examined, and the contribution of the hydrophobic effect to the stability of proteins is discussed. Moreover, by comparison with the correlation for the mutants of T4 lysozyme (Eriksson et al., 1992; Baldwin et al., 1996), a generality of the correlation is also examined.

[#] This work is submitted to *J. Mol. Biol.*, titled "A General Rule for the Relationship between Hydrophobic Effect and Conformational Stability of a Protein: Stability and Structure of a Series of Hydrophobic Mutants of Human Lysozyme".

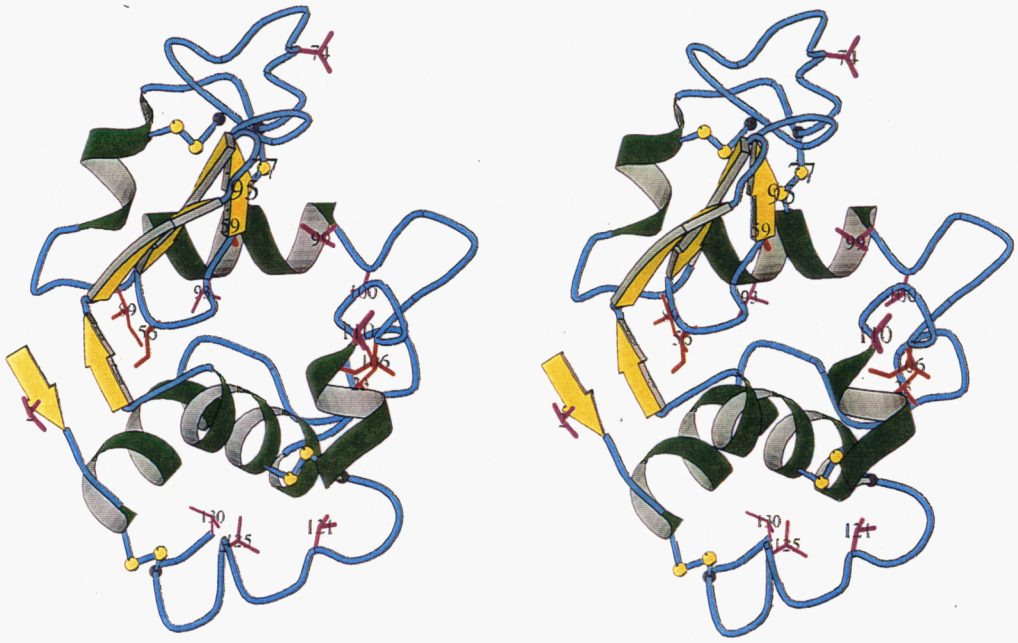

Figure V-1. Stereodrawing of the wild-type (4SS) human lysozyme structure. The yellow circles represent sulfur atoms of disulfide bonds, and Cys77 and Cys95 are labeled. The positions of the substituted Ile and Val residues are indicated. The structure was generated by the program MOLSCRIPT (Kraulis, 1991).

Material and Methods

Mutant proteins

Mutagenesis, expression and purification of the mutant human lysozymes were performed as described in Chapter II. The secretion of the 3SS human lysozyme was increased about five times than that of the wild-type in the yeast secretion system at 30 °C, as described previous report (Taniyama et al., 1988). I23V-3SS, V74A-3SS and V110A-3SS were also secreted effectively at 30 °C. For the other 3SS mutants, the efficient secretions were observed at lower temperature (20 to 25 °C), approximately depending on their stabilities. Then, we cultured the yeast at 30 °C for 3SS, I23V-3SS, V74A-3SS and V110A-3SS, at 25 °C for I59V-3SS, I89V-3SS, V93A-3SS, V99A-3SS, V100A-3SS and V130A-3SS, at 22 °C for I56V-3SS and I106V-3SS, and at 20 °C for V2A-3SS, V121A-3SS and V125A-3SS.

DSC measurements

Calorimetric measurements and data analyses were carried out as described in Chapter II. The thermodynamic parameters for denaturation as a function of temperature were calculated using Equations I-4 to I-6.

X-ray crystallography

The 3SS and 3SS mutant human lysozymes were crystallized, diffraction data collected, and the structures refined as described in Chapter II. All refinements were performed by the program X-PLOR (Brunger, 1992) using the coordinates of the wild-type structure for the 3SS structure and our

3SS model for the 3SS mutant proteins.

The coordinates of the mutant human lysozymes, I106V-3SS, I23V-3SS, I56V-3SS, I59V-3SS, I89V-3SS, V100A-3SS, V110A-3SS, V121A-3SS, V125A-3SS, V130A-3SS, V2A-3SS, V74A-3SS, V93A-3SS and V99A-3SS have been deposited in the Brookhaven Protein Data Bank.

Results

Differential scanning calorimetry (DSC) of 3SS and 3SS mutant human lysozymes

DSC measurements were performed to investigate the thermodynamic parameters for denaturation of the 3SS and 3SS mutant lysozymes at acidic pHs between 2.5 and 3.2. In this pH region, the denaturation of the 3SS protein is reversible (Kuroki et al., 1992a). Figure V-2 shows typical excess heat capacity curves at pH 3.1 for 3SS, I56V-3SS, 4SS (wild-type) and I56V (Chapter II). The 3SS proteins are destabilized compared to the 4SS proteins. For each of the proteins considered in this study, the values of denaturation temperature (T_d), calorimetric enthalpy (ΔH_{cal}), and van't Hoff enthalpy (ΔH_{vH}) of denaturation obtained from an analysis of the DSC curves are shown in Table V-1. The data for 3SS human lysozyme agree with those reported previously (Kuroki et at., 1992a). The T_d values are sensitive to pH and increase linearly with pH for all the proteins measured, as shown in Figure V-3(a). The heat capacity changes (ΔC_p) of denaturation were obtained from the slopes of plot of ΔH_{cal} against T_d (Figure V-3(b)).

The thermodynamic parameters for denaturation of the 3SS proteins at the denaturation temperature of the 3SS protein, 49.2 °C, and at pH 2.7 were calculated as shown in Table V-2. To obtain the most reliable thermodynamic parameters, 49.2 °C was chosen as an intermediate temperature within the range of experimental data with high accuracy for all the proteins examined (Table V-1). It minimizes errors that could result from too long a temperature extrapolation. The effects of the mutations, Ile to Val or Val to Ala, on the stability were different in each mutant protein even for

the same kind of substitution. The $\Delta\Delta G$ values for the 3SS mutants ranged from +0.3 to -7.3 kJ/mol, but for the 4SS mutants, the $\Delta\Delta G$ values ranged from +2.2 to -6.3 kJ/mol at 64.9 °C (Chapters II and III) (Table V-3).

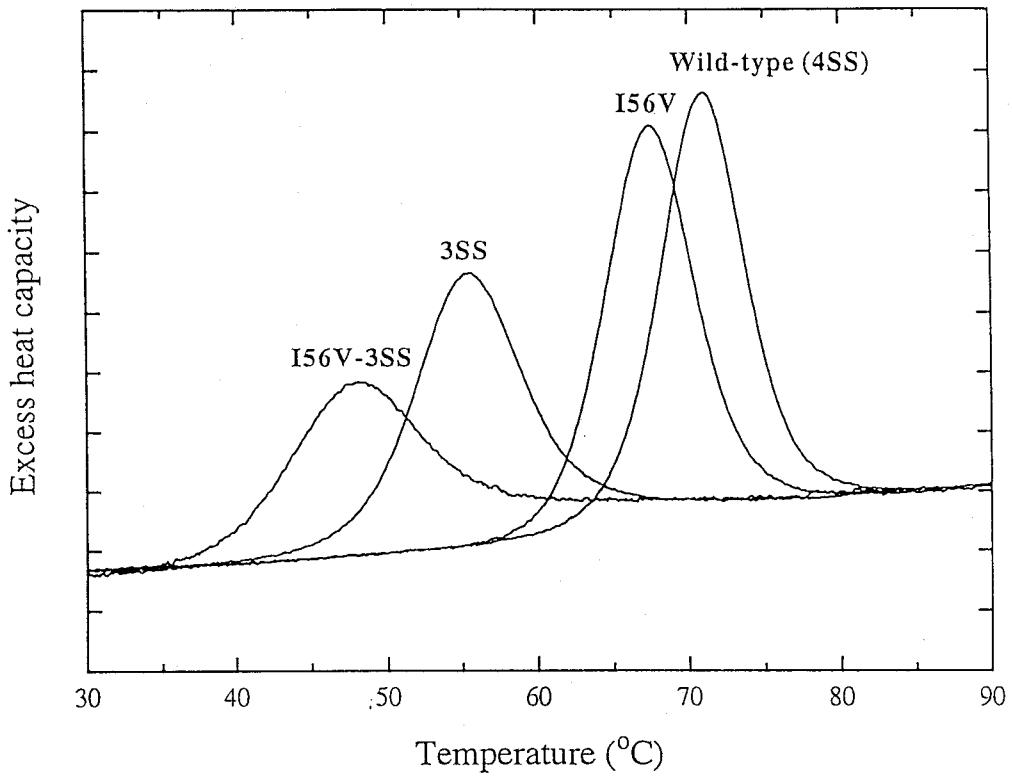

Figure V-2. Typical excess heat capacity curves of the wild-type (4SS), I56V, 3SS and I56V-3SS human lysozymes at pH 3.1. The increments of excess heat capacity were 10 kJ/mol K.

Table V-1. Thermodynamic parameters for denaturation of 3SS, Ile→Val-3SS and Val→Ala-3SS mutant human lysozymes at different pHs.

	pH	T_d (°C)	ΔH_{cal} (kJ/mol)	ΔH_{vH} (kJ/mol)		pH	T_d (°C)	ΔH_{cal} (kJ/mol)	ΔH_{vH} (kJ/mol)
3SS	3.14	57.8	403	407	V93A-3SS	3.16	52.5	342	361
	3.04	55.4	383	397		3.02	50.1	324	347
	2.81	52.0	359	373		2.88	47.7	306	334
	2.70	49.2	345	357		2.70	45.2	297	323
	2.53	45.5	315	327		2.50	41.2	268	297
I23V-3SS	3.09	55.0	381	397	V99A-3SS	3.10	52.6	295	308
	2.96	52.3	357	373		3.02	51.0	288	302
	2.78	49.6	349	359		2.85	48.2	281	295
	2.66	46.7	319	336		2.72	45.3	260	275
	2.49	43.5	292	312		2.54	41.4	234	249
I56V-3SS	3.10	50.5	311	327	V100A-3SS	3.15	54.4	342	354
	3.00	48.2	290	305		3.02	52.0	325	341
	2.80	45.3	279	297		2.90	49.9	303	331
	2.70	42.6	266	273		2.72	46.8	288	307
						2.51	43.5	257	293
I59V-3SS	3.10	52.0	315	329					
	3.00	50.3	310	318	V110A-3SS	3.13	57.2	390	390
	2.81	46.9	282	297		3.00	55.0	372	389
	2.68	44.3	263	280		2.87	52.5	359	366
						2.73	50.0	347	349
I89V-3SS	3.10	53.8	365	369		2.55	46.8	321	326
	2.96	51.8	344	368					
	2.78	48.4	323	344	V121A-3SS	3.14	50.1	281	303
	2.66	45.5	300	320		3.00	47.0	257	282
	2.49	42.5	276	301		2.86	43.6	242	262
						2.72	40.3	224	238
I106V-3SS	3.10	51.3	308	326					
	3.00	49.5	295	316	V125A-3SS	3.17	50.8	339	346
	2.79	46.0	276	292		3.02	47.9	319	326
	2.70	43.6	250	279		2.87	45.9	302	319
						2.72	42.8	281	295
V2A-3SS	3.10	48.3	272	295		2.53	38.7	261	268
	3.02	47.3	259	282					
	2.71	41.4	228	252	V130A-3SS	3.09	52.5	352	377
						2.97	49.9	335	360
V74A-3SS	3.16	54.8	345	361		2.82	47.0	305	331
	3.03	52.8	331	361		2.69	43.8	292	305
	2.85	50.1	311	338		2.50	40.4	255	283
	2.69	47.5	299	316					
	2.51	43.9	274	292					

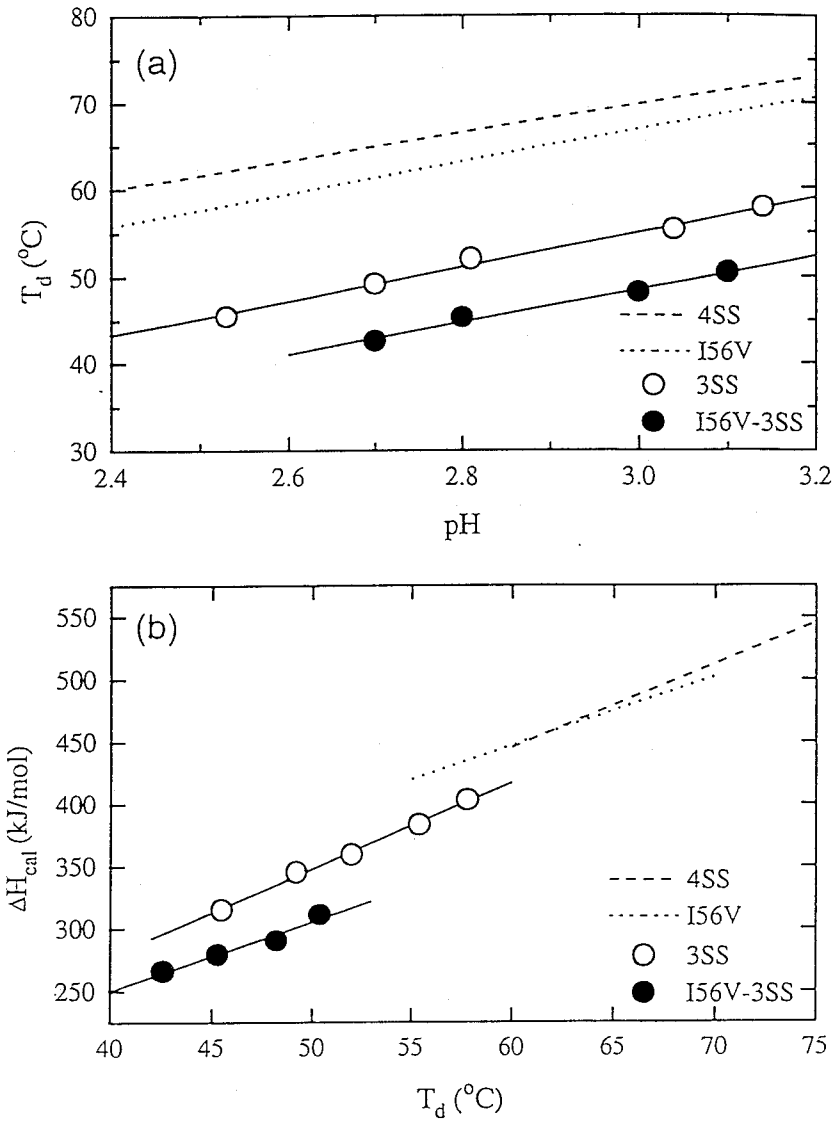

Figure V-3. (a) The denaturation temperature versus pH. 3SS and I56V-3SS are represented by the open and solid circles, respectively. The continuous lines show the linear regressions of the results for 3SS and I56V-3SS. The dashed and dotted lines show those for 4SS and I56V, respectively. (b) The calorimetric enthalpy change as a function of the denaturation temperature. 3SS and I56V-3SS are represented by the open and solid circles, respectively. The continuous lines show the linear regressions of the results for 3SS and I56V-3SS. The dashed and dotted lines show those for 4SS and I56V, respectively.

Table V-2. Thermodynamic parameters for denaturation of 3SS, Ile→Val-3SS and Val→Ala-3SS mutant human lysozymes at the denaturation temperature (49.2°C) of the 3SS protein at pH 2.7.

	T_d (°C)	ΔT_d (°C)	ΔC_p[a] (kJ/mol K)	ΔH_{cal} (kJ/mol)	$\Delta\Delta G$ (kJ/mol)
3SS	49.2 ± 0.5		7.0 ± 0.3	342 ± 3	(0)
I23V-3SS	47.6 ± 0.3	-1.6	7.6 ± 0.6	338 ± 6	-1.7
I56V-3SS	42.9 ± 0.5	-6.3	5.4 ± 0.7	300 ± 4	-5.6
I59V-3SS	44.8 ± 0.1	-4.4	7.0 ± 0.6	298 ± 4	-3.9
I89V-3SS	46.5 ± 0.4	-2.7	7.7 ± 0.3	328 ± 3	-2.7
I106V-3SS	44.5 ± 0.1	-4.7	7.2 ± 0.8	294 ± 5	-4.1
V2A-3SS	41.3 ± 0.3	-7.9	6.0 ± 0.9	274 ± 5	-6.3
V74A-3SS	47.3 ± 0.3	-1.9	6.4 ± 0.2	308 ± 2	-1.8
V93A-3SS	44.8 ± 0.3	-4.4	6.4 ± 0.4	319 ± 3	-4.2
V99A-3SS	44.8 ± 0.3	-4.4	5.3 ± 0.5	280 ± 5	-3.7
V100A-3SS	46.6 ± 0.2	-2.6	7.7 ± 0.4	302 ± 4	-2.4
V110A-3SS	49.5 ± 0.1	+0.3	6.3 ± 0.4	338 ± 3	+0.3
V121A-3SS	39.9 ± 0.1	-9.3	5.7 ± 0.5	273 ± 3	-7.3
V125A-3SS	42.2 ± 0.4	-7.0	6.5 ± 0.4	326 ± 4	-6.7
V130A-3SS	44.4 ± 0.3	-4.8	7.8 ± 0.6	327 ± 6	-4.7

[a] ΔC_p was obtained from the slope of ΔH against T_d.

Table V-3. Comparison of ΔT_d and $\Delta\Delta G$ values between 4SS and 3SS human lysozymes at each substitution.

	ΔT_d (°C)		$\Delta\Delta G$ (kJ/mol)	
	4SS[a]	3SS	4SS[a]	3SS
Substitution			(64.9 °C)	(49.2 °C)
I23V	-1.1	-1.6	-1.5	-1.7
I56V	-3.6	-6.3	-5.0	-5.6
I59V	-3.4	-4.4	-4.6	-3.9
I89V	-1.4	-2.7	-2.0	-2.7
I106V	-2.2	-4.7	-3.0	-4.1
V2A	-4.6	-7.9	-6.3	-6.3
V74A	-1.1	-1.9	-1.5	-1.8
V93A	-2.3	-4.4	-3.1	-4.2
V99A	-3.0	-4.4	-4.1	-3.7
V100A	-0.8	-2.6	-1.1	-2.4
V110A	+1.5	+0.3	+2.2	+0.3
V121A	-4.5	-9.3	-6.0	-7.3
V125A	-4.0	-7.0	-5.5	-6.7
V130A	-2.6	-4.8	-3.5	-4.7

[a] Chapters II and III.

X-ray structural analysis of 3SS and 3SS mutant human lysozymes

For 3SS and 3SS mutant proteins, all the crystals belong to the space group $P2_12_12_1$. Data collection and refinement statistics for the 3SS and 3SS mutant human lysozymes are summarized in Table V-4. All structures were refined at 1.8 Å resolution. The overall X-ray structures examined were essentially identical to that of the wild-type (4SS) structure. In some 3SS mutants, structural changes between the 3SS and 3SS mutants near the substitution residue were observed as described below.

(i) Structure of 3SS (C77A/C95A) human lysozyme

The r.m.s deviation of each residue for the main-chain atoms between the 3SS and 4SS proteins is shown in Figure V-4(a). The shifts for residues near substitution residue 77 are larger than for those near residue 95. Figure V-4(b) shows the increase in the *B*-factors for main-chain atoms around the residue 77 in the 3SS structure (continuous line). This indicates that the region around the residue 77 is more flexible than that around residue 95, because the residue 77 is in a loop on the surface of the native structure but the residue 95 is in an α-helix in the interior of the molecule. The structures of the 3SS and 4SS proteins in the vicinity of the residues 77 and 95 are shown in Figure V-4(c). The main difference observed is the disappearance of sulfur atoms in the structure of the 3SS protein. These results for the 3SS structure in this study are identical with those in the previous report (Inaka et al., 1991a).

(ii) Overall structures of 3SS mutant human lysozymes

Figure V-5(b) shows the r.m.s. deviation of each residue for the main-

chain atoms between I56V (Chapter II) and I56V-3SS (continuous line). It was similar to that between the 3SS and 4SS proteins (dashed line). The *B*-factors for the main-chain atoms of I56V-3SS (continuous line in Figure V-5(c)) were also similar to those of the 3SS protein (dashed line in Figure V-5(c)). However, the structure changes around residue 77 between I56V-3SS and 3SS (continuous line in Figure V-5(a)) were larger than those between I56V and 4SS (dashed line in Figure V-5(a)), due to the flexibility of the region in the 3SS proteins. The results for the other 3SS mutant proteins were similar.

(iii) Structures in the vicinity of mutation site in 3SS mutant human lysozymes

For V93A, V100A, V125A and V130A, the residues around the mutation site have shifted toward the created cavity (Chapter i), and movements of the residues around the mutation site in V93A-3SS, V100A-3SS, V125A-3SS and V130A-3SS were observed (Figures V-6 and V-7). For examples, Figure V-6 shows (a) the structures in the vicinity of the residue 93 in 4SS and V93A (Chapter III), and (b) those in 3SS and V93A-3SS. For V93A-3SS and V93A, the side-chains of Leu15 and Met17 facing the residue 93 shifted toward the created cavity. In contrast, V100A-3SS underwent a shift of Ala100 itself toward the cavity (Figure V-7(b)), as did V100A (Chapter III) (Figure V-7(a)). Except for the substitution of Ile59 to Val, the structural changes around the mutation site were similar between each 3SS and 4SS mutant.

The structures in the vicinity of the residue 59 in I59V and 4SS (Chapter II), and I59V-3SS and 3SS are shown in Figure V-8(a) and (b),

respectively. In I59V a new water molecule was observed in the created cavity and the side-chain conformation of Val59 was different from that of Ile59 (Chapter II) (Figure V-8(a)), but I59V-3SS had no solvent molecule in the cavity and underwent no side-chain conformational change (Figure V-8(b)). The different structural changes in the vicinity of the residue 59 in I59V-3SS and I59V may be caused by the deletion of the disulfide bond (Cys77-95) which is located near residue 59.

Table V-4. X-ray data collection and refinement statistics for 3SS, Ile→Val-3SS and Val→Ala-3SS mutant human lysozymes.

	Data collection (1.8 Å)							Refinement (8-1.8 Å)				
	Cell (Å)			Measured	Independent	Completeness	R_{merge}[a]	Atoms	Solvent	Reflections	Completeness	R factor[b]
	a	*b*	*c*	reflections	reflections	(%)	(%)		atoms		(%)	
3SS	56.93	60.91	33.57	36249	10498	92.3	4.0	1183	156	10210	91.4	0.170
I23V-3SS	56.33	60.82	33.51	33763	10541	94.0	4.4	1204	178	10095	91.6	0.168
I56V-3SS	56.99	60.76	33.47	23543	9229	81.5	6.4	1164	138	8472	76.2	0.170
I59V-3SS	56.93	60.84	33.61	33145	10377	91.3	4.7	1196	170	9872	88.4	0.169
I89V-3SS	56.97	60.83	33.56	34714	10745	94.5	5.5	1183	157	10326	92.5	0.172
I106V-3SS	56.93	60.85	33.53	32471	10568	93.1	3.6	1190	164	10120	90.8	0.170
V2A-3SS	57.33	60.62	33.63	27103	9828	84.3	7.3	1176	151	8921	79.6	0.167
V74A-3SS	56.88	60.89	33.61	26168	11170	98.2	3.4	1194	169	10108	90.5	0.167
V93A-3SS	56.06	60.11	33.62	26365	9944	86.6	5.1	1196	171	9156	84.2	0.168
V99A-3SS	56.89	60.61	33.22	33258	10767	95.0	4.7	1184	159	10237	93.1	0.179
V100A-3SS	57.00	60.96	33.55	29699	10677	93.5	6.1	1207	182	10205	91.3	0.171
V110A-3SS	56.92	60.83	33.57	31232	10594	93.3	5.2	1186	161	10105	90.6	0.175
V121A-3SS	56.96	60.83	33.31	31289	10295	90.9	6.2	1173	148	9613	86.8	0.174
V125A-3SS	56.96	60.86	33.50	35655	10303	90.9	3.6	1196	171	10055	90.3	0.177
V130A-3SS	56.72	60.71	33.43	25803	10257	92.6	7.1	1243	218	9759	88.3	0.187

[a] $R_{merge} = 100\ \Sigma\ |\ I - \langle I \rangle\ |\ /\ \Sigma\ \langle I \rangle$.

[b] R factor $= \Sigma\ ||F_o| - |F_c||\ /\ \Sigma\ |F_o|$.

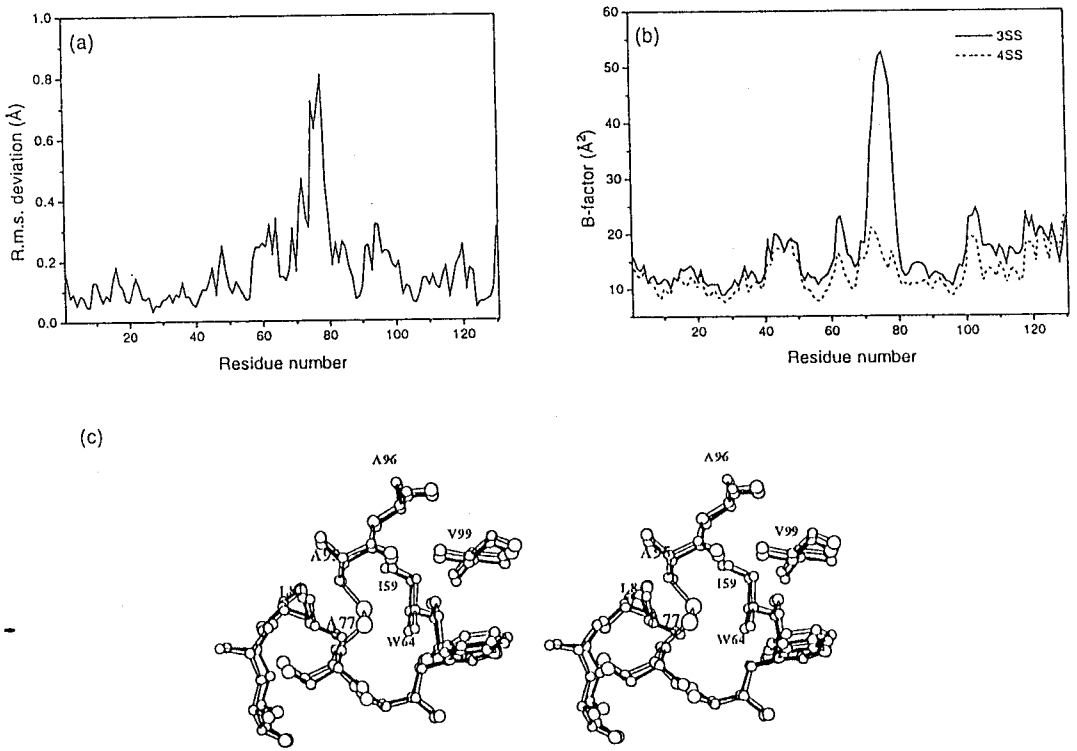

Figure V-4. (a) R.m.s. deviation for the main-chain atoms between the 3SS and 4SS structures after a least-squares fit of both structures using main-chain atoms. (b) *B*-factors of each residue for the main-chain atoms of the 3SS (continuous line) and 4SS (dashed line) structures. (c) Stereodrawing (Johnson, 1976) showing the structures in the vicinity of the Cys77 and Cys95 for the 3SS (solid bonds) and 4SS (open bonds) structures which are superimposed.

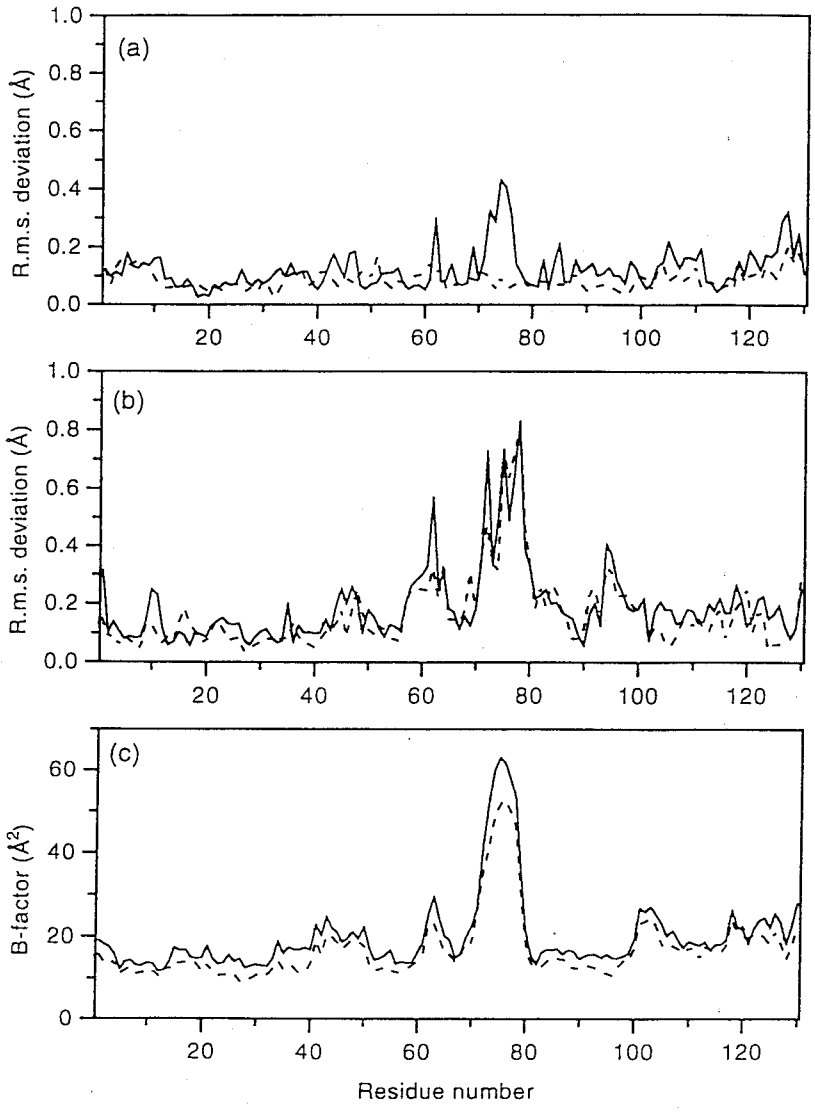

Figure V-5. (a) R.m.s. deviations for the main-chain atoms between I56V-3SS and 3SS structures (continuous line) and between I56V and 4SS structures (dashed line) after a least-squares fit of both structures using main-chain atoms. (b) R.m.s. deviations for the main-chain atoms between I56V-3SS and I56V structures (continuous line) and between the 3SS and 4SS structures (dashed line) after a least-squares fit of both structures using main-chain atoms. (c) *B*-factors of each residue for the main-chain atoms of I56V-3SS (continuous line) and 3SS (dashed line) structures.

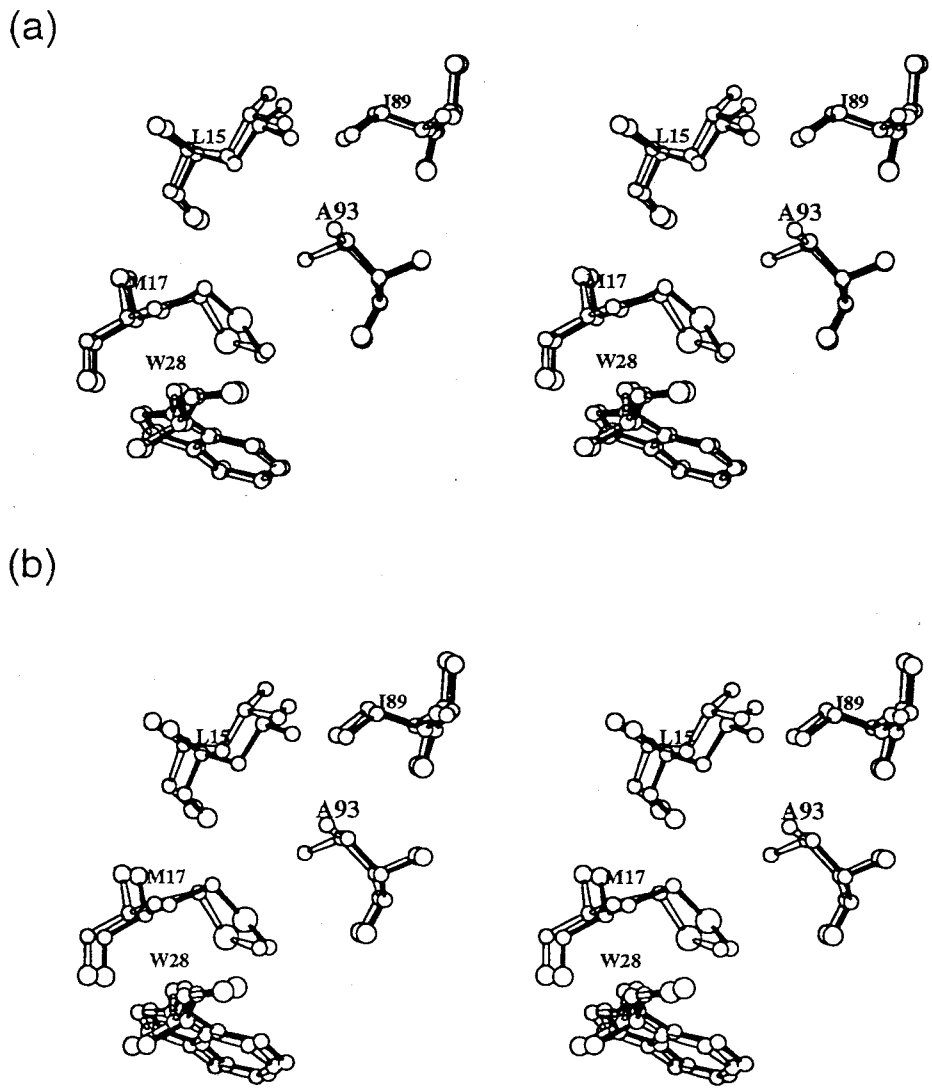

Figure V-6. Stereodrawing (Johnson, 1976) showing the structures in the vicinity of the residue 93. (a) V93A (solid bonds) and 4SS (open bonds) structures are superimposed. (b) V93A-3SS (solid bonds) and 3SS (open bonds) structures are superimposed.

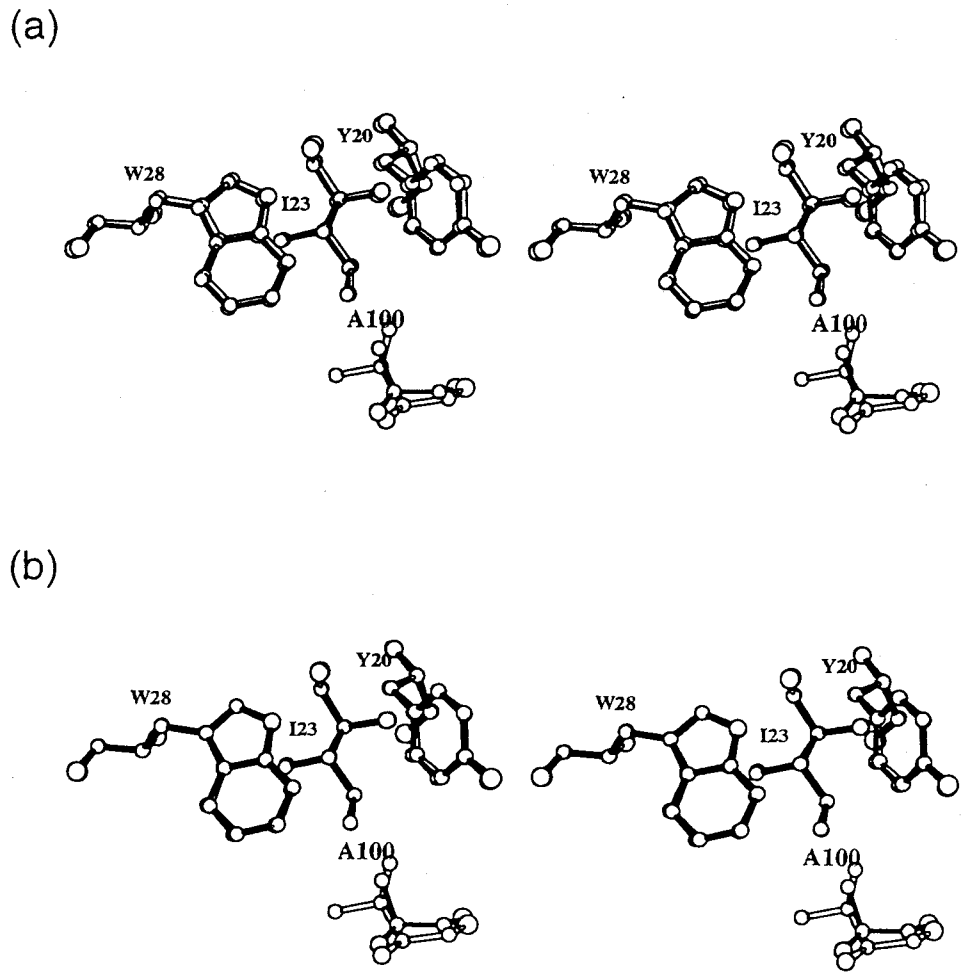

Figure V-7. Stereodrawing (Johnson, 1976) showing the structure in the vicinity of the residue 100. (a) V100A (solid bonds) and 4SS (open bonds) structures are superimposed. (b) V100A-3SS (solid bonds) and 3SS (open bonds) structures are superimposed.

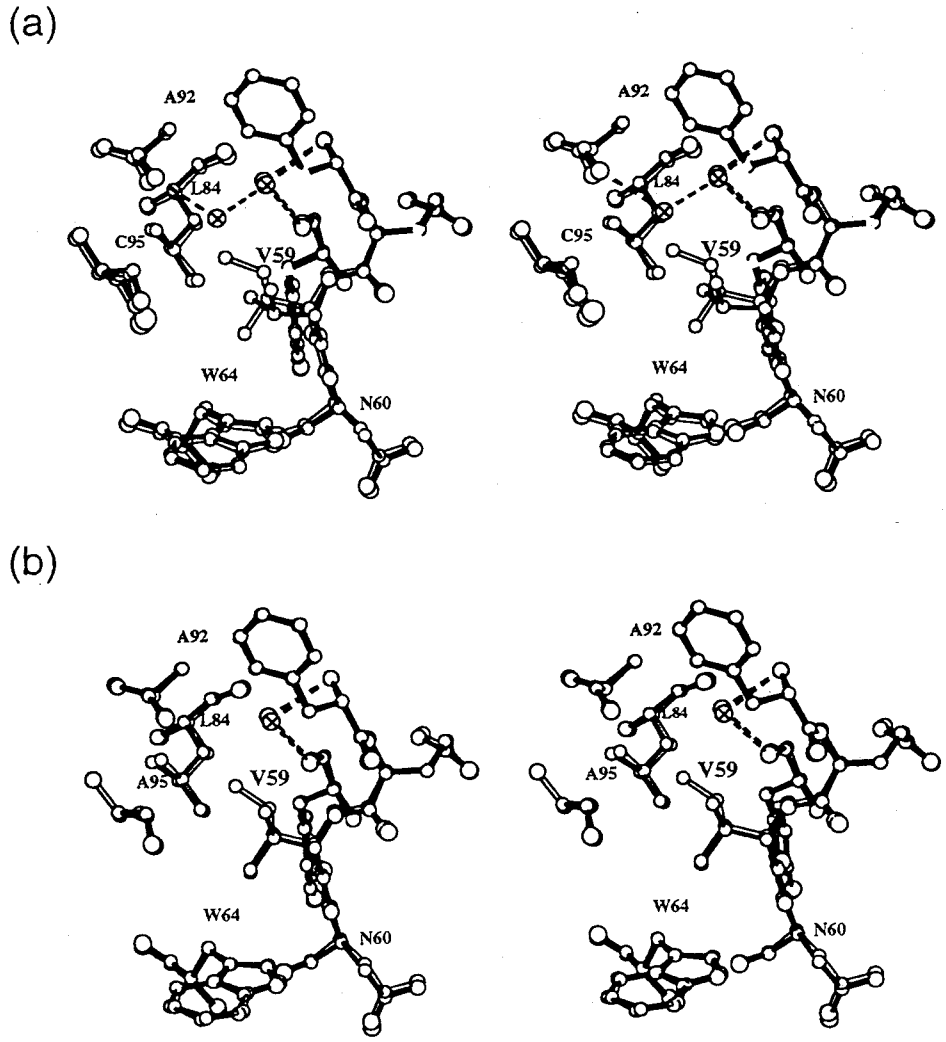

Figure V-8. Stereodrawing (Johnson, 1976) showing the structure in the vicinity of the residue 59. (a) I59V (solid bonds) and 4SS (open bonds) structures are superimposed. (b) I59V-3SS (solid bonds) and 3SS (open bonds) structures are superimposed. Solvent water molecules are drawn as crossed circles. The dashed lines indicate hydrogen bonds.

Discussion

Role of a disulfide bond between Cys77 and Cys95 in the stability and structure of human lysozyme

The destabilization of the 3SS (C77A/C95A) human lysozyme compared to the 4SS (wild-type) protein is caused by a decrease in ΔH, that must be related to the increase of the flexibility of the native state. This is indicated both by an increase in the crystallographic *B*-factors and by an increase in entropy in the binding of *N*-acetylglucosamine trimer observed by isothermal titration calorimetry (Kuroki et al., 1992a). In this study, we constructed 14 hydrophobic mutants from the 3SS protein, and determined their thermodynamic parameters of denaturation using differential scanning calorimetry and their structures by X-ray analysis. By examining each difference in stability and structure between the equivalent mutants from 3SS and 4SS (Chapters II and III), the effect of the cross-linking on the stability of human lysozyme were evaluated.

Table V-5 lists the differences in Gibbs energy change, enthalpy change and entropy change of the 3SS proteins relative to the equivalent 4SS proteins at 57.0 °C. Because the measured denaturation temperatures of the 3SS and 4SS proteins were quite different, this temperature (57.0 °C) was chosen as a midpoint between them in order to minimize extrapolation errors. In all cases, the 3SS proteins are destabilized by about 20 kJ/mol compared with the equivalent 4SS proteins. These $\Delta\Delta G$ values are similar to the value, 20.5 kJ/mol, for the decrease in ΔG due to the increase in entropy in the denatured state by the removal of a disulfide bond between Cys77 and Cys95, estimated by Kuroki et al. (1992a). The destabilizations of all 3SS

proteins, however, is due mainly to decreases in ΔH as shown in Table V-5. From the structural analysis, all 3SS proteins had large B-factors around the residue 77 (Figures V-4(b) and V-5(c)). These results show that the disulfide bond between Cys77 and Cys95 in human lysozyme has an important role in tightly maintaining the tertiary structure (Kuroki et al., 1992a).

Table V-5. Differences in Gibbs energy change, enthalpy change and entropy change of the 3SS proteins relative to the equivalent 4SS proteins at 57.0 °C.

	$\Delta\Delta H$ (kJ/mol)	$T\Delta\Delta S$ (kJ/mol)	$\Delta\Delta G$ (kJ/mol)
3SS	-29	-9	-19.9
I23V-3SS	-26	-5	-20.9
I56V-3SS	-88	-66	-22.6
I59V-3SS	-67	-48	-19.9
I89V-3SS	-32	-8	-22.7
I106V-3SS	-62	-38	-23.1
V2A-3SS	-96	-74	-21.7
V74A-3SS	-69	-46	-22.7
V93A-3SS	-47	-23	-23.2
V99A-3SS	-107	-87	-19.9
V100A-3SS	-66	-43	-22.4
V110A-3SS	-56	-33	-22.5
V121A-3SS	-91	-70	-21.8
V125A-3SS	-52	-29	-23.3
V130A-3SS	-26	-5	-21.3

Effect of the hydrophobic mutations on the stability of the 3SS and 4SS human lysozymes

The stabilities of all of the 3SS hydrophobic mutants were decreased compared with the 3SS protein except for V110A-3SS (Table V-2), coinciding with the result of the 4SS proteins (Table V-3) (Chapters II and III). Moreover, the order of the stability in the 3SS mutants was similar to that in the 4SS mutants. Figure V-9(a) shows the plot of the ΔT_d values for the 3SS mutants against those for the equivalent 4SS mutants at pH 2.7. The slope of the relation between them in this Figure is greater than 1.0, showing a greater destabilization in the double mutations. However, in the plot of $\Delta\Delta G$ of the 3SS mutants at 49.2 °C against those of the corresponding 4SS mutants at 64.9 °C (Figure V-9(b)), the data points were near the diagonal line, indicating the additivity of the stability changes due to double mutations.

The different slopes in Figure V-9(a) and (b) are brought about by the different temperature dependencies of ΔG for the 3SS and 4SS proteins, as shown in Figure V-10(a). Figure V-10(b) displays the temperature dependencies of ΔG for 4SS, I56V, 3SS and I56V-3SS near their denaturation temperatures at pH 2.7. The temperature at $\Delta G = 0$ is denaturation temperature. The values of $\Delta\Delta G$ were similar between the 3SS and 4SS proteins (represented by red), but the decrease in the T_d value for 3SS proteins was bigger than that for 4SS proteins (represented by blue) as illustrated in Figure V-10(b). These results show that changes in T_d values for mutant proteins do not correspond directly to the $\Delta\Delta G$ values.

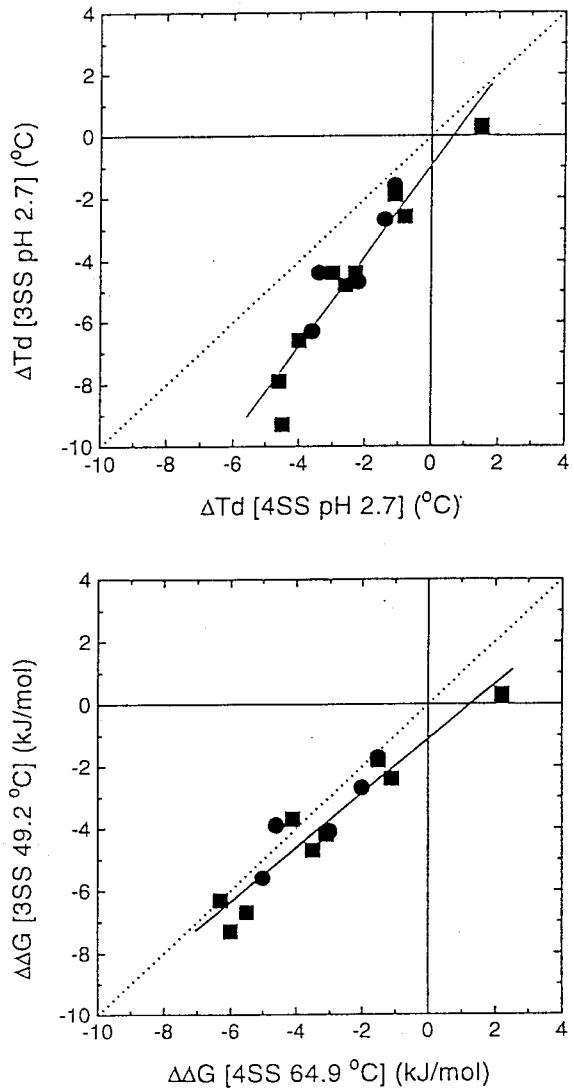

Figure V-9. (a) Plot of the ΔT_d values of the 3SS mutants relative to 3SS against those of the equivalent 4SS mutants relative to 4SS at pH 2.7. (b) Plot of the $\Delta\Delta G$ values of the 3SS mutants relative to 3SS at 49.2 °C against those of the equivalent 4SS mutants relative to 4SS at 64.9 °C. The substitutions of Ile to Val and Val to Ala are shown as solid circles and squares, respectively. The continuous lines indicate the linear regression of all the points.

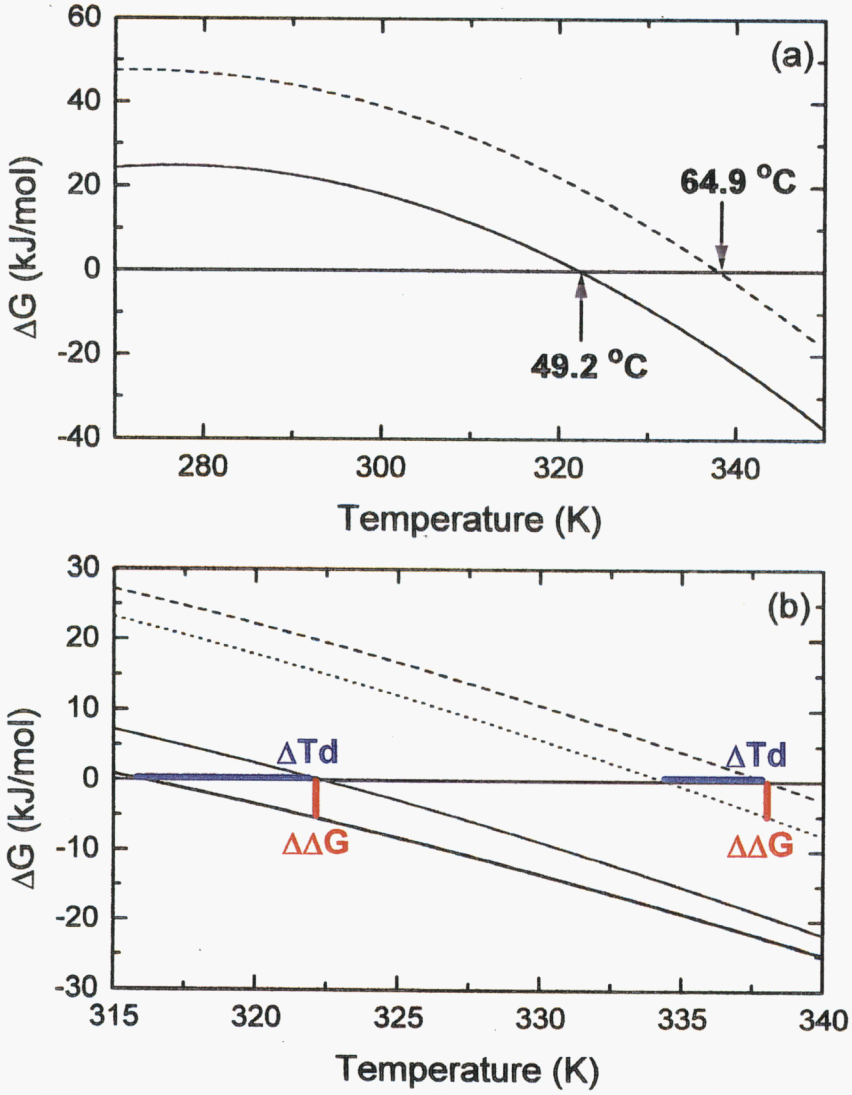

Figure V-10. (a) Temperature dependencies of ΔG for 3SS (continuous line) and 4SS (dashed line) at pH 2.7. (b) Temperature dependencies of ΔG for 3SS (continuous line), I56V-3SS (thick continuous line), 4SS (dashed line) and I56V (dotted line) at pH 2.7.

Contribution of the hydrophobic effect to the stability of human lysozyme

From a series of the hydrophobic mutants (4SS mutants) of wild-type (4SS) human lysozyme, a linear correlation between $\Delta\Delta G$ and $\Delta\Delta ASA_{HP}$ (differences in hydrophobic surface area exposed upon denaturation) for the hydrophobic mutants was observed by taking into account effects of the secondary structural propensity (Chapter II) and water molecules in the cavity (Chapter III). In this correlation, the mutants are divided into three types, according to the type of secondary structure where the mutation is located (Chou & Fasman, 1978). Type I is for the mutations of Val to Ala in α-helices (represented by black in Figure V-11(b)), that is, mutations for which the secondary structural propensity would be expected to increase the stability of the protein; type II is for the mutations of Ile/Val to Ala/Gly in β-sheets (blue), that is, mutations for which the secondary structural propensity would be expected to decrease the stability of the protein; and type III includes the mutations in turns/loops and the mutations of Ile to Val in β-sheets (represented by red in Figure V-11(a)), which are insensitive to the secondary structural propensity. In the mutations for type III of the 4SS mutants (red filled squares in Figure V-11(a)), there is a good correlation, yielding Equation (V-1) (Chapter IV).

$$\Delta\Delta G \text{ (kJ/mol)} = 0.12\ (\pm 0.01)\ \Delta\Delta ASA_{HP}\ (\text{Å}^2) - 0.87\ (\pm 0.80)$$
(correlation coefficient of 0.94 for 14 points) (V-1)

We examined the correlation between $\Delta\Delta G$ and $\Delta\Delta ASA_{HP}$ for the 3SS mutants, represented as open symbols in Figure V-11. There was a good correspondence between correlations for the 3SS and 4SS mutants, except

for one 3SS mutant, V93A-3SS. In the mutations for type III, the correlation including both the 3SS and 4SS mutants was as follows.

$$\Delta\Delta G \text{ (kJ/mol)} = 0.12\ (\pm 0.01)\ \Delta\Delta ASA_{HP}\ (\text{Å}^2) - 0.56\ (\pm 0.59)$$
(correlation coefficient of 0.93 for 22 points) (V-2)

The value of the slope in this correlation, 0.12 kJ/mol Å^2, is comparable with that of accessible surface areas of amino acid side-chains plotted against hydrophobicity, 0.10 kJ/mol Å^2, estimated by Chothia (1974).

In the case of the mutation of type I, Val to Ala in α-helices (represented by black in Figure V-11(b)), the stability was about 3 kJ/mol higher than that expected from the value of $\Delta\Delta ASA_{HP}$ Equation V-1. This stabilization effect of the mutations of Val to Ala on α-helix is similar to the estimations of helix propensities for barnase, 3.7 kJ/mol (Horovitz et al., 1992), and RNase T1 peptide and protein, 2.7 and 2.8 kJ/mol, respectively (Myers et al., 1997a, b).

V93A-3SS of human lysozyme, however, did not have the increment in stabilization due to helix propensity (Figure V-11(b)). The amino acid sequences of the wild-type (4SS), V93A, 3SS and V93A-3SS around the residue 93 are shown in Figure V-12. The sequences of 3SS and V93A-3SS are similar to those of alanine-based peptides used in helix propensity experiments (Rohl et al., 1996; Park et al., 1993). Myers et al., (1997a, b) have described that differences in the local sequence cause solvation differences, leading to differences in the measured propensities. In the case of V93A-3SS, the peptide groups around residue 93 might be more exposed to solvent in the denature state, as compared with those of 4SS proteins.

Since residue 93 is buried in the native state, the solvation of the peptide groups in the denatured state may cause a destabilization.

The values of $\Delta\Delta G$ of the 3SS and 4SS mutants were compared at the different temperatures, 49.2 and 64.9 °C (about 322 and 338 K), respectively, to obtain the most reliable thermodynamic parameters. The free energy for transfer of hydrocarbon from liquid hydrocarbon to water (the hydrophobic effect) increases with temperature (Hermann, 1972; Reynolds et al., 1974), but the increase is small. For the mean values (ΔG_{tr}) of toluene, ethylbenzene, cyclohexane, pentane and hexane, the difference in ΔG_{tr} even at 25 and 100 °C (298 and 373 K) is only 10 % for their values, which is within the error of our estimation (Equations V-1 and V-2).

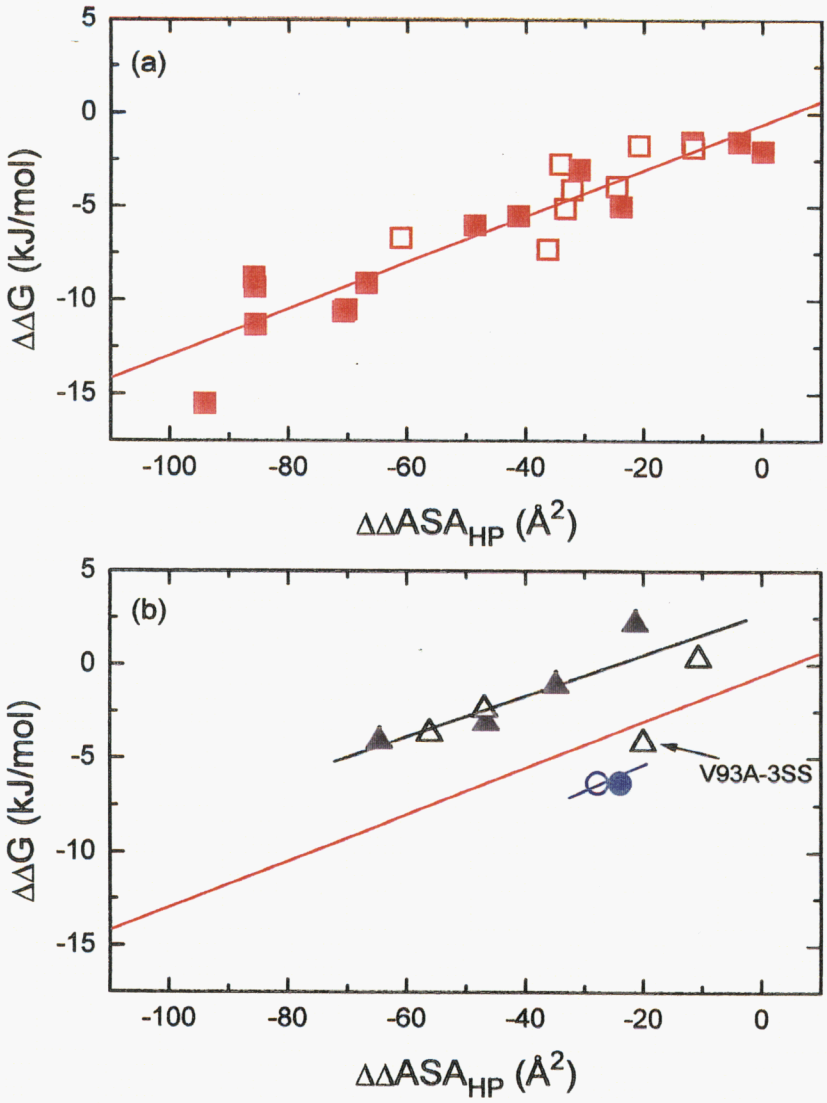

Figure V-11. Correlation of $\Delta\Delta ASA_{HP}$ (changes in hydrophobic surface area exposed upon denaturation) with $\Delta\Delta G$ of the 4SS mutants (solid symbols) and 3SS mutants (open symbols). (a) The mutants of the type III are represented by red squares. The red continuous line shows the linear regression of the type III mutants. (b) The mutants of the type I are represented by black triangles. The black continuous line shows the linear regression of the type I mutants, except for V93A-3SS. The mutants of the type II are represented by blue circles. The red continuous line shows the linear regression of the type III mutants. The ASA values were calculated using the procedure of Connolly (1993) with a probe size of 1.4 Å.

	89	101
Wild-type	I A D A V A C A K R V V R	
V93A	I A D A A A C A K R V V R	
3SS	I A D A V A A A K R V V R	
V93A-3SS	I A D A A A A K R V V R	
	α-Helix	

Figure V-12. Amino acid sequences of the wild-type (4SS), V93A, 3SS and V93A-3SS between residues 89 and 101. The substituted residues are represented by red.

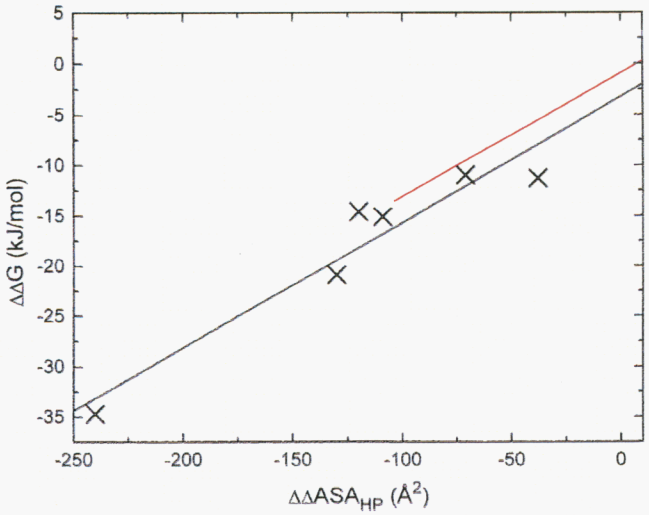

Figure V-13. Correlation of $\Delta\Delta ASA_{HP}$ (changes in hydrophobic surface area exposed upon denaturation) with $\Delta\Delta G$ of the T4 lysozyme mutants (cross symbols). The black continuous line shows the linear regression of the mutants. The red continuous line shows the linear regression of the mutants of human lysozyme (as the same line as red lines in Figure V-11). The ASA values were calculated using the procedure of Connolly (1993) with a probe size of 1.4 Å.

Comparison with T4 lysozyme mutants

The stabilities and structures of some cavity-creating mutants of T4 lysozyme (Eriksson et al., 1992, 1993; Baldwin et al., 1996) have been reported. In order to examine whether the correlation between $\Delta\Delta G$ and $\Delta\Delta ASA_{HP}$ obtained from the 3SS and 4SS human lysozymes is common to globular proteins, we calculated $\Delta\Delta ASA_{HP}$ of all of the hydrophobic residues for the mutants of T4 lysozyme using the crystal structures (L46A, PDB code 1L67; L99A, 1L90; L121A, 200L; L133A, 1L69; F153A, 1L85; L99A/F153A, 1L89) and the wild-type structure (1L63) (Eriksson et al., 1992; Baldwin et al., 1996), which crystals belong to same space group, $P3_221$.

Figure V-13 shows the correlation between $\Delta\Delta G$ and $\Delta\Delta ASA_{HP}$ of all of the hydrophobic residues for six T4 lysozyme mutants. There was a good relation as following.

$$\Delta\Delta G \text{ (kJ/mol)} = 0.12\ (\pm 0.02)\ \Delta\Delta ASA_{HP}\ (\text{Å}^2) - 3.23\ (\pm 2.48)$$
$$\text{(correlation coefficient of 0.96 for 6 points)} \qquad \text{(V-3)}$$

This correlation coefficient was better than that (0.92) obtained by using $\Delta\Delta ASA_{HP}$ values at only substituted residues (not shown), as was the case for human lysozyme (in Figure III-6(c) and (d) of Chapter III). In Figure V-13, although the values of $\Delta\Delta G$ of T4 lysozyme mutants were slightly lower than those of human lysozyme mutants, the slope was a good agreement with that of human lysozymes.

Eriksson et al. (1992) have found that the decrease in the stability of the mutant T4 lysozymes substituted in the core, Leu→Ala, Phe→Ala and

Leu→Ala/Phe→Ala, depends on the change in the size of the cavity. For Ile→Ala mutations in the core of barnase, there is also an approximately linear relation between them (Buckle et al., 1996). This relation seemed to give a successful way to reconcile hydrophobic effect to stability changes of mutant proteins. However, for the mutations expected to create small cavities such as Ile→Val and Val→Ala, and substituted on near the surface, the correlation between $\Delta\Delta G$ and cavity volume has not been seen in human lysozyme (Chapter III) and barnase (Buckle et al., 1993). It could be expected to reconcile a number of conflicting reports concerning the strength of the hydrophobic effect to protein stability.

In this study, we found a good correlation between $\Delta\Delta G$ and $\Delta\Delta ASA_{HP}$ of all of the hydrophobic residues for mutant proteins of the 3SS and 4SS human lysozymes and T4 lysozyme, including the mutations from Ile→Val to Leu→Ala/Phe→Ala, both in the core and on the surface of proteins. That is, the changes in hydrophobic surface area of total hydrophobic residues are correlated with changes in protein stability. It may be concluded that changes in ASA values of hydrophobic residues due to mutations of globular proteins correspond to changes in conformational stability of 0.12 kJ/mol $Å^2$.

Chapter VI

Summary and Conclusions

In this thesis, the relation between the changes in the stability and the structural features of mutants of human lysozyme were investigated to elucidate how a hydrophobic residue contributes to conformational stability. The main results obtained in Chapters II to V are summarized as follows.

Chapter II

In order to understand the contribution of hydrophobic residues to the conformational stability of human lysozyme, five Ile mutants (Ile → Val) in the interior of the protein were constructed. The thermodynamic parameters characterizing the denaturation of these mutant proteins were determined by scanning calorimetry, and the three-dimensional structure of each mutant protein was solved at high resolution by X-ray crystallography.

The thermodynamic analyses at 64.9 °C and at pH 2.7 revealed the following. (1) The stabilities of all the mutant proteins were decreased as compared with that of the wild-type protein. (2) The changes in the calorimetric enthalpies were larger than those in the Gibbs energies, and were compensated by entropy changes. (3) The destabilization mechanism of the mutant proteins differs, depending on the location of the mutation sites.

X-ray analyses showed that the overall structures of all the mutant human lysozymes examined were identical to that of the wild-type protein, and only small structural rearrangements were observed locally around some of the mutation sites. The most striking change among the mutant proteins was found in the mutant protein, I59V, which contains a new water molecule in the cavity created by the mutation. The thermodynamic stabilites of the mutant proteins are discussed in light of the high-resolution X-ray structures of the wild-type and five mutant human lysozymes examined.

Chapter III

To clarify the contribution of the hydrophobic effect to the conformational stability of human lysozyme, a series of Val to Ala mutants were constructed. The thermodynamic parameters for the denaturation of these 9 mutant proteins were determined using differential scanning calorimetry (DSC), and the crystal structures were solved at high resolution. The denaturation Gibbs energy ($\Delta\Delta G$) and enthalpy ($\Delta\Delta H$) values of the mutant proteins ranged from +2.2 to -6.3 kJ/mol and +7 to -17 kJ/mol, respectively. The structural analyses showed that the mutation site and/or the residues around it in some proteins shifted toward the created cavity, and the substitutions affected not only the mutation site but also other parts far from the site, although the structural changes were not as great. Correlation between the changes in the thermodynamic parameters and the structural features of mutant proteins was examined, including the 5 Ile to Val mutant human lysozymes. There was no simple general correlation between $\Delta\Delta G$ and the changes in hydrophobic surface area exposed upon denaturation ($\Delta\Delta ASA_{HP}$). We found only a new correlation between the $\Delta\Delta G$ and $\Delta\Delta ASA_{HP}$ of all of the hydrophobic residues if the effect of the secondary structure propensity was taken into account.

Chapter IV

Water molecules frequently occur in the interior of globular proteins. To elucidate the contribution of buried water molecules to the conformational stability of a protein, we examined the crystal structures and the thermodynamic parameters of denaturation of six Ile to Ala/Gly mutant

human lysozymes, in which a cavity is created at each mutation site by the substitution of a smaller side-chain for a larger one. One or two ordered water molecules were found in the cavities created in some mutants (I106A, I59A and I59G). The cavity volumes for these three mutants were bigger than those that remained empty in the other mutants. The stability of the mutant proteins with the newly introduced water molecules was about 8 kJ/mol higher than that expected from the change in hydrophobic surface area ($\Delta\Delta ASA_{HP}$) exposed upon denaturation. It was concluded that a water molecule in a cavity created in the interior of a protein contributes favorably to the stability.

Chapter V

To get a general rule for the relationship between hydrophobic effect and conformational stability, five Ile to Val and nine Val to Ala mutants (3SS mutants) from 3SS (C77A/C95A) human lysozyme were constructed. As known from previous studies, the 3SS protein lacking a disulfide bond between Cys77 and Cys95 is destabilized by enthalpic factors, as revealed by about 20 kJ/mol decrease in the denaturation Gibbs energy change (ΔG) value, as compared to the wild-type protein which has four disulfide bonds. In this study, the stabilities and structures of the 3SS mutants were determined by differential scanning calorimetry and X-ray crystal analysis, respectively, and compared with those of the mutants (4SS mutants) from the wild-type (4SS) protein shown in Chapters II, III and IV.

The stabilities of all the 3SS mutants except V110A-3SS were decreased as compared with that of the 3SS protein, coinciding with the results for the 4SS mutants. The change in the denaturation Gibbs energy

change ($\Delta\Delta G$) values of the 3SS mutants relative to the 3SS protein at the denaturation temperature (49.2 °C) of the 3SS protein at pH 2.7 were similar to those of the equivalent 4SS mutants relative to the wild-type at that (64.9 °C) of the wild-type protein.

The $\Delta\Delta G$ values of the 3SS mutants correlated with the changes in hydrophobic surface area exposed upon denaturation ($\Delta\Delta ASA_{HP}$) for all of the hydrophobic residues when the effects of the secondary structure propensity were considered. This correlation is identical with that found for the 4SS mutants in Chapters III and IV. The linear relation between $\Delta\Delta G$ and $\Delta\Delta ASA_{HP}$ for all of the hydrophobic residues with the same slope was also found for the mutants of T4 lysozyme already reported, indicating that this is a general relationship between changes in conformational stability and changes in ASA values of hydrophobic residues due to mutations.

In conclusion, we were able to estimate quantitatively the hydrophobic effect on protein stability due to the mutations by systematically investigating hydrophobic mutant human lysozymes. That is, we found, as a general rule for globular proteins, a new correlation between $\Delta\Delta G$ and $\Delta\Delta ASA_{HP}$ due to mutation by considering the secondary structural propensity and the water molecules in the interior of a protein. This relationship indicates that the hydrophobic area buried in the interior of a protein contributes about 0.1 kJ/mol $Å^2$ to the conformational stability. The present work reconciles a number of conflicting reports concerning the strength of the hydrophobic effect on the conformational stability of a protein.

References

Alber, T., Dao-pin, S., Nye, J. A., Muchmore, D. C. & Matthews, B. W. (1987) *Biochemistry*, **26**, 3754-3758.

Anfinsen, C. B. (1973) *Science*, **181**, 223-230.

Artymiuk, P. J. & Blake, C. C. F. (1981) *J. Mol. Biol.* **152**, 737-762.

Baldwin, E., Xu, J., Hajiseyedjavadi, O., Baase, W. A. & Matthews, R. W. (1996) *J. Mol. Biol.* **259**, 542-559.

Becktel, W. J. & Schellman, J. A. (1987) *Biopolymers*, **26**, 1859-1877.

Bernal, J. D. & Crowfoot, D.C. (1934) *Nature*, **133**, 794.

Berndt, K. D., Beunink, J., Schroder, W. & Wuthrich, K. (1993) *Biochemistry*, **32**, 4564-4570.

Blaber, M., Zhang, X. J. & Matthews, B. W. (1993) *Science,* **260**, 1637-1640.

Blow, D. M. & Crick, F. H. C. (1959) *Acta Cryst.* **12**, 794-802.

Booth, D. R., Sunde, M., Bellotti, V., Robinson, C. V., Hutchinson, W. L., Fraser, P. E., Hawkins, P. N., Dobson, C. M., Radford, S. E., Blake, C. C. & Pepys, M. B. (1997) *Nature*, **385**, 787-793.

Bowie, J. U., Clarke, N. D., Pabo, C. O. & Sauer, R. T. (1990) *Proteins: Struct. Funct. Genet.* **7**, 257-264.

Bowie, J. U., Luthy, R. & Eisenberg, D. (1991) *Science*, **253**, 164-170.

Brandts, J. F. (1964a) *J. Am. Chem. Soc.* **86**, 4291-4301.

Brandts, J. F. (1964b) *J. Am. Chem. Soc.* **86**, 4302-4314.

Braun, W., Wider, G., Lee, H. H. & Wuthrick, K. (1983) *J. Mol. Biol.* **169**, 921-948.

Brunger, A. T. (1992) X-PLOR manual Ver. 3.1, Yale University, NH, USA.

Buckle, A. M., Henrick, K. & Fersht, A. R. (1993) *J. Mol. Biol.* **234**, 847-860.

Buckle, A. M., Cramer, P. & Fersht, A. R. (1996) *Biochemistry,* **35**, 4298-4305.

Chothia, C. (1974) *Nature*, **248**, 338-339.

Chothia, C. (1992) *Nature*, **357**, 543-544.

Chou, P. Y. & Fasman, G. D. (1978) *Adv. Enzymol.* **47**, 45-148.

Connolly, M. L. (1985) *J. Am. Chem. Soc.* **107**, 1118-1124.

Connolly, M. L. (1993) *J. Mol. Graphics*, **11**, 139-141.

Crowther, R. A. & Blow, D. M. (1967) *Acta Cryst.* **23**, 544-548.

Damodaran, S. & Song, K. B. (1986) *J. Biol. Chem.* **261**, 7220-7222.

Dao-Pin, S., Baase, W. A. & Matthews, B. W. (1990) *Proteins: Struct. Funct. Genet.* **7**, 198-204.

Dao-Pin, S., Anderson, D. E., Baase, W. A., Dahlquist, F. W. & Matthews, B. W. (1991) *Biochemistry*, **30**, 11521-11529.

Das, G., Hickey, D. R., McLendon, D., McLendon, G. & Sherman, F. (1989) *Proc. Natl Acad. Sci. USA*, **86**, 496-499.

Dill, K. A. & Shortle, D. (1991) *Annu. Rev. Biochem.* **60**, 795-825.

Driscoll, P. C., Gronenborn, A. M., Wingfield, P. T. & Clore, G. M. (1990) *Biochemistry*, **29**, 4668-4682.

Dunitz, J. D. (1994) *Science*, **264**, 670.

Eriksson, A. E., Baase, W. A., Zhang, X.-J., Heinz, D. W., Blaber, M., Baldwin, E. P. & Matthews, B. W. (1992) *Science*, **255**, 178-183.

Eriksson, A E., Baase, W. A. & Matthews, B. W. (1993) *J. Mol. Biol.* **229**, 747-769.

Ernst, J. A., Clubb, R. T., Zhou, H.-X., Gronenborn, A. M. & Clore, M. (1995) *Science*, **267**, 1813-1817.

Evans, P. A., Toppmg, K. D., Woolfson, D. N. & Dobson, C. M. (1991) *Proteins: Struct. Funct. Cenet.* **9**, 248-296.

Fauchere, J.-L. & Pliska, V. (1983) *Eur. J. Med. Chem.* **18**, 369-375.

Fitzgerald, M. M., Churchill, M. J., McRee, D. E. & Goodin, D. B. (1994) *Biochemistry*, **33**, 3807-3818.

Funahashi, J., Takano, K., Ogasahara, K., Yamagata, Y. & Yutani, K. (1996) *J. Biochem.* **120**, 1216-1223.

Green, D. W., Ingram, V. M. & Perutz, M. F. (1954) *Proc. Roy. Soc.* **A225**, 287-292.

Gros, F. & Tocchini-Valentin, G. G. (1994) *Nature*, **369**, 11-12.

Hajdu, J., Machin, P. A., Campbell, J. W., Greenhough, T. J., Clifon, I. J., Zurek, S., Gover, S., Johnson, L. N. & Elder, M. (1987) *Nature*, **329**, 178-181.

Hawkers, R., Grutter, M. G. & Schellmann, J. A. (1984) *J. Mol. Biol.* **175**, 195-212.

Helms, V. & Wade, R. C. (1995) *Biophys. J.* **69**, 810-824.

Henderson, R., Baldwin, J. M., Ceska, T. A., Zemlin, F., Beckmann, E. & Downing, K. H. (1990) *J. Mol. Biol.* **213**, 899-928.

Hermann, R. B. (1972) *J. Phys. Chem.* **76**, 2754-2759.

Herning, T., Yutani, K., Taniyama, Y. & Kikuchi, M. (1991) *Biochemistry*, **30**, 9882-9891.

Herning, T., Yutani, K., Inaka, K., Kuroki, R., Matsushima, M. & Kikuchi, M. (1992) *Biochemistry*, **31**, 7077-7085.

Hickey, D. R., Berghuis, A. M., Lafond, G., Jaeger, J. A., Cardillo, T. S., McLendon, D., Das, G., Sherman, F., Brayer, G. D. & McLendon, G. (1991) *J. Biol. Chem.* **266**, 11686-11694.

Hiraga, K. & Yutani, K. (1996) *Protein Eng.* **9**, 425-431.

Horovitz, A., Matthews, J. M. & Fersht, A. R. (1992) *J. Mol. Biol.* **227**, 560-568.

Hubbard, S. J., Gross, K.-H. & Argos, P. (1994) *Protein Eng.* **7**, 613-626.

Ikura, M., Kay, L. E.. Krinks, M. & Bax, A. (1991) *Biochemistry*, **30**, 5498-5504.

Inaka, K., Taniyama, Y., Kikuchi, M., Morikawa, K. & Matsushima, M. (1991a) *J. Biol. Chem.* **266**, 12599-12603.

Inaka, K., Kuroki, R., Kikuchi, M. & Matsushima, M. (1991b) *J. Biol. Chem.* **266**, 20666-20671.

Ishikawa, K., Nakamura, H., Morikawa, K. & Kanaya, S. (1993) *Biochemistry*, **32**, 6171-6178.

Jackson, S. E., Moracci, M., elMasry, N., Johnson, C. M. & Fersht, A. R. (1993) *Biochemistry*, **32**, 11259-11269.

Johnson, C. K. (1976) ORTEPII, Oak Ridge National Laboratory, TN, USA.

Jones, T. A. (1978) *J. Appl. Cryst.* **11**, 268.

Kabsch, W. & Sander, C. (1983) *Biopolymers*, **22**, 2577-2637.

Kanaya, E. & Kikuchi, M. (1992) *J. Biol. Chem.* **267**, 15111-15115.

Karpusas, M., Baase, W. A., Matsumura, M. & Matthews, B. (1989) *Proc. Natl Acad. Sci. USA*, **86**, 8237-8241.

Kauzmann, W. (1959) *Adv. Protein Chem.* **14**, 1-63.

Kellis, J. T., Jr. Nyberg, K., Sali, D. & Fersht, A. R. (1988) *Nature*, **333**, 784-786.

Kellis, J. T. Jr, Nyberg, K. & Fersht, A. R. (1989) *Biochemistry*, **28**, 4914-4922.

Kendrew, J. C., Bodo, G., Dintzis, H. M., Parrish, R. G., Wykoff, H. & Phillips, D. C. (1958) *Nature*, **181**, 662-666.

Kidera, A., Inaka, K. & Go, N. (1992) *J. Mol. Biol.* **225**, 477-486.

Kidera, A., Inaka, K. & Go, N. (1994) *Protein Sci.* **3**, 92-102.

Kikuchi, M., Yamamoto, Y., Taniyama, Y., Ishimaru, K., Yoshikawa, W., Kaisho, Y. & Ikehara., M. (1988) *Proc. Natl Acad. Sci. USA*, **85**, 9411-9415.

Kikuchi, M. & Ikehara, M. (1994) *Protein Eng.* **7**, 735-742.

Kim, C. A. & Berg, J. M. (1993) *Nature,* **362**, 267-270.

Kossiakoff, A. A., Sintchak, M. D., Shpungin, J. & Presta, L. G. (1992) *Proteins: Struct. Funct. Genet.* **12**, 223-236.

Kraulis, P. J. (1991) *J. Appl. Crystallog.* **24**, 946-950.

Kuroki, R., Inaka, K., Taniyama, Y., Kidokoro, S., Matsushima, M., Kikuchi, M. & Yutani, K. (1992a) *Biochemistry*, **31**, 8323-8328.

Kuroki, R., Kawakita, S., Nakamura, H. & Yutani, K. (1992b) *Proc. Natl Acad. Sci. USA*, **89**, 6803-6807.

Lee, B. (1993) *Protein Sci.* **2**, 733-738.

Lesser, G. J. & Rose, G. D. (1990) *Proteins: Struct. Funct. Genet.* **8**, 6-13.

Lett, C. M., Berghuis, A. M., Frey, H. E., Lepock, J. R. & Guillemette, J. G. (1996) *J. Biol. Chem.* **271**, 29088-29093.

Luzzati, P. V. (1952) *Acta Cryst.* **5**, 802-810.

Makhatadze, G. I. & Privalov, P. (1993) *J. Mol. Biol.* **232**, 639-659.

Makhatadze, G. I. & Privalov, P. L. (1995) *Adv. Protein Chem.* **47**, 307-429.

Matsumura, M., Becktel, W. J. & Matthews, B. W. (1988) *Nature*, **334**, 406-410.

Matthews, B. W. (1993) *Annu. Rev. Biochem.* **62**, 139-160.

Matthews, B. W. (1995) *Adv. Protein Chem.* **46**, 249-278.

Matthews, B. W. (1996) *FASEB J.* **10**, 35-41.

Minor, D. L., Jr. & Kim, P. S. (1994) *Nature,* **367**, 660-663.

Minor, D. L., Jr. & Kim, P. S. (1996) *Nature*, **380**, 730-734.

Miyahara, J., Takahashi, K., Amemiya, Y., Kamiya, N. & Satow, Y. (1986) *Nucl. Inst. Methods Phys. Res.* **A246**, 572-578.

Miyanohara, A., Toh-e, A., Nozaki, C., Hamada, F., Ohtomo, N. & Matsubara, K. (1983) *Proc. Natl Acad. Sci. USA*, **80**, 1-5.

Moffat, K., Szebenyi, D. & Bilderback, D. (1984) *Science*, **223**, 1423-1425.

Muraki, M., Harata, K. & Jigami, Y. (1992) *Biochemistry*, **31**, 9212-9219.

Muraki, M., Goda, S., Nagahora, H. & Harata, K. (1997) *Protein Sci.* **6**, 473-476.

Myers, J. K., Pace, C. N. & Scholtz, J. M. (1997a) *Proc. Natl Acad. Sci.*

USA, **94**, 2833-2837.

Myers, J. K., Pace, C. N. & Scholtz, J. M. (1997b) *Biochemistry*, **36**, 10923-10929.

Nakasako, M., Ueki, T., Toyoshima, C. & Umeda, Y. (1995) *J. Appl. Cryst.* **28**, 856-857.

Nozaki, Y. & Tanford, C. (1971) *J. Biol. Chem.* **246**, 2211-2217.

Oobatake, M. & Ooi, T. (1993) *Prog. Biophys. Mol. Biol.* **59**, 237-284.

Otwinowski, Z. (1993) DENZO data processing package. Yeal University, New Haven, CT.

Otzen, D. E. & Fersht, A. R. (1995) *Biochemistry,* **34**, 5718-5724.

Otzen, D. E., Rheinnecker, M. E. & Fersht, A. R. (1995) *Biochemistry,* **34**, 13051-13058.

Pace, C. N. (1986) *Methods Enzymol.* **131**, 266-280.

Pace, C. N. (1992) *J. Mol. Biol.* **226**, 29-35.

Pace C. N., Laurents, D. V. & Thomson, J. A. (1990) *Biochemistry,* **29**, 2564-2572.

Pace C. N., Laurents, D. V. & Erickson, R. E. (1992) *Biochemistry,* **31**, 2728-2734.

Pace, C. N., Shirley, B. A., Mcnutt, M. & Gajiwala, K. (1996) *FASEB J.* **10**, 75-83.

Park S. H., Shalongo, W. & Stellwagen, E. (1993) *Biochemistry*, **32**, 7048-7053.

Parry, R. M., Chandan, R. C. & Shahani, K. M. (1969) *Arch. Biochem. Biophys.* **130**, 59-65.

Pedersen, J. T., Olsen, O. H., Betzel, C., Eschenburg, S., Branner, S. & Hastrup, S. (1994) *J. Mol. Biol.* **242**, 193-202.

Pepys, M. B., Hawkins, P. N., Booth, D. R., Vigushin, D. M., Tennent, G. A., Soutar, A. K., Totty, N., Nguyen, O., Blake, C. C., Terry, C. J., Feest, T. G., Zalin, A. M. & Hsuan, J. J. (1993) *Nature*, **362**, 553-557.

Peters, C. W. B., Kruse, U. K., Pollwein, R., Grzeschik, K.-H. & Sippel, A. E. (1989) *Eur. J. Biochem.* **182**, 507-516.

Phillips, D. C. (1966) *Sci. Am.* **215**, 78-90.

Pinker, R. J., Lin, L., Rose, G. D. & Kallenbach, N. R. (1993) *Protein Sci.* **2**, 1099-1106.

Plotnikov, V. V., Brandts, J. M., Lin, L.-N. & Brandts, J. F. (1997) *Anal. Biochem.* **250**, 237-244.

Privalov, G., Kavina, V., Freire, E. & Privalov, P. L. (1995) *Anal. Biochem.* **232**, 79-85.

Privalov, P. L. (1974) *FEBS Lett.* **40S**, S140-153.

Privalov, P. L. (1979) *Adv. Protein Chem.* **33**, 167-241.

Privalov, P. L. & Khechinashvili, N. N. (1974) *J. Mol. Biol.* **86**, 665-684.

Privalov, P. L. & Makhataze, G. I. (1993) *J. Mol. Biol.* **232**, 660-679.

Privalov, P. L. & Potekhin, S. A. (1986) *Methods Enzymol.* **131**, 4-51.

Radzicka, A. & Wolfenden, R. (1988) *Biochemistry*, **27**, 1644-1670.

Rashin, A. A., Iofin, M. & Honig, B. (1986) *Biochemistry*, **25**, 3619-3625.

Reynolds, J. A., Gilbert, D. B. & Tanford, C. (1974) *Proc. Natl Acad. Sci. USA*, **71**, 2925-2927.

Richards, F. M. (1977) *Annu. Rev. Biophys. Bioeng.* **6**, 151-176.

Rohl, C. A., Chakrabartty, A. & Baldwin, R. L. (1996) *Protein Sci.* **5**, 2623-2637.

Rose, G. D., Gierasch, L. M. & Smith, J. A. (1985) *Adv. Protein Chem.* **37**, 1-109.

Rossmann, M. G., & Blow, D. M. (1962) *Acta Cryst.* **15**, 24-31.

Sakabe, N. (1991) *Nucl. Instr. Methods Phys. Res.* **A303**, 448-463.

Sandberg, W. S. & Terwilliger, T. C. (1991) *Proc. Natl Acad. Sci. USA*, **88**, 1706-1710.

Serrano, L., Horovitz, A., Avron, B., Bycroft, M. & Fersht, A. R. (1990) *Biochemistry*, **29**. 9343-9352.

Serrano, L., Kellis, J. T., Jr., Cann, P., Matouschek, A. & Fersht, A. R. (1992a) *J. Mol. Biol.* **224**, 783-804.

Serrano, L., Sancho, J., Hirshberg, M. & Fersht, A. R. (1992b) *J. Mol. Biol.* **227**, 544-559.

Shortle, D., Stites, W. E. & Meeker, A. K. (1990) *Biochemistry*, **29**, 8033-8041.

Smith, C. K., Withka, J. M. & Regan, L. (1994) *Biochemistry,* **33**, 5510-5517.

Stokes, D. L & Green, N. M. (1990) *J. Mol. Biol.* **213**, 529-538.

Sturtevant, J. M. (1994) *Curr. Opin. Struct. Biol.* **4**, 69-78.

Takano, K., Ogasahara, K., Kaneda, H., Yamagata, Y., Fujii, S., Kanaya, E., Kikuchi, M., Oobatake, M. & Yutani, K. (1995). *J. Mol. Biol.* **254**, 62-76.

Takano, K., Yamagata, Y., Fujii, S. & Yutani, K. (1997a). *Biochemistry*, **36**, 688-698.

Takano, K., Funahashi, J., Yamagata, Y., Fujii, S. & Yutani, K. (1997b). *J. Mol. Biol.* **274**, 132-142.

Tamura, A. & Sturtevant, J. M. (1995) *J. Mol. Biol.* **249**, 625-635.

Tanford, C. (1962) *J. Am. Chem. Soc.* **84**, 4240-4247.

Taniyama, Y., Yamamoto, Y., Nakao, M., Kikuchi, M. & Ikehara, M. (1988) *Biochem. Biophys. Res. Commun.* **152**, 962-967.

Taniyama, Y., Seko, C. & Kikuchi, M. (1990) *J. Biol. Chem.* **265**, 16767-16771.

Taniyama, Y., Ogasahara, K., Yutani, K. & Kikuchi, M. (1992) *J. Biol. Chem.* **267**, 4619-4624.

Toh-e, A., Ueda, Y., Kakimoto, S. & Oshima, Y. (1973) *J. Bacteriol.* **113**, 727-738.

Vriend, G., Berendsen, H. J. C., van der Zee, J. R., van den Burg, B., Venema, G. & Eijsink, V. G. H. (1991) *Protein Eng.* **4**, 941-945.

Wade, R. C., Mazor, M. H., McCammon, J. A. & Quiocho, F. A. (1991) *Biopolymers*, **31**, 919-931.

Williams, M. A., Goodfellow, J. M. & Thornton, J. M. (1994) *Protein Sci.* **3**, 1224-1235.

Yamamoto, Y., Taniyama, Y., Kikuchi, M. & Ikehara, M. (1987) *Biochem. Biophys. Res. Commun.* **149**, 431-436.

Yoshimura, K., Toibana, A., Kikuchi, K., Kobayashi, M., Hayakawa, T., Nakahama, K., Kikuchi, M. & Ikehara, M. (1987) *Biochem. Biophys. Res. Commun.* **145**, 712-718.

Yu, M.-H., Weissman, J. S. & Kim, P. S. (1995) *J. Mol. Biol.* **249**, 388-397.

Yutani, K., Ogasahara, K., Sugino, Y. & Matsushiro, A. (1977) *Nature*, **267**, 274-275.

Yutani, K., Ogasahara, K., Tsujita, T. & Sugino, Y. (1987) *Proc. Natl Acad. Sci. USA*, **84**, 4441-4444.

Yutani, K., Hayashi, S., Sugisaki, Y. & Ogasahara, K. (1991) *Proteins: Struct. Funct. Cenet.* **9**, 90-98.

Zhang, L. & Hermans, J. (1996) *Proteins: Struct. Funct. Genet.* **24**, 433-438.

Zimmerman, S. S., Pottel, M. S., Nemethy, G. & Scheraga, H. A. (1977) *Macromolecules,* **10**, 1-9.

List of Publications

[1] **Contribution of Hydrophobic Residues to the Stability of Human Lysozyme: Calorimetric Studies and X-ray Structural Analysis of the Five Isoleucine to Valine Mutants**
Kazufumi Takano, Kyoko Ogasahara, Hidetomo Kaneda, Yuriko Yamagata, Satoshi Fujii, Eiko Kanaya, Masakazu Kikuchi, Motohisa Oobatake & Katsuhide Yutani
J. Mol. Biol. (1995) **254**, 62-76.

[2] **Contribution of the Hydrophobic Effect to the Stability of Human Lysozyme: Calorimetric Studies and X-ray Structural Analyses of the Nine Valine to Alanine Mutants**
Kazufumi Takano, Yuriko Yamagata, Satoshi Fujii & Katsuhide Yutani
Biochemistry (1997) **36**, 688-698.

[3] **Contribution of Water Molecules in the Interior of a Protein to the Conformational Stability**
Kazufumi Takano, Jun Funahashi, Yuriko Yamagata, Satoshi Fujii & Katsuhide Yutani
J. Mol. Biol. (1997) **274**, 132-142.

[4] **A General Rule for the Relationship between Hydrophobic Effect and Conformational Stability of a Protein: Stability and Structure of a Series of Hydrophobic Mutants of Human Lysozyme**
Kazufumi Takano, Yuriko Yamagata & Katsuhide Yutani
Submitted to *J. Mol. Biol.*

[5] **The Structure, Stability, and Folding Process of Amyloidgenic Mutant Human Lysozyme**
Jun Funahashi, Kazufumi Takano, Kyoko Ogasahara, Yuriko Yamagata & Katsuhide Yutani
J. Biochem. (1996) **120**, 1216-1223.

[6] **Contribution of Hydrogen Bonds to the Conformational Stability of Human Lysozyme: Calorimetry and X-ray Analysis of Six Tyr → Phe Mutants**
Yuriko Yamagata, Masahiro Kubota, Jun Funahashi, Kazufumi Takano, Yohei Sumikawa, Satoshi Fujii & Katsuhide Yutani
Submitted to *Biochemistry*.

[7] **Quantitative Analysis of Various Factors that Affect Protein Stability due to Amino Acid Substitution**
Jun Funahashi, Kazufumi Takano, Yuriko Yamagata & Katsuhide Yutani
in preparation.